



**HAL**  
open science

# Modeling and simulation in nonlinear stochastic dynamic of coupled systems and impact

Roberta de Queiroz Lima

► **To cite this version:**

Roberta de Queiroz Lima. Modeling and simulation in nonlinear stochastic dynamic of coupled systems and impact. Other. Université Paris-Est; Pontificia universidade católica (Rio de Janeiro, Brésil), 2015. English. NNT: 2015PESC1049 . tel-01238847

**HAL Id: tel-01238847**

**<https://theses.hal.science/tel-01238847>**

Submitted on 7 Dec 2015

**HAL** is a multi-disciplinary open access archive for the deposit and dissemination of scientific research documents, whether they are published or not. The documents may come from teaching and research institutions in France or abroad, or from public or private research centers.

L'archive ouverte pluridisciplinaire **HAL**, est destinée au dépôt et à la diffusion de documents scientifiques de niveau recherche, publiés ou non, émanant des établissements d'enseignement et de recherche français ou étrangers, des laboratoires publics ou privés.

UNIVERSITÉ PARIS-EST et PUC-Rio

**THÈSE**

pour obtenir le grade de

**DOCTEUR de l'UNIVERSITÉ PARIS-EST et de la PUC-Rio**

**ROBERTA DE QUEIROZ LIMA**

Date de la soutenance: le 13 mai 2015.

Lieu de la soutenance: PUC-Rio, Rua Marquês de São Vicente,  
225 CEP 22451-900, Rio de Janeiro, Brésil.

Titre: **Modeling and simulation in nonlinear stochastic dynamics  
of coupled systems and impacts**

**Directeurs de thèse**

**Professeur CHRISTIAN SOIZE**  
**Professeur RUBENS SAMPAIO**

**JURY**

FERNANDO ALVES ROCHINHA	UFRJ	Professeur Président
ROGER OHAYON	CNAM	Professeur Rapporteur
DOMINGOS ALVES RADE	ITA	Professeur Rapporteur
THIAGO GAMBOA RITTO	UFRJ	Professeur Examineur
HANS INGO WEBER	PUC-Rio	Professeur Examineur
CHRISTIAN SOIZE	Univ. Paris-Est	Professeur Directeur de thèse
RUBENS SAMPAIO	PUC-Rio	Professeur Directeur de thèse



**Roberta de Queiroz Lima**

**Modeling and simulation in nonlinear  
stochastic dynamics of coupled systems and  
impacts**

**PhD Thesis**

Thesis presented to the Postgraduate Program in Applied Mechanics of the Department of Mechanical Engineering of PUC-Rio and Université Paris-Est as partial fulfillment of the requirements for the degree of Doctor in Applied Mechanics

Adviser: Prof. Rubens Sampaio

Adviser: Prof. Christian Soize

Rio de Janeiro  
May 2015



**Roberta de Queiroz Lima**

**Modeling and simulation in nonlinear  
stochastic dynamics of coupled systems and  
impacts**

Thesis presented to the Post-graduate Program in Applied Mechanics of the Department of Mechanical Engineering of PUC-Rio and Université Paris-Est as partial fulfillment of the requirements for the degree of Doctor in Philosophy in Applied Mechanics. Approved by the following commission:

**Prof. Rubens Sampaio**

Adviser

Departamento de Engenharia Mecânica — PUC-Rio

**Prof. Christian Soize**

Adviser

Laboratoire de Modélisation et Simulation Multi-Echelle  
(MSME) — Université Paris-Est Marne-la-Vallée

**Prof. Fernando Alves Rochinha**

President

Departamento de Engenharia Mecânica — UFRJ

**Prof. Roger Ohayon**

Rapporteur

Laboratoire de Mécanique des Structures et des Systèmes  
Couplés — CNAM

**Prof. Domingos Alves Rade**

Rapporteur

Technological Institute of Aeronautics — ITA

**Prof. Hans Ingo Weber**

Examineur

Departamento de Engenharia Mecânica — PUC-Rio

**Prof. Thiago Gamboa Ritto**

Examineur

Departamento de Engenharia Mecânica — UFRJ

**Prof. José Eugênio Leal**

Coordinator of the Centro Técnico Científico da PUC-Rio

Rio de Janeiro — May 13, 2015

All rights reserved.

### Roberta de Queiroz Lima

Roberta Lima graduated as mechanical engineering in 2009 from PUC-Rio (Rio de Janeiro, RJ), and she got her master degree in 2011 from the same institution. This DSc. Thesis was a joint work between PUC-Rio and Université Paris-Est in a program of double diploma.

#### Bibliographic data

Lima, Roberta de Queiroz

Modeling and simulation in nonlinear stochastic dynamics of coupled systems and impacts / Roberta de Queiroz Lima; adviser: Rubens Sampaio; adviser: Christian Soize. — Rio de Janeiro : PUC-Rio, Department of Mechanical Engineering of PUC-Rio and Université Paris-Est, 2015.

v., 89 f: il. ; 29,7 cm

1. PhD Thesis - Pontificia Universidade Católica do Rio de Janeiro, Department of Mechanical Engineering of PUC-Rio and Université Paris-Est.

Bibliography included.

1. Department of Mechanical Engineering of PUC-Rio and Université Paris-Est – Thesis. 2. Coupled systems; Embarked system; Vibro-impact; Stochastic analysis; Robust design optimization; Nonlinear dynamics. I. Sampaio, Rubens. II. Pontificia Universidade Católica do Rio de Janeiro. Department of Department of Mechanical Engineering of PUC-Rio and Université Paris-Est. III. Title.

CDD: 621

## Acknowledgments

First I would like to thank my family for their incentive and support. Then, I would like to say thanks to my advisers Rubens Sampaio and Christian Soize for all dedication, attention and teaching. They were always available, full of ideas, and guided me throughout the period of the thesis. I learned a lot with them. I would also like to say thanks to the jury: Prof. Ohayon, Prof. Rade, Prof. Weber, Prof. Ritto and Prof. Rochinha. Also, I would like to say thanks to all the professors and friends of PUC-Rio and Paris-Est. Finally, I would like to thank the financial support of the Brazilian agencies FAPERJ, CNPq and CAPES (project CAPES-COFECUB 672/10) and of the universities PUC-Rio and Paris-Est.

## Abstract

Lima, Roberta de Queiroz; Sampaio, Rubens and Soize, Christian.  
**Modeling and simulation in nonlinear stochastic dynamics of coupled systems and impacts.** Rio de Janeiro, 2015. 89p.  
PhD Thesis — Department of Mechanical Engineering of PUC-Rio and Université Paris-Est.

In this Thesis, the robust design with an uncertain model of a vibro-impact electromechanical system is done. The electromechanical system is composed of a cart, whose motion is excited by a DC motor (motor with continuous current), and an embarked hammer into this cart. The hammer is connected to the cart by a nonlinear spring component and by a linear damper, so that a relative motion exists between them. A linear flexible barrier, placed outside of the cart, constrains the hammer movements. Due to the relative movement between the hammer and the barrier, impacts can occur between these two elements. The developed model of the system takes into account the influence of the DC motor in the dynamic behavior of the system. Some system parameters are uncertain, such as the stiffness and the damping coefficients of the flexible barrier. The objective of the Thesis is to perform an optimization of this electromechanical system with respect to design parameters in order to maximize the impact power under the constraint that the electric power consumed by the DC motor is lower than a maximum value. To choose the design parameters in the optimization problem, a sensitivity analysis was performed in order to define the most sensitive system parameters. The optimization is formulated in the framework of robust design due to the presence of uncertainties in the model. The probability distributions of random variables are constructed using the Maximum Entropy Principle and statistics of the stochastic response of the system are computed using the Monte Carlo method. The set of nonlinear equations are presented, and an adapted time domain solver is developed. The stochastic nonlinear constrained design optimization problem is solved for different levels of uncertainties, and also for the deterministic case. The results are different and this shows the importance of the stochastic modeling.

## Keywords

Coupled systems; Embarked system; Vibro-impact; Stochastic analysis; Robust design optimization; Nonlinear dynamics.

## Résumé

Lima, Roberta de Queiroz; Sampaio, Rubens and Soize, Christian.  
**Modélisation et simulation en dynamique stochastique non linéaire des systèmes couplés avec phénomènes d'impact.**  
Rio de Janeiro, 2015. 89p. PhD Thesis — Département de Génie Mécanique de la PUC-Rio and Université Paris-Est.

Dans cette Thèse, nous étudions l'optimisation robuste avec un modèle incertain d'un système électromécanique avec vibro-impact. Le système électromécanique est constitué d'un chariot dont le mouvement est généré par un moteur à courant continu, et d'un marteau embarqué dans ce chariot. Le marteau est relié au chariot par un ressort non linéaire et par un amortisseur linéaire, de façon qu'un mouvement relatif existe entre eux. Une barrière flexible linéaire, placée à l'extérieur du chariot limite les mouvements du marteau. En raison du mouvement relatif entre le marteau et la barrière, des impacts peuvent se produire entre ces deux éléments. Le modèle du système développé prend en compte l'influence du moteur à courant continu dans le comportement dynamique du système. Certains paramètres du système sont incertains, tels que les coefficients de rigidité et d'amortissement de la barrière flexible. L'objectif de la Thèse est de réaliser une optimisation de ce système électromécanique en jouant sur les paramètres de conception. Le but est de maximiser la puissance d'impact sous la contrainte que la puissance électrique consommée par le moteur à courant continu soit inférieure à une valeur maximale. Pour choisir les paramètres de conception dans le problème d'optimisation, une analyse de sensibilité a été réalisée afin de définir les paramètres du système les plus sensibles. L'optimisation est formulée dans le cadre de la conception robuste en raison de la présence d'incertitudes dans le modèle. Les lois de probabilités des variables aléatoires du problème sont construites en utilisant le Principe du Maximum d'Entropie. Les statistiques de la réponse stochastique du système sont calculées en utilisant la méthode de Monte Carlo. L'ensemble des équations non linéaires est présenté, et un solveur temporel adapté est développé. Le problème d'optimisation non linéaire stochastique est résolu pour différents niveaux d'incertitudes, ainsi que pour le cas déterministe. Les résultats sont différents, ce qui montre l'importance de la modélisation stochastique.

## Mots-clés

Systèmes couplés; Système embarqué; Vibro-impact; Analyse stochastique; Optimisation robuste; Dynamique non-linéaire.

## Resumo

Lima, Roberta de Queiroz; Sampaio, Rubens and Soize, Christian.  
**Modelagem e simulação em dinâmica estocástica não-linear de sistemas acoplados e impactos.** Rio de Janeiro, 2015. 89p.  
PhD Thesis — Departamento de Engenharia Mecânica da PUC-Rio and Université Paris-Est.

Nesta Tese, o design robusto, com um modelo incerto de um sistema de vibro-impacto eletromecânico é feito. O sistema é composto de um carrinho, cujo movimento é acionado por um motor de corrente contínua e um martelo embarcado neste carrinho. O martelo é ligado ao carrinho por um mola não linear e por um amortecedor linear, de modo que existe um movimento relativo entre eles. Uma barreira linear flexível, colocada fora do carrinho, restringe aos movimentos do martelo. Devido ao movimento relativo entre o martelo e a barreira, impactos podem ocorrer entre estes dois elementos. O modelo matemático desenvolvido para sistema leva em conta a influência do motor no comportamento dinâmico do sistema. Alguns parâmetros do sistema são incertos, tais como a rigidez e os coeficientes de amortecimento da barreira flexível. O objectivo da Tese é realizar uma otimização deste sistema electromecânico com respeito a parâmetros de projeto, a fim de maximizar a potência de impacto sob a restrição de que a potência elétrica consumida pelo motor seja menor do que um valor máximo. Para escolher os parâmetros de projeto no problema de otimização, uma análise de sensibilidade foi realizada a fim de definir os parâmetros mais sensíveis do sistema. O problema de otimização é formulado no âmbito de otimização robusta, devido à presença de incertezas no modelo. As distribuições de probabilidades das variáveis aleatórias são construídas através do Princípio da Máxima Entropia e estatísticas da resposta estocástica do sistema são calculadas pelo método de Monte Carlo. O conjunto de equações não-lineares é apresentado, e um integrador temporal adaptado é desenvolvido. O problema de otimização não-linear estocástico com restrição é resolvido para diferentes níveis de incertezas e também para o caso determinístico. Os resultados são diferentes e isto mostra a importância da modelagem estocástica.

## Palavras-chave

Sistemas acoplados; Sistema embarcado; Vibro-impacto; Análise estocástica; Otimização robusta; Dinâmica não linear.

# Contents

1	Introduction	<b>14</b>
1.1	Motivation of the Thesis	14
1.2	Percussive systems	16
1.3	Hierarchical electromechanical systems analyzed	17
1.4	Organization of the Thesis	19
2	Motor-cart system: a parametric excited nonlinear system due to electromechanical coupling	<b>20</b>
2.1	Dynamics of the motor-cart system	20
	Electrical system: DC motor	20
	Cart-motor system: a master-slave relation	22
2.2	Dimensionless cart-motor system	23
2.3	Numerical simulations of the dynamics of the motor-cart system	24
2.4	Asymptotically stable periodic orbit	29
2.5	Summary of the Chapter	32
3	Motor-cart-pendulum system: introduction of a mechanical energy reservoir	<b>33</b>
3.1	Dynamics of the motor-cart-pendulum system	33
3.2	Dimensionless cart-motor-pendulum system	34
3.3	Numerical simulations of the dynamics of the motor-cart-pendulum system	36
3.4	Pumping Leads To Revolution	39
3.5	Summary of the Chapter	43
4	Electromechanical system with internal impacts and uncertainties	<b>44</b>
4.1	Dynamics of the motor-cart-pendulum-barrier system	45
4.2	Dimensionless motor-cart-pendulum-barrier system	46
4.3	Impact energy	48
4.4	Numerical simulations of the dynamics of the coupled system	48
	No coupling between the motor and the mechanical system	48
	Coupled system	49
4.5	Probabilistic model	51
4.6	Numerical simulations of the stochastic vibro-impact electromechanical system	52
4.7	Summary of the Chapter	56
5	Robust design optimization with an uncertain model of a nonlinear percussive electromechanical system	<b>58</b>
5.1	Dynamics of the vibro-impact electromechanical system	58

5.2	Dimensionless vibro-impact electromechanical system	61
5.3	Measure of the system performance	63
5.4	Sensitivity analysis and choice of the design parameters	63
5.5	Construction of the probability model	68
5.6	Robust design optimization problem	69
5.7	Results of the robust optimization problem	69
5.8	Summary of the Chapter	71
6	Summary, future works and publications	<b>75</b>
6.1	Future works	76
6.2	Publications	76
	Bibliography	<b>81</b>

## List of Figures

1.1	First system: cart-motor system.	17
1.2	Second system: cart-motor-pendulum system.	18
1.3	Third system: motor-cart-pendulum-barrier system.	18
1.4	Fourth system: motor-cart-hammer coupled system.	19
2.1	Electrical DC motor.	21
2.2	Coupled cart-motor system.	22
2.3	Motor-cart system with $\Delta = 0.001$ m: (a) angular speed of the motor shaft over time and (b) Fast Fourier Transform of the cart displacement.	25
2.4	Motor-cart system with $\Delta = 0.01$ m: (a) angular speed of the motor shaft over time and (b) Fast Fourier Transform of the cart displacement.	26
2.5	Motor-cart system: Fast Fourier Transform of the current (a) when $\Delta = 0.001$ m and (b) when $\Delta = 0.01$ m.	26
2.6	Motor-cart system with $\Delta = 0.01$ m: (a) cart displacement and (b) motor current over time.	27
2.7	Motor-cart system with $\Delta = 0.01$ m: (a) horizontal force $f$ and (b) torque $\tau$ during one cycle of the cart movement.	27
2.8	Motor-cart system with $\Delta = 0.01$ m: (a) current variation during one cart movement cycle and (b) torque variation as function of the current.	28
2.9	Motor-cart system with $\Delta = 0.01$ m: (a) angular velocity of the motor shaft during one cart movement cycle and (b) current variation as function of the angular velocity of the motor shaft.	28
2.10	Motor-cart system $\Delta = 0.01$ m: (a) torque variation as function of the horizontal force $f$ and (b) horizontal force variation as function of the angular velocity of the motor shaft.	29
2.11	Motor-cart system: period of one cart movement cycle (a) as function of $\Delta$ with $m = 5.0$ kg and (b) as function of $m$ with $\Delta = 0.005$ m.	29
2.12	Comparison between numerical findings and the asymptotic approximation.	31
2.13	Coupled cart-motor-spring-damper system.	32
3.1	Cart-motor-pendulum system.	33
3.2	Motor-cart-pendulum system with $\Delta = 0.001$ m: (a) angular velocity of the motor shaft and (b) current over time.	37
3.3	Motor-cart-pendulum system with $\Delta = 0.001$ m: (a) pendulum displacement and (b) cart displacement over time.	37
3.4	Motor-cart-pendulum system with $\Delta = 0.001$ m: Fast Fourier Transform of (a) cart and pendulum displacements and (b) of current.	38
3.5	Motor-cart-pendulum system with $\Delta = 0.01$ m: (a) angular velocity of the motor shaft and (b) current over time.	38

3.6	Motor-cart-pendulum system with $\Delta = 0.01$ m: (a) pendulum and (b) cart displacement over time.	39
3.7	Motor-cart-pendulum system with $\Delta = 0.01$ m: Fast Fourier Transform of (a) pendulum and (b) cart displacements.	39
3.8	Motor-cart-pendulum system with $\Delta = 0.01$ m: Fast Fourier Transform of (a) current and (b) angular speed of the motor shaft over time.	40
3.9	Motor-cart-pendulum system with $\Delta = 0.01$ m: (a) angular velocity of the motor shaft and (b) current over time.	40
3.10	Motor-cart-pendulum system with $\Delta = 0.01$ m: (a) pendulum and (b) cart displacement over time.	41
3.11	Motor-cart-pendulum system with $\Delta = 0.01$ m: portrait graphs of (a) $\ddot{\alpha}$ graph as function of $\dot{\alpha}$ and (b) $\dot{\alpha}$ graph as function of $x$ .	41
3.12	Motor-cart-pendulum system with $\Delta = 0.01$ m: portrait graphs of (a) $\dot{\theta}$ graph as function of $\dot{\alpha}$ and (b) $\theta$ as function of $\dot{\alpha}$ .	42
3.13	Motor-cart-pendulum system with $\Delta = 0.01$ m: portrait graphs of (a) tangent $\ddot{\theta}$ graph as function of $\dot{\alpha}$ and (b) $\tau$ as function of $\dot{\alpha}$ .	42
4.1	Coupled motor-cart-pendulum-barrier system.	44
4.2	No coupling ( $\Delta = 0$ m): normalized average of the maximum impact energy as function of the parameter gap/ $l_p$ for different values of $k_i$ N/m.	49
4.3	Coupled system ( $\Delta > 0$ ): normalized average of the impact energy as function of the parameter gap/ $l_p$ for different values of $\Delta$ (units in meters).	51
4.4	Coupled system ( $\Delta > 0$ ): normalized average of the impact energy as function of the parameter gap/ $l_p$ for different values of $k_i$ N/m with $\Delta = 10^{-3}$ m.	52
4.5	Mean and 90% confidence interval of $\Lambda/\lambda^{ref}$ as function of gap/ $l_p$ with $\delta = 0.15$ for (a) $E\{K_i\} = 10^4$ N/m and (b) $E\{K_i\} = 10^5$ N/m .	53
4.6	(a) Mean and 90% confidence interval of $\Lambda$ as function of gap/ $l_p$ with $\delta = 0.15$ and $E\{K_i\} = 10^6$ N/m and (b) normalized histogram of $\Lambda/\lambda^{ref}$ for gap/ $l_p = 0.63$ m, $E\{K_i\} = 10^6$ N/m and $\delta = 0.15$ .	54
4.7	Mean and 90% confidence interval of $\Lambda/\lambda^{ref}$ as function of gap/ $l_p$ with $E\{K_i\} = 10^4$ N/m for (a) $\delta = 0.25$ and (b) $\delta = 0.35$ .	54
4.8	Mean and 90% confidence interval of $\Lambda/\lambda^{ref}$ as function of gap/ $l_p$ with $E\{K_i\} = 10^5$ N/m for (a) $\delta = 0.25$ and (b) $\delta = 0.35$ .	55
4.9	Mean and 90% confidence interval of $\Lambda/\lambda^{ref}$ as function of gap/ $l_p$ with $E\{K_i\} = 10^6$ N/m for (a) $\delta = 0.25$ and (b) $\delta = 0.35$ .	55
5.1	Motor-cart-hammer coupled system. The nonlinear component spring is drawn as a linear spring with constant $k_{h1}$ and a nonlinear cubic spring with constant $k_{h3}$ .	58
5.2	Parallelization of the simulations in the sensitivity analysis.	65

- 5.3 For the optimal values  $(m_c/m_h)^*$  and  $\Delta^*$ : (a) graph of  $\pi_{\text{imp}}$  as a function of  $g$  and  $k_{h1}/m_h$  (varying in all its range of values), (b) graph of  $\pi_{\text{imp}}$  as a function of  $g$  and  $k_{h1}/m_h$  (varying in  $[0.06, 0.02]$  and  $[1\ 250, 1\ 953]$  respectively). 66
- 5.4 (a) Graph of  $\pi_{\text{imp}}$  as a function of  $m_c/m_h$  with  $(k_{h1}/m_h)^*$ ,  $g^*$ , and  $\Delta^*$ . (b) Graph of  $\pi_{\text{imp}}$  as a function of  $k_{h1}/m_h$  with  $(m_c/m_h)^*$ ,  $g^*$ , and  $\Delta^*$ . 66
- 5.5 (a) Graph of  $\pi_{\text{imp}}$  as a function of  $g$  with  $(m_c/m_h)^*$ ,  $(k_{h1}/m_h)^*$ , and  $\Delta^*$ . (b) Graph of  $\pi_{\text{imp}}$  as a function of  $\Delta$  with  $(m_c/m_h)^*$ ,  $(k_{h1}/m_h)^*$ , and  $g^*$ . 66
- 5.6 (a) Graph of  $\pi_{\text{elec}}$  as a function of  $m_c/m_h$  with  $(k_{h1}/m_h)^*$ ,  $g^*$ , and  $\Delta^*$ . (b) Graph of  $\pi_{\text{elec}}$  as a function of  $k_{h1}/m_h$  with  $(m_c/m_h)^*$ ,  $g^*$ , and  $\Delta^*$ . 67
- 5.7 (a) Graph of  $\pi_{\text{elec}}$  as a function of  $g$  with fix  $(m_c/m_h)^*$ ,  $(k_{h1}/m_h)^*$ , and  $\Delta^*$ . (b) Graph of  $\pi_{\text{elec}}$  as a function of  $\Delta$  with fix  $(m_c/m_h)^*$ ,  $(k_{h1}/m_h)^*$ , and  $g^*$ . 67
- 5.8 Parallelization of the simulations performed to solve the robust optimization problem. 70
- 5.9 (a) Cost function as function of the design parameters for the deterministic case. (b) Cost function as function of the design parameters for the case in which  $\delta_{K_i} = \delta_{C_i} = 0.1$  and  $\delta_{K_{h1}} = 0$ . 71
- 5.10 (a) Cost function as function of the design parameters for the case in which  $\delta_{K_i} = \delta_{C_i} = \delta_{K_{h1}} = 0.1$ . (b) Cost function as function of the design parameters for the case in which  $\delta_{K_i} = \delta_{C_i} = 0.1$  and  $\delta_{K_{h1}} = 0.4$ . 72
- 5.11 (a) Cost function as function of  $g$  with  $(\underline{K}_{h1}/m_h)^{\text{opt}}$ . (b) Cost function as function of  $\underline{K}_{h1}/m_h$  with  $g^{\text{opt}}$ . In both graphs, the  $E\{\Pi_{\text{imp}}(\mathbf{p}_{\text{des}}^{\text{opt}})\}$  is highlighted for each level of uncertainties with markers. 72
- 5.12 (a) Mean value of the time average of electric power as function of  $g$  with  $(\underline{K}_{h1}/m_h)^{\text{opt}}$ . (b) Mean value of the time average of electric power as function of  $\underline{K}_{h1}/m_h$  with  $g^{\text{opt}}$ . In both graphs, the  $E\{\Pi_{\text{elec}}(\mathbf{p}_{\text{des}}^{\text{opt}})\}$  is highlighted for each level of uncertainties with markers. 73
- 5.13 (a) Coefficient variation of  $\Pi_{\text{imp}}$  as function of  $g$  with  $(\underline{K}_{h1}/m_h)^{\text{opt}}$ . (b) Coefficient variation of  $\Pi_{\text{imp}}$  as function of  $\underline{K}_{h1}/m_h$  with  $g^{\text{opt}}$ . In both graphs, the  $\delta_{\Pi_{\text{imp}}}(\mathbf{p}_{\text{des}}^{\text{opt}})$  is highlighted for each level of uncertainties with markers. 73

## List of Tables

2.1	Values of the motor parameters used in simulations.	25
5.1	Values of the system parameters used in simulations.	64

# 1 Introduction

## 1.1 Motivation of the Thesis

The oil well drilling is still an interesting topic of research. There are still many challenges involving the modeling of the complex dynamics of a drill string. It presents interesting phenomena, such as coupled axial, lateral and torsional vibrations [86], bit-rock interaction, geometric nonlinearities, impacts, fluid-structure interaction. The literature dealing with modeling the drill string dynamics is vast (see [14, 36, 69, 79, 77]).

Besides this complex dynamics, the drill string dynamics involves also numerous sources of uncertainties. In this context of modeling, uncertainties should be taken into account in the computational models in order to improve the robustness of the numerical predictions [39, 92, 38, 67].

Recently this problem of modeling and simulation of nonlinear dynamics of a drill-string including uncertainty modeling has been intensively studied, as [74, 76, 80, 74, 82, 78].

Due to the growth of perforation depth over the years, the drilling process requires a constant improvement in energy efficiency. Reduction of costs and increase in bit life and in rate of penetration are always challenges for oil companies.

During conventional rotary drilling, many different forms of dissipation, as axial vibrations, can generate the waste of the energy applied in the drillstring. To compensate these losses, many new concepts of drilling were proposed over the years. These new approaches consider the efficient use of energy as an important factor, bringing an increase in rate of penetration, and consequently a reduction the cost of hard rock drilling. One example, is the concept of percussive drilling, introduced in the last decades [5]. The percussion proposes to insert energy into the drilling process through impacts to fracture the rock, and then facilitate the penetration of the bit [3, 2, 28, 27, 60, 58, 70, 22]. The objective is to combine rotary and impact action in order to increase the drilling rate.

This concept of use of impacts in drilling motivates this Thesis. We are interested in simple systems that present the phenomenon that somehow mimic the dynamical behavior found in the percussive drilling process: the vibro-

impact action. Despite the systems analyzed do not consider the rotary action, we do believe that they represent an initial step to study the percussive drilling.

As percussive dynamical systems can be affected by many factors, their analysis requires to take into account uncertainties in the computational models that are used (see for instance [87]). Thus, we are interested also in problems that involve uncertainty quantification and stochastic modeling.

The analysis of vibro-impact systems is not a new subject, and is frequently encountered in technical applications of mechanisms. The interest of analyzing their performance is reflected by the increasing amount of research in this area (see for instance [63, 68, 98, 75, 33, 96], and also the book by Ibrahim [32], which is completely devoted to this problem). Besides the theoretical research in vibro-impact dynamics, numerous applications to vibro-impact systems have also been developed, such as vibration hammer, impact damper, and gears. The vibro-impact dynamics appears also in several other situations, as for example in earthquakes, where the interest is the seismic mitigation [66].

The focus of this Thesis is to analyze numerically the performance of vibro-impact systems with motion driven by an electrical motor. This performance is measured by the impact power (transferred from the system to an external barrier) and by the electric power consumed by the electrical motor that drives the system motion. In the developed model of the system, the influence of the DC motor in the dynamic behavior of the system is taken into account.

The electromechanical systems analyzed in this Thesis were first designed by R.R. Aguiar in his PhD Thesis [1]. He investigated experimentally a vibro-impact system with motion driven by an electrical motor, with a similar coupling mechanism between the mechanical and electrical parts of the system, the *scotch yoke* mechanism. The main objective of R.R. Aguiar was to characterize the impact force magnitude and to make numerical analysis through bifurcation diagrams, Peterka map [72] and basins of attraction. Aguiar published some journal papers about his work, as [3, 2].

Mechanical systems with motion driven by electric motors are usually modeled eliminating the motor and saying that the force between the mechanical and electric systems is imposed, so no electromechanical coupling is present, and it is harmonic with frequency given by the nominal frequency of the motor. In this Thesis, it is shown that this hypothesis is far from true and leads to a completely different dynamics. In the systems we analyze here, the coupling force is not prescribed by a function, it comes from the coupling, varying with the coupling conditions [44, 18]. Therefore, the dynamics of electromechanical systems is characterized by a mutual interaction between the

mechanical and electric parts, that is, the dynamics of the motor is heavily influenced by the mechanical system and the dynamics of the mechanical part depends on the dynamics of the motor [4].

After an extensive literature review, no references dealing with this mutual interaction between electric and percussive systems were found. Hence we believe that this Thesis is a first work on this topic.

## 1.2 Percussive systems

Percussive systems are usually composed by a cart with motion driven by an external system (in our case it is an electrical DC motor) and, by an embarked hammer in the cart. The cart acts like a hammer case and induces the hammer motion. An external barrier (representing the soil, in the case of percussive drilling systems) constrains the hammer movements. Due to the relative movement between the hammer and the barrier, impacts can occur between these two elements. The interaction between those components (DC motor, cart, hammer, and barrier) gives to the system dynamical special features, and turns the dynamical behavior very nonlinear. These interactions are described as following:

- Between the mechanical and electrical parts of the system appears an electromechanical coupling in which the coupling force varies with the coupling conditions. The result is a mutual interaction between the mechanical and electric parts.
- The motion of the hammer is induced by the motion of the cart, in a way that there is no direct control on the hammer motion. Therefore, the hammer introduces a new feature since its motion acts as a reservoir of energy, i.e. energy from the electrical system is pumped to the hammer and stored in the hammer motion, changing the characteristics of the mechanical system (see [13, 59]).
- Part of the energy stored in the hammer motion is transferred to the external barrier through the impacts. The impact power achieved is one the variables used for measuring the system performance. In the case of drilling, this power would be used to fracture the soil and enhance the penetration.

To understand the role played by each one of these phenomena in the dynamics of the electromechanical percussive systems, we decided to split the problem into four simpler problems, in hierarchical complexity: from simpler to more complexity. With this division, to every concluded step, we gained some

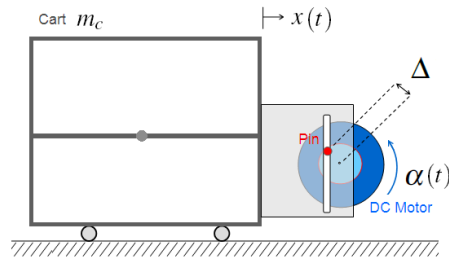


Figure 1.1: First system: cart-motor system.

insight into the behavior of the electromechanical percussive systems and, we published some works. The systems studied are described in the next Section.

### 1.3 Hierarchical electromechanical systems analyzed

We started the study analyzing the dynamics of a very simple system, composed of a cart whose motion is driven by an electrical DC motor, as shown in Fig. 1.1. The coupling between the motor and the cart is made by a mechanism called *scotch yoke* so that the motor rotational motion is transformed into a cart horizontal motion. This system is a bare minimum to analyze the effect of the electromechanical coupling, i.e., the mutual interaction between the mechanical and electric systems, in which the coupling torque appears as a parametric excitation, i.e., a time variation of the system parameters (see for instance [10, 97]). In this simple motor-cart system the coupling is a sort of master-slave condition: the motor drives, the cart is driven, and that is all.

The second system analyzed has the same two elements of the first and also a pendulum with suspension point fixed in cart, as shown in Fig. 1.2. The pendulum is the embarked system and its motion is driven by the motion of the cart. So there is no direct control of the motion of the pendulum. The pendulum introduces a new feature since its motion acts as a reservoir of energy, i.e. energy from the electrical system is pumped to the pendulum and stored in the pendulum motion, changing the characteristics of the mechanical system. The objective of the study of this motor-cart-pendulum system is to analyze the influence of an embarked element in the dynamics of the electromechanical system. One of the main results is that the master-slave condition, that appeared in the cart-motor system, is not anymore a characteristic of the system.

The third system analyzed has the same three elements of the first and also a flexible barrier placed inside the cart that constrains the pendulum

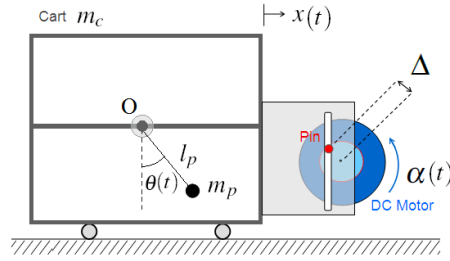


Figure 1.2: Second system: cart-motor-pendulum system.

motion, as shown in Fig. 1.3. Due to the relative movement between the cart and the pendulum, it is possible that occur impact between these two elements. Thus, the third electromechanical system analyzed has internal impacts. The impacts are caused by the motion of the cart that induces the motion of the pendulum. As the impacts are internal, the energy stored in the pendulum motion it is not transferred outside the system, it stays within, with a possible dissipation. This system configuration helps to understand the difference between an internal and an external barrier. The objective in this part of the Thesis is to analyze the maximal energy stored in the barrier in impacts as function of some parameters of the electromechanical system. Due to the presence of uncertainties in the computational nonlinear dynamics model of the electromechanical system with internal impacts, the energy analysis is performed from a stochastic view point for different levels of uncertainties, and also for the deterministic case.

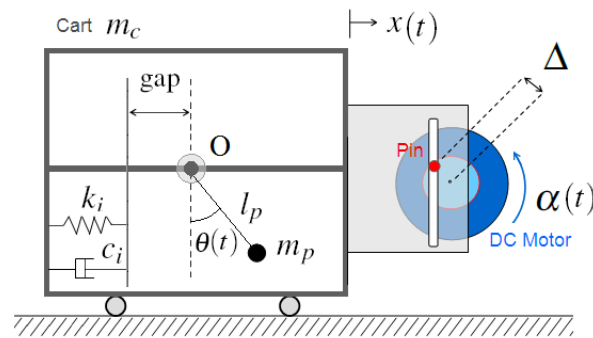


Figure 1.3: Third system: motor-cart-pendulum-barrier system.

The fourth system analyzed is the percussive electromechanical system. It is composed of a cart coupled to a DC motor by the *scotch yoke* mechanism, and of an embarked hammer in the cart. In this percussive system, we opted to change the geometry of the embarked element. We do not consider anymore a pendulum. We took a particle with concentrate mass able to move in only one direction. This hammer is connected to the cart by a nonlinear spring component and by a linear damper, so that a relative motion exists between

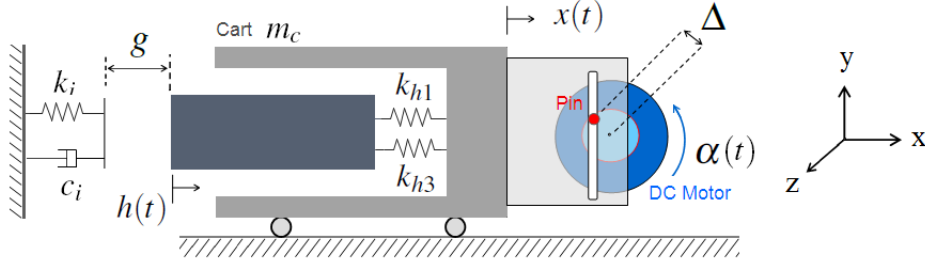


Figure 1.4: Fourth system: motor-cart-hammer coupled system.

them. A linear flexible barrier, placed outside of the cart, constrains the hammer movements, as shown in Fig. 1.4. Due to the relative movement between the hammer and the barrier, impacts can occur between these two elements. As the impacts are in an external barrier, the energy stored in the hammer motion it is transferred outside the system. The objective in this part of the Thesis is to analyze the performance of this percussive system with motion driven by a DC motor. We performed an optimization of the system with respect to design parameters in order to maximize the impact power under the constraint that the electric power consumed by the DC motor is lower than a maximum value. This optimization problem is formulated in the framework of robust design (see [81, 9]) and it is solved for different levels of uncertainties and also for the deterministic case.

## 1.4 Organization of the Thesis

The Thesis is organized as follows. In Chapter 2, we analyze the simplest electromechanical system: the motor-cart system. Then, in Chapter 3, we analyze the system that has the same elements of the first system and has a pendulum that is embarked in the cart: the motor-cart-pendulum system. In Chapter 4, we include inside the cart a flexible barrier constraining the pendulum motion. Thus we deal with an electromechanical system with internal impacts. In Chapter 5, we analyze the performance of a percussive electromechanical system. The objective is to optimize of this system with respect to some chosen design parameters in order to maximize the impact power under the constraint that the electric power consumed by the DC motor is bounded. Finally, in Chapter 6, the results are summarized and future works are discussed.

## 2

# Motor-cart system: a parametric excited nonlinear system due to electromechanical coupling

The analysis of electromechanical systems is not a new subject. The interest of analyzing their dynamic behavior is reflected by the increasing amount of research in this area (see for instance [99, 84, 41, 7, 8]). In [83] there is a chapter dedicated to the coupled problem and it is remarked that it is a problem different from parametric resonance. In [37] the whole book is dedicated to the problem but the analytical treatment supposes some small parameter, a hypothesis avoided here. Recently, the problem is been intensely studied again, see [6, 1, 4], but the literature is vast.

The mutual interaction between electrical and mechanical parts leads us to analyze a very interesting nonlinear dynamical systems [64, 24, 31, 23, 10], in which the nonlinearity comes from the coupling and varies with the coupling conditions.

In this Chapter, we analyze the dynamical behavior of a simple electromechanical system composed by a cart whose motion is driven by a DC motor. The coupling between the motor and the cart is made by a mechanism called *scotch yoke* so that the motor rotational motion is transformed into a cart horizontal motion.

## 2.1 Dynamics of the motor-cart system

### 2.1.1 Electrical system: DC motor

The mathematical modeling of DC motors is based on the Kirchhoff's law [35]. It is written as

$$l\dot{c}(t) + r c(t) + k_e\dot{\alpha}(t) = \nu , \quad (2.1)$$

$$j_m\ddot{\alpha}(t) + b_m\dot{\alpha}(t) - k_e c(t) = -\tau(t) , \quad (2.2)$$

where  $t$  is the time,  $\nu$  is the source voltage,  $c$  is the electric current,  $\dot{\alpha}$  is the angular speed of the motor,  $l$  is the electric inductance,  $j_m$  is the inertia moment of the motor,  $b_m$  is the damping ratio in the transmission of the torque

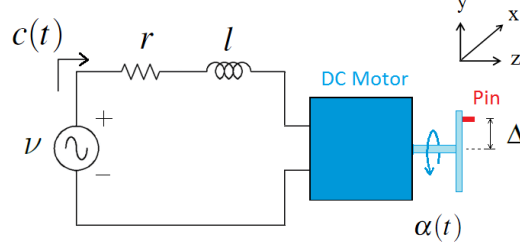


Figure 2.1: Electrical DC motor.

generated by the motor to drive the coupled mechanical system,  $k_e$  is the motor electromagnetic force constant and  $r$  is the electrical resistance. Figure 2.1 shows a sketch of the DC motor. The available torque delivered to the coupled mechanical system is represented by  $\tau$ , that is the component of the torque vector  $\boldsymbol{\tau}$  in the  $z$ -direction shown in Fig. 2.1. Some relevant situations when we analyze electrical motors are described as following:

- Assuming that  $\tau$  and  $\nu$  are constant in time, the motor achieves a steady state in which the electric current and the angular speed become constant in time. By Eqs. (2.1) and (2.2), the angular speed of the motor shaft and the current in steady state, respectively  $\dot{\alpha}_{steady}$  and  $c_{steady}$ , are written as

$$\dot{\alpha}_{steady} = \frac{-\tau r + k_e \nu}{b_m r + k_e^2} \quad , \quad c_{steady} = \frac{\nu}{r} - \frac{k_e}{r} \left( \frac{-\tau r + k_e \nu}{b_m r + k_e^2} \right) . \quad (2.3)$$

- When  $\tau$  is not constant in time, the angular speed of the motor shaft and the current do not reach a constant value. This kind of situation happens when, for example, a mechanical system is coupled to a motor. In this case,  $\dot{\alpha}$  and  $c$  vary in time in a way that the dynamics of the motor will be influenced by the coupled mechanical system. When there is no load applied in the motor (i.e.  $\tau(t) = 0, \forall t \in \mathbb{R}^{\geq 0}$ ) and the source voltage is constant in time, the motor achieves its maximum angular speed that is called the *no load speed*. It is calculated by

$$\dot{\alpha}_{no \text{ load}} = \frac{k_e \nu}{b_m r + k_e^2} \quad , \quad c_{no \text{ load}} = \frac{b_m}{k_e} \left( \frac{k_e \nu}{b_m r + k_e^2} \right) . \quad (2.4)$$

- The motor delivers the maximum torque, when the load applied in the motor is such that the motor does not move at all. This is called the *stall torque*. If the source voltage is constant in time, it is calculated by

$$\tau_{stall} = \frac{k_e \nu}{r} . \quad (2.5)$$

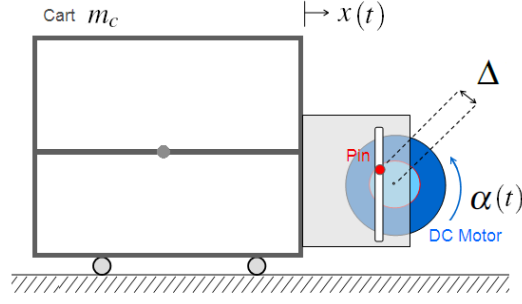


Figure 2.2: Coupled cart-motor system.

### 2.1.2 Cart-motor system: a master-slave relation

As described in the introduction, the system is composed by a cart whose motion is driven by the DC motor. The motor is coupled to the cart through a pin that slides into a slot machined in an acrylic plate that is attached to the cart, as shown in Fig. 2.2. The off-center pin is fixed on the disc at distance  $\Delta$  of the motor shaft, so that the motor rotational motion is transformed into a cart horizontal movement. It is noticed that with this configuration, the center of mass of the mechanical system is always located in the center of mass of the cart, so its position does not change. To model the coupling between the motor and the mechanical system, the motor shaft is assumed to be rigid. Thus, the available torque vector to the coupled mechanical system,  $\boldsymbol{\tau}$ , can be written as

$$\boldsymbol{\tau}(t) = \boldsymbol{\Delta}(t) \times \mathbf{f}(t), \quad (2.6)$$

where  $\boldsymbol{\Delta} = (\Delta \cos \alpha(t), \Delta \sin \alpha(t), 0)$  is the vector related to the eccentricity of the pin, and where  $\mathbf{f}$  is the coupling force between the DC motor and the cart. Assuming that there is no friction between the pin and the slot, the vector  $\mathbf{f}$  only has a horizontal component,  $f$  (the horizontal force that the DC motor exerts in the cart). The available torque  $\tau$  is written as

$$\tau(t) = -f(t) \Delta \sin \alpha(t). \quad (2.7)$$

Due to constraints, the cart is not allowed to move in the vertical direction. The mass of the mechanical system,  $m$ , is equal the cart mass,  $m_c$ , and the horizontal cart displacement is represented by  $x$ . Since the cart is modeled as a particle, it satisfies the equation

$$m \ddot{x}(t) = f(t). \quad (2.8)$$

Due to the system geometry,  $x(t)$  and  $\alpha(t)$  are related by the following constraint

$$x(t) = \Delta \cos(\alpha(t)). \quad (2.9)$$

Substituting Eqs. (2.7) to (2.9) into Eqs. (2.1) and (2.2), we obtain the initial value problem for the motor-cart system that is written as follows. Given a constant source voltage  $\nu$ , find  $(\alpha, c)$  such that, for all  $t > 0$ ,

$$l \dot{c}(t) + r c(t) + k_e \dot{\alpha}(t) = \nu , \quad (2.10)$$

$$\ddot{\alpha}(t) [j_m + m\Delta^2(\sin \alpha(t))^2] + \dot{\alpha} [b_m + m\Delta^2\dot{\alpha}(t) \cos \alpha(t) \sin \alpha(t)] - k_e c(t) = 0 , \quad (2.11)$$

with the initial conditions,

$$\dot{\alpha}(0) = 0 \quad , \quad \alpha(0) = 0 \quad , \quad c(0) = \frac{\nu}{r} . \quad (2.12)$$

Comparing Eq. (2.11) with Eq. (2.2), it is seen that the mechanical system influences the motor in a parametric way, [40, 65, 93, 62, 71]. The coupling torque,  $\tau$ , that appears in the right side of Eq. (2.2), appears now as a time variation of the system parameters.

## 2.2 Dimensionless cart-motor system

In this section, the initial value problem to the motor-cart system is presented in a dimensionless form. The development of this form is a strategy to determine the dimensionless parameters of the system, which were useful in the prove of existence and asymptotic stability of a periodic orbit to this electromechanical system, discussed in Section 2.4. Beside this, the dimensionless equations were very useful for simulations, since it reduced significantly the computation time.

Consider the system of (2.10) to (2.11). Taking  $\dot{\alpha}(t) = u(t)$ , the system can be written as a first-order system, thus one gets that

$$\begin{aligned} \dot{c}(t) &= -\frac{k_e u(t) + r c(t) - \nu}{l}, \\ \dot{\alpha}(t) &= u(t), \\ \dot{u}(t) &= \frac{-\left(-c(t) k_t + \Delta^2 m u(t)^2 \cos(\alpha(t)) \sin(\alpha(t)) + b_m u(t)\right)}{\left(\Delta^2 m \sin^2(\alpha(t)) + j_m\right)}. \end{aligned} \quad (2.13)$$

Writing

$$t = \frac{l}{r}s, \quad \alpha\left(\frac{ls}{r}\right) = p(s), \quad u\left(\frac{ls}{r}\right) = \frac{r q(s)}{l}, \quad c\left(\frac{ls}{r}\right) = \frac{k_e w(s)}{l} \quad (2.14)$$

one gets that  $s$  is dimensionless parameter. The functions  $p(s)$ ,  $q(s)$  and  $w(s)$  are dimensionless functions. Substituting (2.14) into (2.13) one obtains

$$\begin{aligned}
 w'(s) &= -w(s) - q(s) + v_0 \\
 p'(s) &= q(s), \\
 q'(s) &= \frac{-\left(v_1 q(s)^2 \cos(p(s)) \sin(p(s)) - v_2 w(s) + v_3 q(s)\right)}{\left(v_1 \sin^2(p(s)) + 1\right)}
 \end{aligned} \tag{2.15}$$

where ' denotes the derivative with respect to  $s$  and  $v_i, i = 0, \dots, 3$ , are dimensionless parameters given by

$$v_0 = \frac{\nu l}{k_e r}, \quad v_1 = \frac{\Delta^2 m}{j_m}, \quad v_2 = \frac{k_e l k_t}{j_m r^2}, \quad v_3 = \frac{b_m l}{j_m r}. \tag{2.16}$$

The strategy to obtain the dimensionless form of the initial value problem to the motor-cart system, was writing the time  $t$  as function of the dimensionless parameter  $s$  and as function of motor parameters (the inductance,  $l$ , and resistance,  $r$ ). Thus, the new dimensionless time  $s$  appeared as a parameter that is independent of the parameters of the mechanical part of the system. Due to this independence, this strategy of writing  $t$  as function of  $s, l$ , and  $r$  could be applied to the others electromechanical systems analyzed in this Thesis. We used the same dimensionless parameter  $s$  to obtain their dimensionless initial value problems.

### 2.3 Numerical simulations of the dynamics of the motor-cart system

Looking at Eqs. (2.10) to (2.12), it can be observed that if the nominal eccentricity of the pin,  $\Delta$ , is small, the initial value problem of the motor-cart system tends to the linear system equations of the DC motor, Eq. (2.1) and (2.2), in case of no load. But as the eccentricity grows, the non-linearities become more pronounced. The nonlinearity also increases with the attached mass,  $m$ . To understand the influence of  $\Delta$  and  $m$  in the dynamic behavior of the motor-cart system, a parametric excited system, simulations with different values to these system parameters were performed. The objective was to observe the graphs of the system variables, as the motor current over time, angular displacement of the motor shaft and coupling force. For computation, the initial value problem defined by Eqs. (2.10) to (2.12) has been rewritten in the dimensionless form given by Eqs. (2.15) to (2.16). Despite of using the dimensionless initial value problem for numerical simulations, the results are presented in the dimensional form because we believe that in this way they have an easier physical interpretation. The duration chosen is 2.0 s. The 4th-order Runge-Kutta method is used for the time-integration scheme with a time-

step equal to  $10^{-4}$ . The motor parameters used in all simulations are listed in Table 2.1. The source voltage is assumed to be constant in time and equal to 2.4 V. To observe the influence of the eccentricity of the pin in the behavior

Parameter	Value
$l$	$1.880 \times 10^{-4}$ H
$j_m$	$1.210 \times 10^{-4}$ kg m <sup>2</sup>
$b_m$	$1.545 \times 10^{-4}$ Nm/(rad/s)
$r$	0.307 $\Omega$
$k_e$	$5.330 \times 10^{-2}$ V/(rad/s)

Table 2.1: Values of the motor parameters used in simulations.

of the system, the mass was fixed to 5 kg and the results of simulations with two values of  $\Delta$  were compared. The selected values are  $\Delta = 0.001$  m and  $\Delta = 0.01$  m. For  $\Delta = 0.001$  m, Figs. 2.3(a) and 2.3(b) displays  $\dot{\alpha}$  as function of time and the Fast Fourier Transform (FFT) of the cart displacement,  $\hat{x}$ . It can be noted that the angular speed of the motor shaft oscillates with a small amplitude around 7 Hz and the FFT graph of  $x$  presents only one peak at this frequency. In contrast to this, when  $\Delta$  is bigger, as  $\Delta = 0.01$  m, observing Figs. 2.4(a) and 2.4(b), it is verified that the amplitude of the oscillations of  $\dot{\alpha}$  grows and, due to the non-linearity effects, the FFT graph of  $x$  presents more than one peak. The first of them is at 6.56 Hz and the others are at odd multiples of this value, characterizing a periodic function.

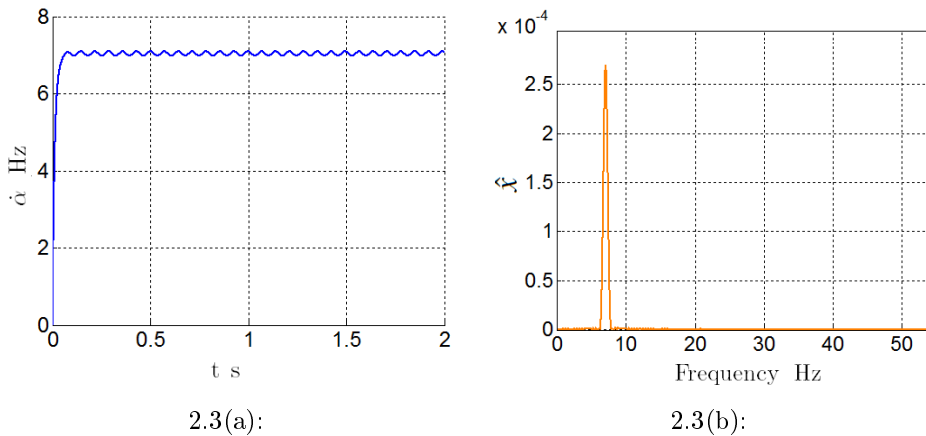


Figure 2.3: Motor-cart system with  $\Delta = 0.001$  m: (a) angular speed of the motor shaft over time and (b) Fast Fourier Transform of the cart displacement.

As said in the introduction of this Thesis, normally problems of coupled systems are modeled as uncoupled saying that the force is imposed, and it is harmonic with frequency given by the nominal frequency of the motor. The dynamic of the motor is not considered. The graphs of Fig. 2.3(a) and 2.4(a) confirm that this hypothesis does not correspond to reality. As  $\Delta$  increases,

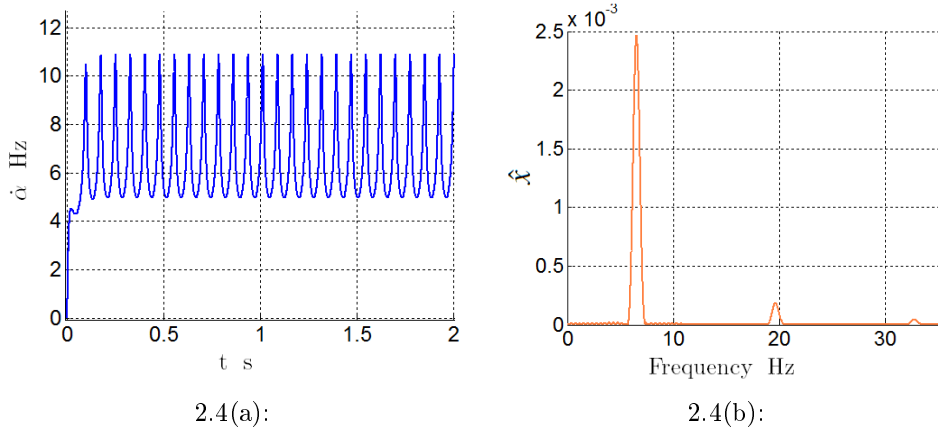


Figure 2.4: Motor-cart system with  $\Delta = 0.01$  m: (a) angular speed of the motor shaft over time and (b) Fast Fourier Transform of the cart displacement.

increases the nonlinearity of the problem, and the hypothesis of harmonic force is inadequate since it falsifies the dynamics. Even when  $\Delta$  is small, the angular speed of the motor shaft does not reach a constant value. After a transient it achieves a periodic state. It oscillates around a mean value and these oscillations are periodic. To enrich the analysis in the frequency domain, the Fast Fourier Transform of the current over time,  $\hat{c}$ , was computed for the two values of  $\Delta$ . The results are shown in Fig. 2.5(a) and 2.5(b). It can be observed that in both cases, the FFT graph of  $\hat{c}$  presents a peak at a frequency that is twice the peak frequency of the FFT  $\hat{x}$  indicating the parametric excitation, [40]. In the following analysis of the motor-cart system, the nominal eccentricity

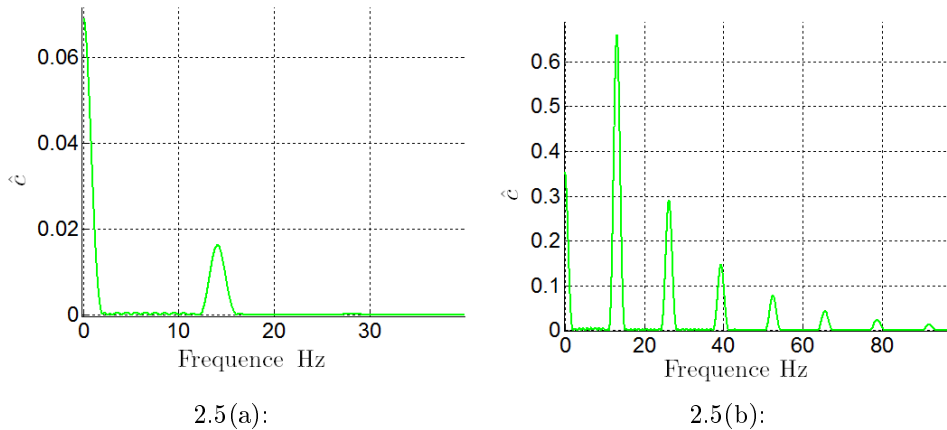


Figure 2.5: Motor-cart system: Fast Fourier Transform of the current (a) when  $\Delta = 0.001$  m and (b) when  $\Delta = 0.01$  m.

of the pin was consider to be 0.01 m. This value was selected to highlight the non-linearity effects. The results obtained to the cart displacement and current in motor over time are observed in Fig. 2.6(a) and Fig. 2.6(b). The behavior found for the current over time is similar to the behavior found for

the angular speed of the motor shaft, Fig. 2.4(a). It achieves a periodic state after a transient phase. Other graphs to be analyzed are the  $f(t)$  and  $\tau(t)$

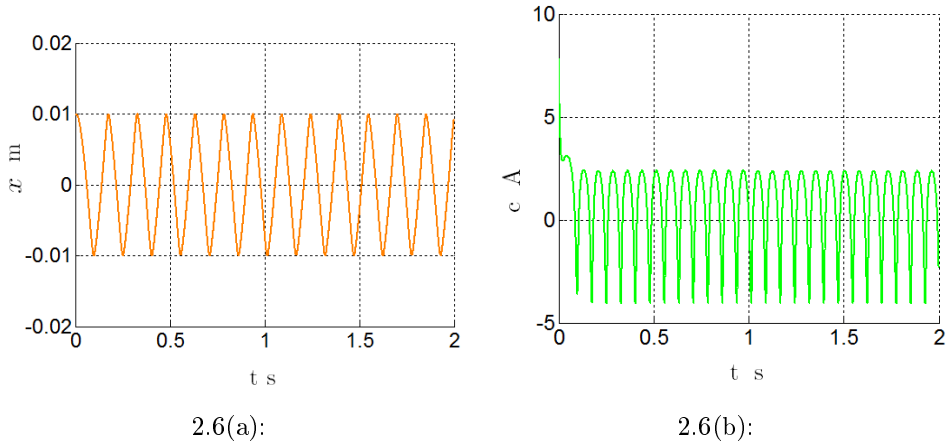


Figure 2.6: Motor-cart system with  $\Delta = 0.01$  m: (a) cart displacement and (b) motor current over time.

variation during one cart movement cycle in the periodic state, *phase portraits* of the system, as it is shown in Figs. 2.7(a) and 2.7(b). Observing the  $f$  graph, we see that the coupling force is not harmonic. Remembering the constrain  $x(t) = \Delta \cos \alpha(t)$ , it is verified that the horizontal force presents its maximum value when  $x(t) = -\Delta$  and its minimum value when  $x(t) = \Delta$ . Besides this, the coupling force changes its sign twice. Observing the  $\tau$  graph, it is verified that the torque presents four points of sign change. Two of them occur when  $x(t) = -\Delta$  and  $x(t) = \Delta$ , corresponding respectively to  $\alpha$  multiple of  $\pi$  and  $\alpha$  multiple of  $2\pi$ . This changes were expected from Eq. (2.7). The others two changes occur exactly in the same cart positions that we have the sign of  $f$  changing. In each cart movement cycle, the horizontal force  $f$  and the torque  $\tau$  follow once the paths shown in Fig. 2.7(a) and 2.7(b). Figures 2.8(a) and

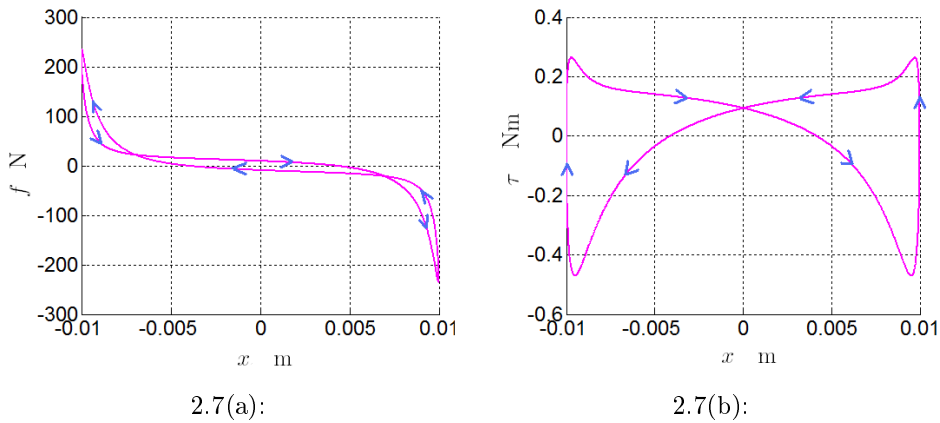


Figure 2.7: Motor-cart system with  $\Delta = 0.01$  m: (a) horizontal force  $f$  and (b) torque  $\tau$  during one cycle of the cart movement.

2.8(b) show the *phase portraits* graphs of the current variation during one cart movement cycle and the torque variation in function of the current. In the left graph, it is noted that the current presents four points of sign change in each cart movement cycle. Observing the right graph, it is verified that the current follows two times the path shown in Fig. 2.8(b). Thus, there is a relation 2:1 between the period of rotation of the disk (part of the electromechanical system) and the period of the current in the DC motor. This relation 2:1 between periods is a common phenomenon of parametric excited systems. Others phase portrait graphs are shown in Figs. 2.9(a), 2.9(b), 2.10(a) and

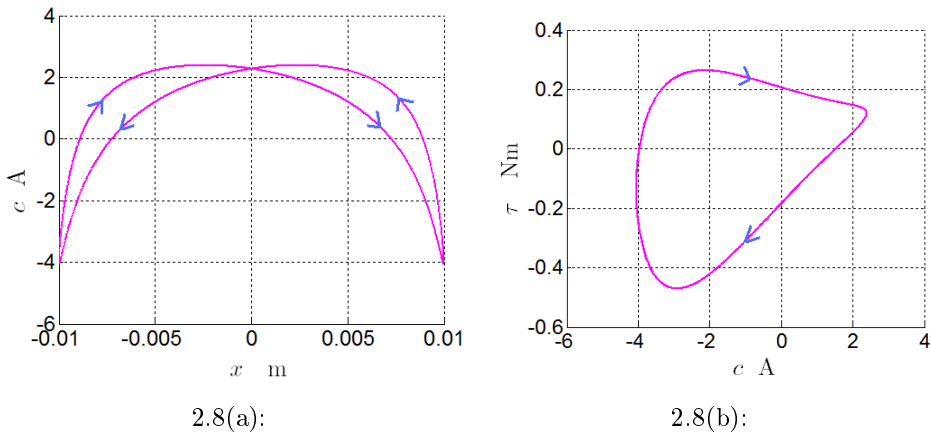


Figure 2.8: Motor-cart system with  $\Delta = 0.01$  m: (a) current variation during one cart movement cycle and (b) torque variation as function of the current.

2.10(b).

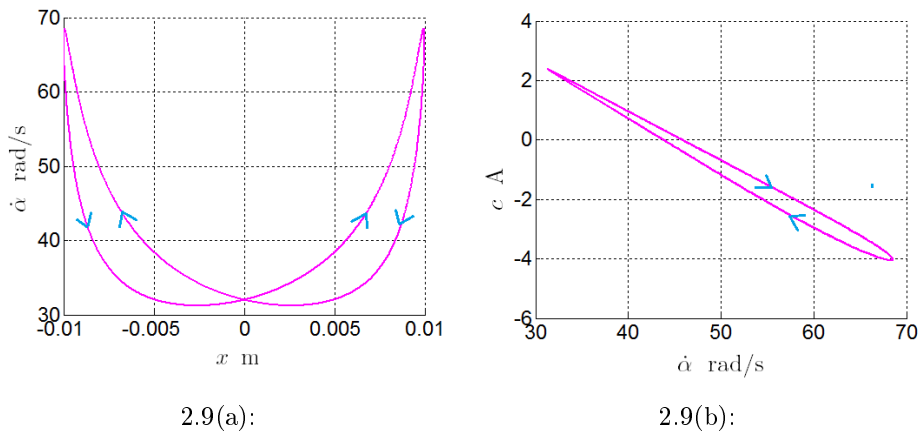


Figure 2.9: Motor-cart system with  $\Delta = 0.01$  m: (a) angular velocity of the motor shaft during one cart movement cycle and (b) current variation as function of the angular velocity of the motor shaft.

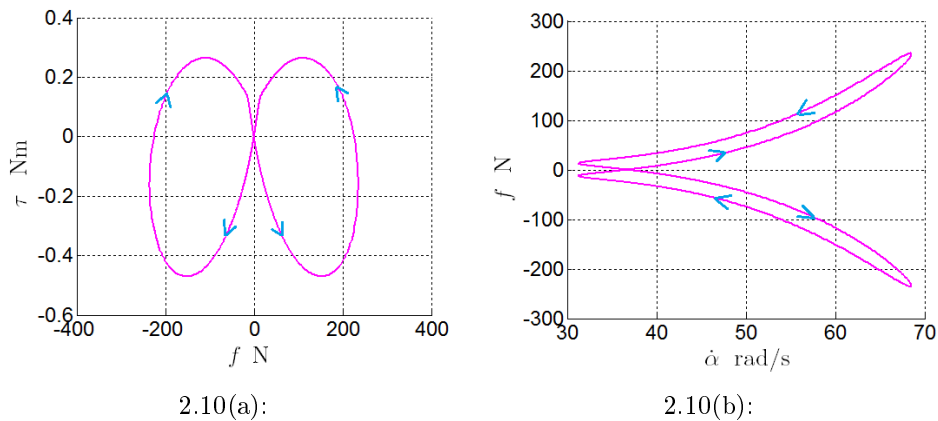


Figure 2.10: Motor-cart system  $\Delta = 0.01$  m: (a) torque variation as function of the horizontal force  $f$  and (b) horizontal force variation as function of the angular velocity of the motor shaft.

## 2.4 Asymptotically stable periodic orbit

Due to the coupling mechanism, the coupling torque,  $\tau$ , varies in time. Thus, the angular speed of the motor shaft and the current are not constant values after the transient. To compare the response of the coupled systems for different values of  $\Delta$  and  $m$ , the duration of one cart movement cycle,  $T_p$ , were computed in the periodic state. Figures 2.11(a) and 2.11(b) show the graphs of the computed periods as function of  $\Delta$  and  $m$ . In both graphs it is observed that, the bigger  $\Delta$ , or  $m$ , is, the bigger is the period of the cart movement cycle in the periodic state. It is noted too that this increment is more pronounced in relation to  $\Delta$ . This result guided the development of

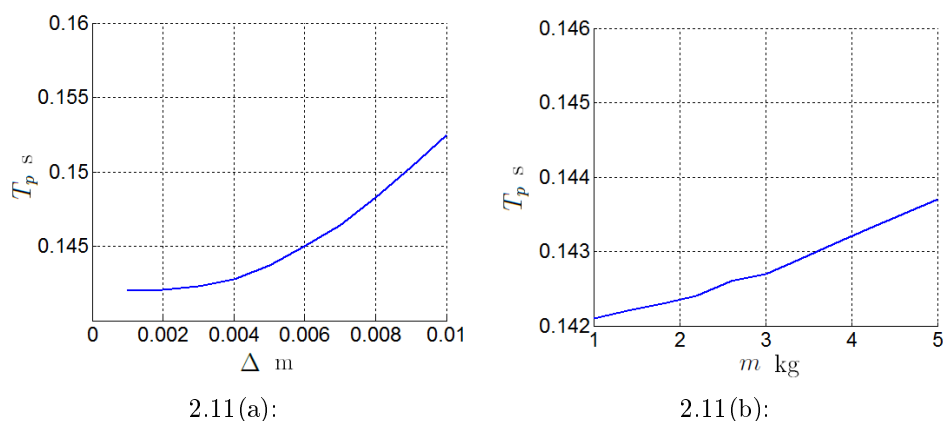


Figure 2.11: Motor-cart system: period of one cart movement cycle (a) as function of  $\Delta$  with  $m = 5.0$  kg and (b) as function of  $m$  with  $\Delta = 0.005$  m.

the paper [18], in which a similar electromechanical motor-cart system was analyzed and the existence and asymptotic stability of a periodic orbit to this system were obtained in a mathematically rigorous way. To prove the

existence and asymptotic stability of periodic orbits, the authors of [18] used the dimensionless initial value problem given by Eq. (2.15) and, assumed the following Ansatz

$$q(s) = \omega_0 + \epsilon z(s), \quad (2.17)$$

$$w(s) = k_1 + \epsilon w_1(s) \quad (2.18)$$

where

$$k_1 = \frac{v_0 v_3}{v_3 + v_2}, \quad \omega_0 = \frac{v_0 v_2}{v_3 + v_2}, \quad (2.19)$$

and  $v_1 = \epsilon$ . Substituting the expressions of  $v_0$ ,  $v_2$  and,  $v_3$  given in Eq. (2.16), one obtains that

$$k_1 = \frac{l k_e \nu}{r(b_m r + k_e^2)} = \frac{l}{r} \dot{\alpha}_{\text{no load}}, \quad \omega_0 = \frac{b_m \nu l}{k_e(b_m r + k_e^2)} = \frac{l}{k_e} c_{\text{no load}}. \quad (2.20)$$

From a mechanical point of view, Eq. (2.17) means that the disk, that is a part of the mechanical system modeled by Eqs. (2.10) and (2.11), will rotate at an angular speed near  $\omega_0$  (which is the velocity  $\dot{\alpha}_{\text{no load}}$  in a dimensionless form) and (2.18) means that electrical current will oscillate near  $k_1$  (which is current  $c_{\text{no load}}$  in a dimensionless form).

After a mathematical proof of existence and asymptotic stability of periodic orbits, the authors of [18] obtained the following expression to the period  $T_p$  of the system

$$T_p(\epsilon) = \frac{\pi}{\omega_0} + \frac{\pi \omega_0 (v_2 + (4\omega_0^2 + 1) v_3) \epsilon^2}{4 E_1} + O(\epsilon^3). \quad (2.21)$$

where  $v_2$  and  $v_3$  are given in Eq. (2.16), and

$$E_1 = 2 (v_3 + v_2) Q_1 \quad (2.22)$$

$$Q_1 = (4\omega_0^2 + 1) v_3^2 + 2 v_2 v_3 + v_2^2 - 8\omega_0^2 v_2 + 16\omega_0^4 + 4\omega_0^2. \quad (2.23)$$

Observing this expression, one concludes that the nonlinear effects on the period are significant at second order of that expansion. Beside this, using the expressions given in Eq. (2.16), it is verified that the period grows proportionally to  $m^2 \Delta^4$ , and so the growing of the period is faster in relation to  $\Delta$  than to  $m$ . These results are compatible with the numerical findings shown in Figs. 2.11(a) and 2.11(b). Another interesting consequence is the following one: from Eqs. (2.17) and (2.8) it follows that the period of rotation of the disk, in the electromechanical system, is given by  $\frac{2\pi}{\omega_0} + O(\epsilon)$ . So, it follows from Eq. (2.21) that there is a 2:1 relation between the period of the disk and the current. Those results are compatible with the numerical findings shown previously in Figs. 2.8(b) and 2.9(b). To analyze the domain of validity

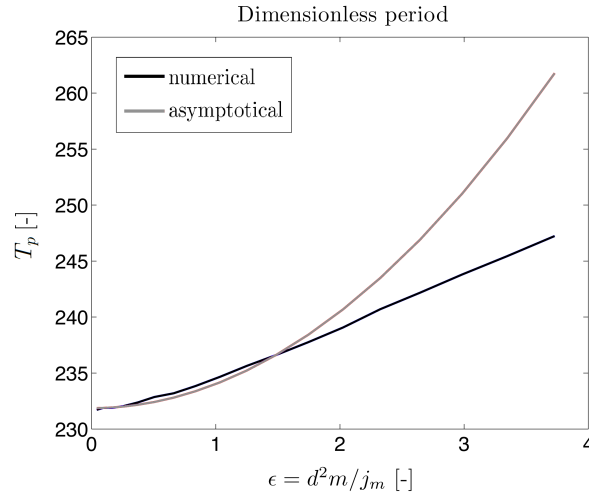


Figure 2.12: Comparison between numerical findings and the asymptotic approximation.

of the approximation of expression to the period  $T_p$ , approximations to the period were computed to different values of  $\epsilon$  considering just the first and second orders terms of the Eq. (2.21). The obtained approximations were compared with the values of period obtained from numerical simulations. The results displayed in Fig. 2.12 shows that domain of validity of the approximation considering only the first and second orders terms is rather large, a fact that is not evident from perturbation theory. The paper [18] treats the problem of electromechanical coupling by a mathematical approach. As no other references dealing with this kind of approach to electromechanical systems were found, we believe that [18] is a first work on the topic. Some others articles have been written in this way, as [20, 19, 17, 16]. Among the several routes for research coming from this mathematical approach, some have been studied. The objective is to prove the existence and asymptotic stability for electromechanical systems in which

- a capacitor is included in the circuit sketched in Fig. 2.1. This leads to a system with four degrees of freedom and the possibility of resonances. The guessing is that if the techniques used here can be useful for this problem.
- the cart is fixed to a wall by a linear spring and damper, as shown in Fig. 2.13. Beside this, the motor has a time-dependent voltage source given by  $\nu_t(t) = \nu + \chi \sin(\omega_1 t)$ . Without the spring, the system is driven by the constraint and the dynamics is a sort of master-slave relation, a very simple one. With the inclusion of the spring, the dynamics changes completely, now the constraints cannot always impose the dynamics and

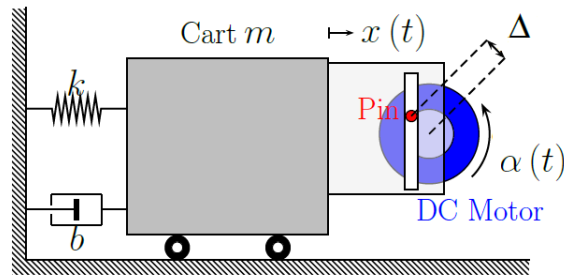


Figure 2.13: Coupled cart-motor-spring-damper system.

it is richer. The techniques used in [18] do not work any more and new techniques to show existence and stability have to be used. If the spring has a high rigidity it does not let the motor to drive the cart all the way to the end of the track and the cart oscillates around a position that depends on the rigidity of the spring and the voltage that drives the system. Some of the results already obtained for this problem are published [21].

## 2.5 Summary of the Chapter

The developed models revealed that the electromechanical motor-cart system is parametric excited, in which the coupling torque appears as a time variation of the system parameters. Simulations of these systems were performed for different values of  $\Delta$  and  $m$  and the results of these numerical simulations, as the graphs the systems variables over time, graphs of the FFT of systems variables and *phase portraits* graphs were analyzed. From these graphs, a typical phenomenon of parametric excited systems was observed: the existence of a periodic solution with a relation 2:1 between the period of rotation of the disk and the period of the current. This result is compatible with earlier numerical findings in [42] and guided us in the development of [18], in which the existence and asymptotic stability of a periodic orbit to an electromechanical system are obtained in a mathematically rigorous way. Besides this, the nominal eccentricity of the pin of the motor, was characterized as a parameter that controls the nonlinearities of the equations of motion of the system.

### 3

## Motor-cart-pendulum system: introduction of a mechanical energy reservoir

The second electromechanical system analyzed in this Thesis has the same elements of the first system and a pendulum that is embarked into the cart, as shown in Fig. 3.1. Its suspension point is fixed in the cart, hence moves with it. The main point here is that the pendulum can have a relative motion with respect to the cart.

### 3.1 Dynamics of the motor-cart-pendulum system

The pendulum is modeled as a mathematical pendulum (bar without mass and particle of mass  $m_p$  at the end). Its length is noted as  $l_p$  and the pendulum angular displacement as  $\theta$ . The equations of the cart-pendulum were obtained with the Lagrange principle. They are

$$m_p l_p^2 \ddot{\theta}(t) + m_p l_p \ddot{x}(t) \cos \theta(t) + m_p g_a l_p \sin \theta(t) = 0 , \quad (3.1)$$

$$(m_p + m_c) \ddot{x}(t) + m_p l_p \ddot{\theta}(t) \cos \theta(t) - m_p l_p \dot{\theta}^2(t) \sin \theta(t) = f(t) , \quad (3.2)$$

where, again,  $f$  represents the horizontal coupling force between the DC motor and the cart,  $g_a$  is the acceleration of gravity, and the horizontal cart displacement is  $x$ . The mass of the mechanical system,  $m$ , is equal the cart mass plus the pendulum mass,  $m_c + m_p$ . The relative motion of the embarked pendulum causes a variation in the position of the center of mass of the mechanical system. As in the first coupled system, the cart is not allowed to move in the vertical direction. Due to the problem geometry,  $x(t)$  and  $\alpha(t)$

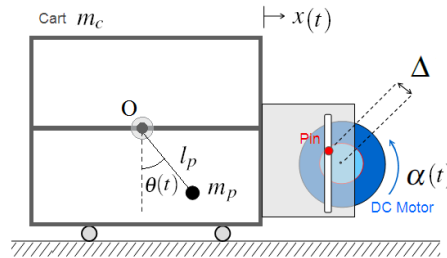


Figure 3.1: Cart-motor-pendulum system.

are related by Eq. (2.9). Once again, it is assumed that the motor shaft is rigid and that there is no friction between the pin and the slot. Thus, the available torque to the coupled mechanical system,  $\tau$ , is written as Eq. (2.6). Substituting the Eq. (2.7), (2.9), (3.1) and (3.2) into Eqs. (2.1) and (2.2), we obtain the initial value problem for the motor-cart-pendulum system that is written as follows. Given a constant source voltage  $\nu$ , find  $(\alpha, c, \theta)$  such that, for all  $t > 0$ ,

$$l\dot{c}(t) + rc(t) + k_e\dot{\alpha}(t) = v ,$$

$$\begin{aligned} \ddot{\alpha}(t) & [j_m + (m_c + m_p)\Delta^2(\sin \alpha(t))^2] + k_e c(t) \\ & + \dot{\alpha}(t) [b_m + (m_c + m_p)\Delta^2\dot{\alpha}(t) \cos \alpha(t) \sin \alpha(t)] \\ & - \ddot{\theta}(t) [m_p l_p \cos \theta(t)\Delta \sin \alpha(t)] + \dot{\theta}(t) [m_p l_p \dot{\theta}(t) \sin \theta(t)\Delta \sin \alpha(t)] = 0 , \end{aligned}$$

$$\begin{aligned} \ddot{\theta}(t) & [m_p l_p^2] - \ddot{\alpha}(t) [m_p l_p \cos \theta(t)\Delta \sin \alpha(t)] \\ & - \dot{\alpha}(t) [m_p l_p \cos \theta(t)\Delta \cos \alpha(t)\dot{\alpha}(t)] + m_p g_a l_p \sin \theta(t) = 0 , \end{aligned} \quad (3.3)$$

with the initial conditions,

$$\dot{\alpha}(0) = 0 \quad , \quad \alpha(0) = 0 \quad , \quad \dot{\theta}(0) = 0 \quad , \quad \theta(0) = 0 \quad , \quad c(0) = \frac{\nu}{r} . \quad (3.4)$$

Observing Eq. (3.3), it is verified that the motor-pendulum system influences the cart in a parametric way.

## 3.2 Dimensionless cart-motor-pendulum system

In this section, the initial value problem to the motor-cart-pendulum system is presented in a dimensionless form. Taking  $\dot{\alpha}(t) = u(t)$  and  $\dot{\theta}(t) = n(t)$ , the system can be written as a first order system

$$\begin{aligned}
 \dot{c}(t) &= \frac{-k_e u(t) - rc(t) + \nu}{l}, \\
 \dot{u}(t) &= \left\{ -n(t)^2 m_p l_p \sin \theta(t) \Delta \sin(\alpha(t)) - u(t)^2 (m_c + m_p) \Delta^2 \cos(\alpha(t)) \sin(\alpha(t)) \right. \\
 &\quad - b_m u(t) + k_e c(t) + [\cos(\theta(t)) \Delta \sin(\alpha(t))] [u(t)^2 m_p \cos \theta(t) \Delta \cos \alpha(t) \\
 &\quad \left. - m_p g_a \sin(\theta(t))] \right\} \\
 &\quad \left\{ \frac{1}{j_m + \Delta^2 \sin(\alpha(t))^2 (m_c + m_p \sin(\theta(t))^2)} \right\}, \\
 \dot{n}(t) &= \left\{ m_p \cos(\theta(t)) \Delta \sin(\alpha(t)) [k_e c(t) - u(t)^2 (m_c + m_p) \Delta^2 \cos(\alpha(t)) \sin(\alpha(t)) \right. \\
 &\quad \left. - b_m u(t) - n(t)^2 m_p l_p \sin \theta(t) \Delta \sin(\alpha(t))] + [j_m + (m_p + m_c) \Delta^2 \sin(\alpha(t))^2] \right. \\
 &\quad \left. [-m_p g_a \sin(\theta(t)) + u(t)^2 m_p \cos \theta(t) \Delta \cos \alpha(t)] \right\} \\
 &\quad \left\{ \frac{1}{m_p l_p [j_m + \Delta^2 \sin(\alpha(t))^2 (m_c + m_p \sin(\theta(t))^2)]} \right\}.
 \end{aligned} \tag{3.5}$$

Writing

$$t = \frac{l}{r} s, \quad \alpha \left( \frac{l}{r} s \right) = \gamma(s), \quad u \left( \frac{l}{r} s \right) = \frac{r q(s)}{l}, \quad \theta \left( \frac{l}{r} s \right) = \beta(s), \tag{3.6}$$

$$n \left( \frac{l}{r} s \right) = \frac{r y(s)}{l}, \quad c \left( \frac{l}{r} s \right) = \frac{k_e w(s)}{l},$$

one gets that  $s$  is dimensionless parameter. The functions  $\gamma(s)$ ,  $q(s)$ ,  $\beta(s)$ ,  $y(s)$  and  $w(s)$  are dimensionless functions. By substituting Eq. (3.6) into Eq. (3.5) one obtains

$$\begin{aligned}
 w'(s) &= -w(s) - q(s) + v_0, \\
 q'(s) &= \left\{ -v_3 q(s) - y(s)^2 v_5 \sin(\gamma(s)) \sin(\beta(s)) - v_6 \sin(\beta(s)) \cos(\beta(s)) \sin(\gamma(s)) \right. \\
 &\quad \left. + v_2 w(s) - q(s)^2 \cos(\gamma(s)) \sin(\gamma(s)) [v_9 - v_4 \cos(\beta(s))^2] \right. \\
 &\quad \left. \left\{ \frac{1}{1 + \sin(\gamma(s))^2 [v_1 + v_4 \sin(\beta(s))^2]} \right\} \right\}
 \end{aligned} \tag{3.7}$$

$$\begin{aligned}
 y'(s) &= \left\{ -v_3 v_7 q(s) \cos(\beta(s)) \sin(\gamma(s)) + q(s)^2 v_7 \cos(\gamma(s)) \cos(\beta(s)) \right. \\
 &\quad \left. - v_4 y(s)^2 \sin(\gamma(s))^2 \sin(\beta(s)) \cos(\beta(s)) + v_2 v_7 w(s) \cos(\beta(s)) \sin(\gamma(s)) \right. \\
 &\quad \left. [1 - v_9 \sin(\gamma(s))^2] [-v_8 \sin(\beta(s))] \right\} \left\{ \frac{1}{1 + \sin(\gamma(s))^2 [v_1 + v_4 \sin(\beta(s))^2]} \right\},
 \end{aligned} \tag{3.8}$$

where ' denotes the derivative with respect to  $s$  and  $a_i$ ,  $i = 1, \dots, 16$  are dimensionless parameters given by

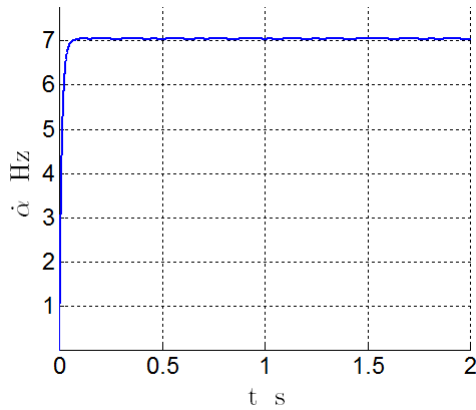
$$\begin{aligned}
 v_0 &= \frac{\nu l}{k_e r}, & v_1 &= \frac{\Delta^2 m_c}{j_m}, & v_2 &= \frac{l k_e^2}{j_m r^2}, & v_3 &= \frac{b_m l}{j_m r}, & v_4 &= \frac{\Delta^2 m_p}{j_m}, \\
 v_5 &= \frac{m_p l_p \Delta}{j_m}, & v_6 &= \frac{m_p \Delta g_a l^2}{j_m r^2}, & v_7 &= \frac{\Delta}{l_p}, & v_8 &= \frac{g_a l^2}{l_p r^2}, & v_9 &= \frac{(m_c + m_p) \Delta^2}{j_m}.
 \end{aligned}
 \tag{3.9}$$

Comparing the dimensionless parameters of the motor-cart-pendulum system with the dimensionless parameters of the motor-cart system given by Eq. 2.16, it can be observed that the parameters  $v_0$  to  $v_3$  appear in both cases and, the inclusion of the embarked pendulum introduces six news parameters:  $v_4$  to  $v_9$ .

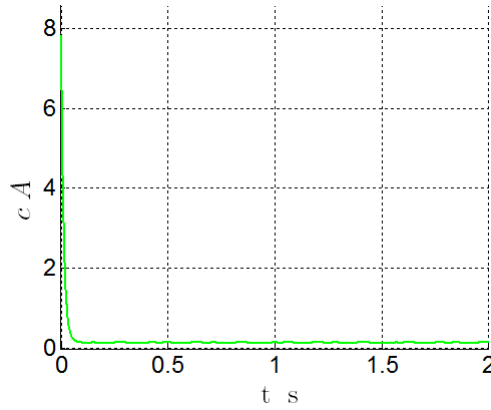
### 3.3 Numerical simulations of the dynamics of the motor-cart-pendulum system

A similar analysis to the one made to the motor-cart system, based on the results of numerical simulations, was developed for the motor-cart-pendulum system. The 4th-order Runge-Kutta method is used for the time-integration scheme with a time-step equal to  $10^{-4}$ . The motor parameters used in all simulations are listed in Table 2.1. The source voltage is assumed to be constant in time and equal to 2.4 V. Despite of using the dimensionless initial value problem for numerical simulations, the results are presented in the dimensional form because we believe that in this way they have an easier physical interpretation. Looking at the initial value problem Eqs. (3.3) to (3.4), it is observed that if the nominal eccentricity of the pin,  $\Delta$ , is small and the angle,  $\theta(t)$ , is near zero, Eq. (3.3) tends to a linear system. But as the eccentricity grows, the nonlinearities become more pronounced. To understand the influence of  $\Delta$  in the dynamic behavior of the motor-cart system, simulations with two different values to this system parameter were performed. The selected values are  $\Delta = 0.001$  m and  $\Delta = 0.01$  m. In these simulations, the cart and the pendulum masses were  $m_c = 0.0$  kg and  $m_p = 5.0$  kg, so that the total mass,  $m = m_c + m_p = 5.0$  kg, is equal to the embarked mass. Although the masses are equal, this configuration contrasts with the one of the motor-cart system used in the previous simulations. In spite of having the same masses, the pendulum has a relative motion with respect to the cart, and this makes a huge difference. The pendulum length was assumed to be 0.075 m. For  $\Delta = 0.001$  m, Figs. 3.2(a), 3.2(b), 3.3(a) and 3.3(b) show the graphs of the angular velocity of the motor shaft, current, pendulum displacement and cart displacement over time. These results reveal that when  $\Delta$  is small, the angular speed of the motor shaft oscillates over time with a very small amplitude around 7 Hz, the current also oscillates with a small amplitude around 0.13 A, and the angular displacement of pendulum is near

zero. The Fast Fourier Transform was computed to the cart and pendulum

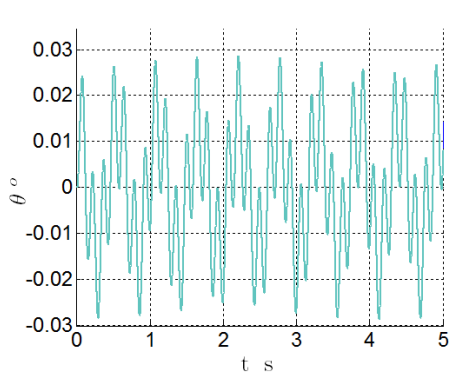


3.2(a):

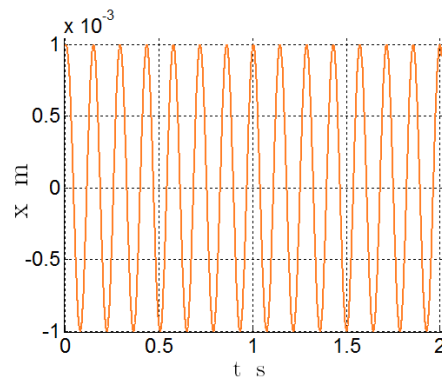


3.2(b):

Figure 3.2: Motor-cart-pendulum system with  $\Delta = 0.001$  m: (a) angular velocity of the motor shaft and (b) current over time.



3.3(a):



3.3(b):

Figure 3.3: Motor-cart-pendulum system with  $\Delta = 0.001$  m: (a) pendulum displacement and (b) cart displacement over time.

displacements and to the current for this small value of  $\Delta$ . The obtained graphs are shown in Figs. 3.4(a) and 3.4(b). The FFT graph of  $\hat{x}$ , shown in Fig. 3.4(a), presents only one peak at the frequency at 7.04 Hz. This peak was expected, since this is close to the angular speed of the motor shaft. The FFT graph of  $\hat{\theta}$  presents two peaks. One of them coincides with the  $\hat{x}$  peak and the other one is at the natural frequency of the pendulum, i.e.,  $\omega_n = \sqrt{g/l_p}/(2\pi) = 1.82$  Hz. The FFT graph of  $\hat{c}$  presents three peaks. The first one is at 5.22 Hz, the second one is at 8.86 Hz and the third one at 14.08 Hz, that is twice the peak frequency of the FFT  $\hat{x}$ . This relation 2:1 between the peak frequency of  $\hat{c}$  and  $\hat{x}$  indicates the parametric excitation. Figures 3.5(a), 3.5(b), 3.6(a) and 3.6(b) show the graphs of angular speed of the motor, current, pendulum and

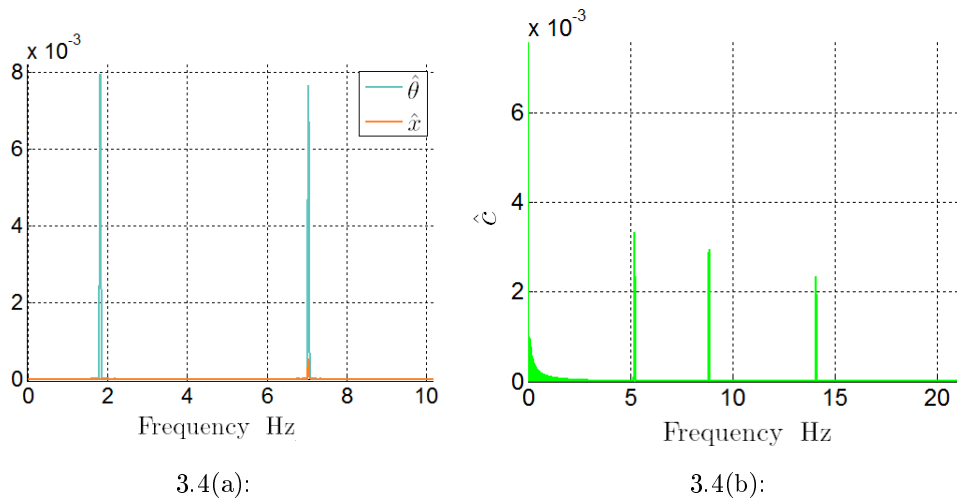


Figure 3.4: Motor-cart-pendulum system with  $\Delta = 0.001$  m: Fast Fourier Transform of (a) cart and pendulum displacements and (b) of current.

cart displacement over time when  $\Delta = 0.01$  m. Comparing these graphs with Figs. 3.2(a), 3.2(b), 3.3(a) and 3.3(b), It is verified that with a bigger  $\Delta$ , the amplitude of the oscillations of  $\dot{\alpha}$ ,  $c$ , and  $\theta$  in the steady state will be also bigger. As done to the results with small  $\Delta$ , the FFT was computed to the

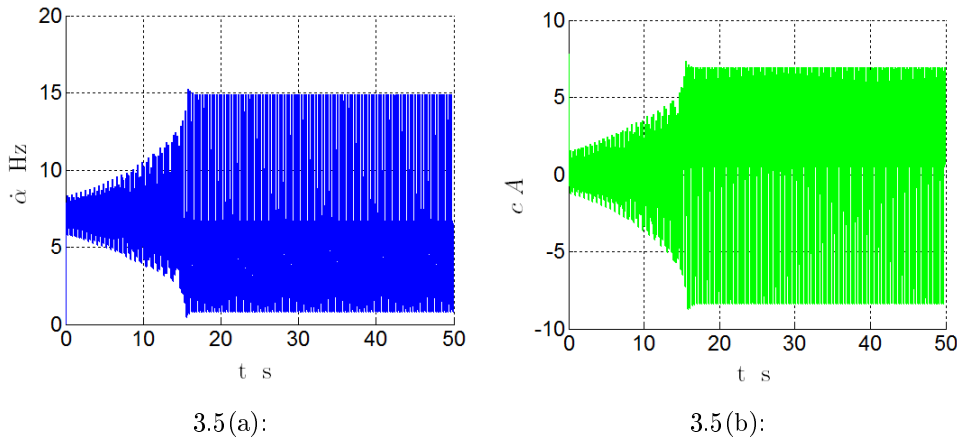
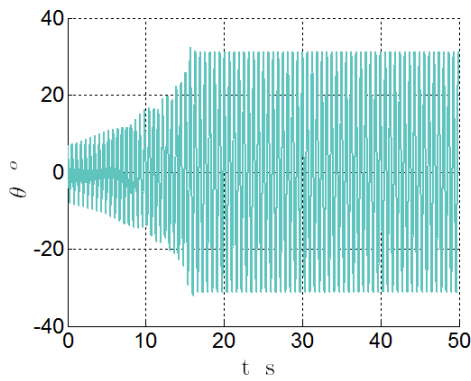
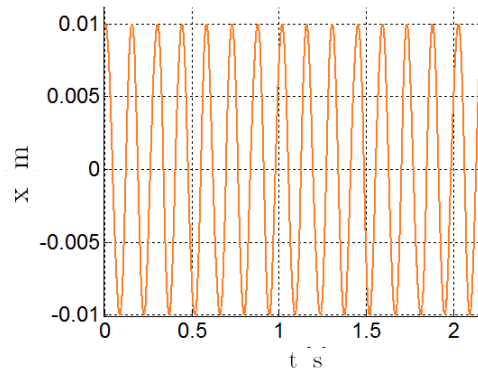


Figure 3.5: Motor-cart-pendulum system with  $\Delta = 0.01$  m: (a) angular velocity of the motor shaft and (b) current over time.

cart and pendulum displacements, angular speed of the motor shaft and to the current for the new value of  $\Delta$ . Figures 3.7(a), 3.7(b), 3.7(a), 3.7(b) display the obtained graphs. Observing Figs. 3.7(a) and 3.7(b), it can be noted that  $\hat{x}$  and  $\hat{\theta}$  present peaks at the same frequencies. The first of them is at 1.61 Hz and the following are at odd multiples of this value. Comparing  $\hat{x}$  with  $\Delta = 0.001$  m and with  $\Delta = 0.01$  m, it is verified that the peak at the natural frequency of the pendulum,  $\omega_n = 1.82$  Hz, vanished when  $\Delta$  grows. This result certifies that the system behavior is far from linear. Regarding Figs. 3.8(a) and 3.8(b),

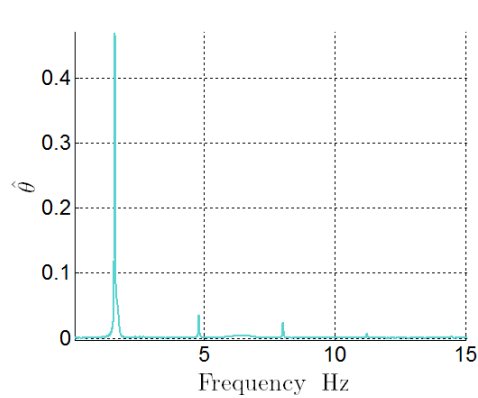


3.6(a):

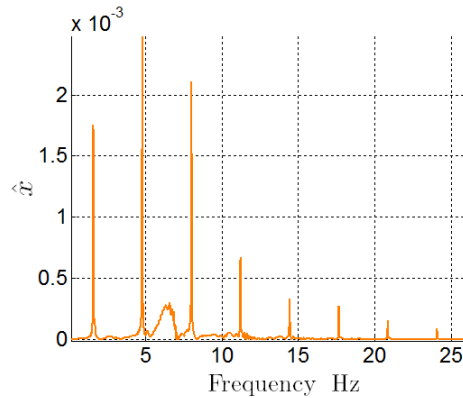


3.6(b):

Figure 3.6: Motor-cart-pendulum system with  $\Delta = 0.01$  m: (a) pendulum and (b) cart displacement over time.



3.7(a):



3.7(b):

Figure 3.7: Motor-cart-pendulum system with  $\Delta = 0.01$  m: Fast Fourier Transform of (a) pendulum and (b) cart displacements.

it can be noted that the FFT graphs of the current and of the angular speed of the motor shaft over time also present peaks at the same frequencies. The first of them is at 3.21 Hz and the following are at multiples of this value. Comparing Figs. 3.8(a) and 3.7(b), it can be verified that the frequencies in which  $\hat{c}$  presents peaks are twice the frequencies in which  $\hat{x}$  presents peaks.

### 3.4 Pumping Leads To Revolution

In Section 3.3, the cart mass was considered to be zero and the pendulum mass 5.0 kg. Next, it is presented an analysis of the behavior of this system with a different mass configuration. The cart mass is kept as 0.0 kg (a limit case) and a smaller value is selected to the pendulum mass,  $m_p = 4.0$  kg, so that the total mass,  $m_c + m_p = 4.0$  kg, is still equal to the embarked mass. Figures 3.9(a), 3.9(b), 3.10(a) and 3.10(b) show the graphs of the angular speed

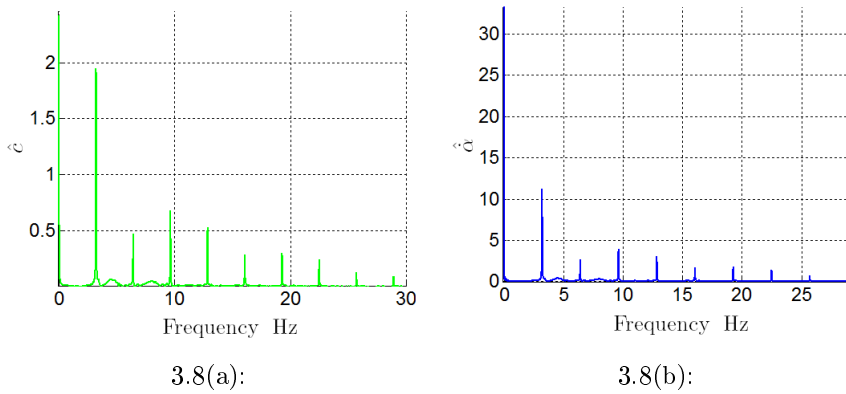


Figure 3.8: Motor-cart-pendulum system with  $\Delta = 0.01$  m: Fast Fourier Transform of (a) current and (b) angular speed of the motor shaft over time.

of the motor shaft, current and cart and pendulum displacements over time for this new mass configuration when  $\Delta = 0.01$  m. Regarding these graphs, it can be observed that after the transient state, the dynamics achieves a periodic state, in which  $\dot{\alpha}$  takes negatives values. With this new mass configuration, the mechanical system pumps energy from the motor and the amplitude of the pendulum grows reaching a point where the mechanical system starts to drive the motion, [30, 29, 12]. This is seen observing that  $\dot{\alpha}$  takes negative values, indicating that the motor shaft sometimes changes its motion direction. When the angular speed of the motor shaft is positive, it is considered that the motor drives the cart motion, the cart is driven. But when it is negative, the motor loses the control over the cart and drives it no more, it is now driven by the mechanical system. In these situations, it will be said that the relation master-slave is reversed. To understand the sign changing of the angular speed

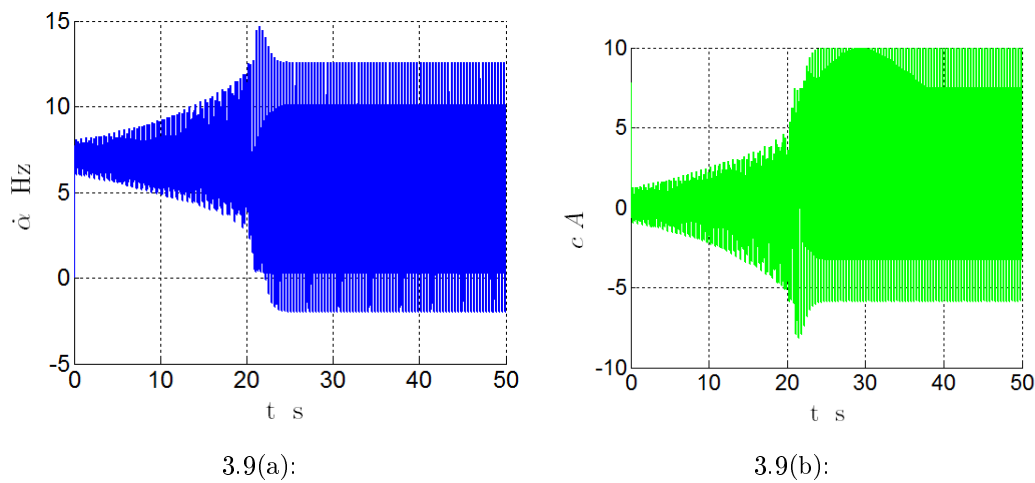


Figure 3.9: Motor-cart-pendulum system with  $\Delta = 0.01$  m: (a) angular velocity of the motor shaft and (b) current over time.

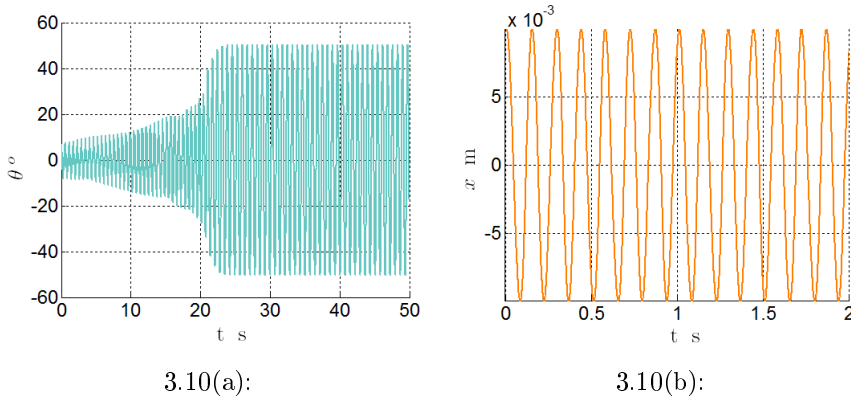


Figure 3.10: Motor-cart-pendulum system with  $\Delta = 0.01$  m: (a) pendulum and (b) cart displacement over time.

of the motor shaft, some phase portrait graphs were plotted. Figures 3.11(a) and 3.11(b) show the  $\ddot{\alpha}$  graph as function of  $\dot{\alpha}$  and the  $\dot{\alpha}$  graph as function of  $x$  during one movement cycle. It is verified that when  $\dot{\alpha}(t)$  turns negative, the motor shaft has a negative acceleration. After a short period of time, its acceleration becomes positive and brakes the motor shaft motion. This causes other sign changing in  $\dot{\alpha}(t)$  and consequently, it turns positive again. Thus, the motor recovers the control over the cart motion. Looking at Fig. 3.11(b),

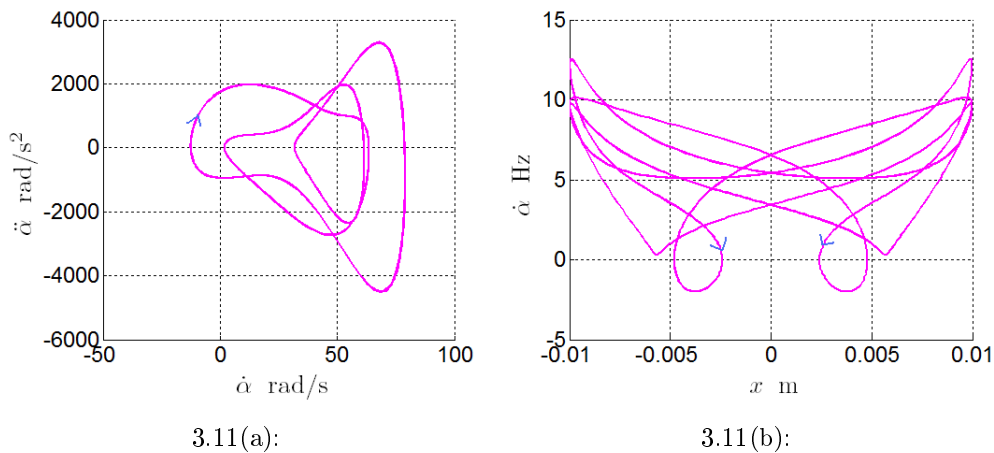
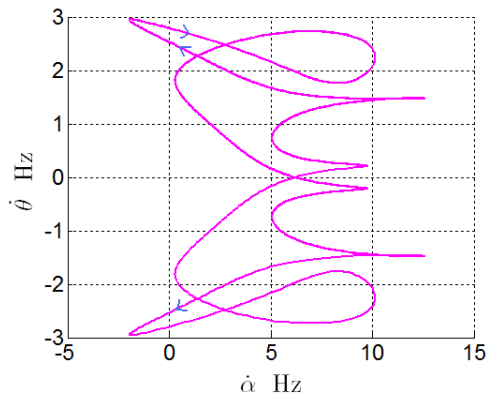
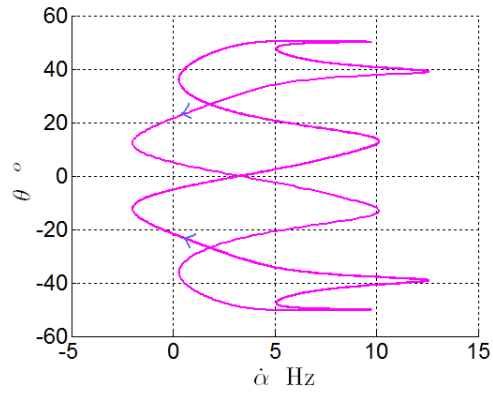


Figure 3.11: Motor-cart-pendulum system with  $\Delta = 0.01$  m: portrait graphs of (a)  $\ddot{\alpha}$  graph as function of  $\dot{\alpha}$  and (b)  $\dot{\alpha}$  graph as function of  $x$ .

it is noted that this reversion in the relation master-slave occurs two times in each movement cycle. The position and angular speed of the pendulum, at the moment of the reversion, can be observed by the graphs of  $\dot{\theta}$  as function of  $\dot{\alpha}$  and  $\theta$  in function of  $\dot{\alpha}$ , shown in Figs. 3.12(a) and 3.12(b). It is verified that when the the motor loses the control over the cart by the sign changing of  $\dot{\alpha}$ , the pendulum angle is around  $21.6^\circ$  or around  $-21.6^\circ$ . When the motor recovers the control, the pendulum angle is around  $6.0^\circ$  or around  $-6.0^\circ$ . It



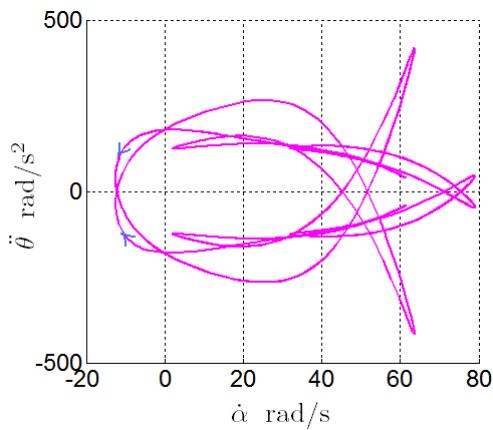
3.12(a):



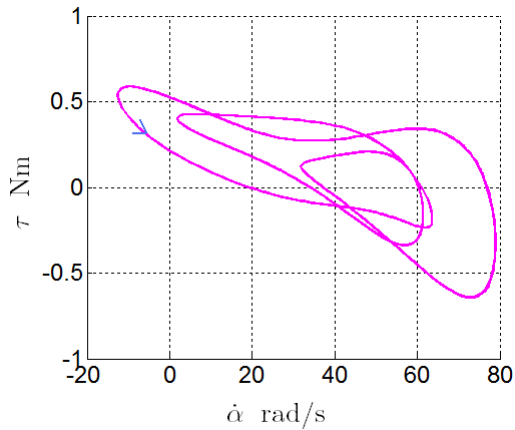
3.12(b):

Figure 3.12: Motor-cart-pendulum system with  $\Delta = 0.01$  m: portrait graphs of (a)  $\dot{\theta}$  graph as function of  $\ddot{\alpha}$  and (b)  $\theta$  as function of  $\ddot{\alpha}$ .

is also noted that, during the period of reversion, the pendulum does not change its direction of motion in spite of its angular speed presents a change of behavior. In the beginning of the reversion the modulus of  $\dot{\theta}$  grows, but when it achieves the value 2.95 Hz, it starts to decrease. This change occurs due to the sign changing in the tangent angular acceleration of the pendulum, as can be observed in Fig. 3.13(a). The graph of the torque variation in function of the angular speed of the motor shaft shows that the maximum torque is achieved during the period of reversion.



3.13(a):



3.13(b):

Figure 3.13: Motor-cart-pendulum system with  $\Delta = 0.01$  m: portrait graphs of (a) tangent  $\ddot{\theta}$  graph as function of  $\ddot{\alpha}$  and (b)  $\tau$  as function of  $\ddot{\alpha}$ .

### 3.5 Summary of the Chapter

The influence of a embarked mass was demonstrated and it was shown the changes it causes in the solutions of the dynamic equations. The motor-cart system has no capacity to pump energy from the motor, it is a master-slave system: the motor drives the cart motion, the cart is driven. The only interesting feature is how the nonlinearity changes with  $\Delta$  and  $m$ , the mass of the cart. The motor-cart-pendulum system has a new feature, the capacity to store energy in the motion of the pendulum. With this, the mechanical system can pump energy from the motor and, in certain cases, revert the relation master-slave, that is the mechanical system can be itself the master stopping the motor and reversing its motion.

## 4

# Electromechanical system with internal impacts and uncertainties

The system analyzed in this chapter is composed by a cart whose motion is driven by a DC motor, sketched in Fig. 2.1, and a embarked pendulum into this cart. The motor is coupled to the cart through a pin that slides into a slot machined on an acrylic plate that is attached to the cart, as shown in Fig. 4.1. The off-center pin is fixed on the disc at distance  $\Delta$  of the motor shaft, so that the motor rotational motion is transformed into a cart horizontal movement. The suspension point of the pendulum is fixed in the cart, so that exists a relative motion between cart and pendulum induced by the motion of the cart. The embarked pendulum is modeled as a mathematical pendulum (bar without mass and particle of mass  $m_p$  at the end). The pendulum length is represented by  $l_p$  and the pendulum angular displacement by  $\theta$ . The mass of the mechanical system,  $m$ , is equal the cart mass plus pendulum mass,  $m_c + m_p$ . The horizontal cart position is represented by  $x$ . Due to constraints, the cart is not allowed to move in the vertical direction. A flexible barrier is attached inside the cart, constraining the pendulum motion. Due to the relative motion between the cart and the pendulum, it is possible that occur impacts between the pendulum and the barrier, as suggested in Fig. 4.1. As the impacts are internal, the energy

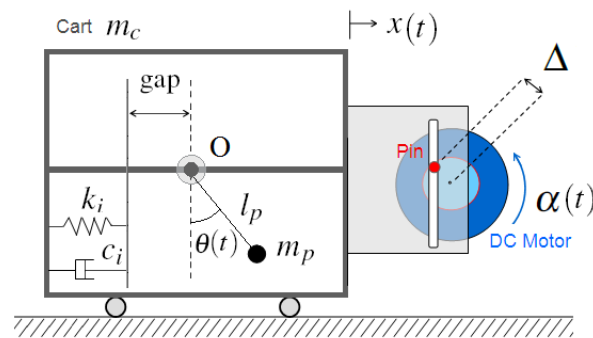


Figure 4.1: Coupled motor-cart-pendulum-barrier system.

stored in the pendulum motion it is not transferred outside the system, it stays within, with a possible dissipation. This system configuration helps to understand the difference between an internal and an external barrier. The objective is to analyze the maximal energy stored in the barrier in impacts as function of some parameters of the electromechanical system. Due to the presence of uncertainties in the computational nonlinear dynamics model of the

electromechanical system, the energy analysis is performed from a stochastic view point for different levels of uncertainties, and also for the deterministic case.

In the deterministic analysis, these parameters are the horizontal distance from the suspension point of the pendulum to the equilibrium position of the barrier and the coupling parameter between motor and the mechanical system,  $\Delta$ . Numerical simulations were performed with different values of these parameters. The coupling parameter has been varied from zero, an asymptotic case, (meaning no coupling between motor and the mechanical system) up to  $10^{-3}$  m. Comparing the results obtained with  $\Delta = 0$  and with  $\Delta > 0$ , it is possible to observe the influence of the coupling in the maximal energy stored in the barrier.

## 4.1 Dynamics of the motor-cart-pendulum-barrier system

A continuous contact dynamic model is developed and the impact is described using the spring-dashpot model. The spring-damper element of the impact is represented by a spring with stiffness  $k_i$  and a damper with damping coefficient  $c_i$ . The equations of the cart-pendulum-barrier system were obtained with the Lagrange principle. They are

$$m_p l_p^2 \ddot{\theta}(t) + m_p l_p \ddot{x}(t) \cos \theta(t) + m_p g_a l_p \sin \theta(t) = f_{\text{imp}}(t) l_p \cos \theta(t), \quad (4.1)$$

$$(m_p + m_c) \ddot{x}(t) + m_p l_p \ddot{\theta}(t) \cos \theta(t) - m_p l_p \dot{\theta}^2(t) \sin \theta(t) = f(t), \quad (4.2)$$

where,  $g_a$  is the acceleration of gravity,  $f$  represents the horizontal coupling force between the DC motor and the cart and  $f_{\text{imp}}$  the impact force exerted in the pendulum. This force is written as:

$$f_{\text{imp}}(t) = -\phi(t) \left[ k_i (l_p \sin \theta(t) + \text{gap}) + c_i (l_p \dot{\theta}(t) \cos \theta(t)) \right], \quad (4.3)$$

$$\phi(t) = \begin{cases} 1, & \text{if } -l_p \sin \theta(t) > \text{gap}, \\ 0, & \text{if } -l_p \sin \theta(t) \leq \text{gap}, \end{cases} \quad (4.4)$$

in Eq. (4.4) gap is the horizontal distance from the suspension point to the equilibrium position of the barrier. Due to the system geometry,  $x(t)$  and  $\alpha(t)$  are related by the following constraint

$$x(t) = \Delta \cos \alpha(t). \quad (4.5)$$

Substituting Eqs. (2.6) and (4.1) to (4.5) into Eqs. (2.1) and (2.2), we obtain the initial value problem for the motor-cart-pendulum-barrier system. Given

a constant source voltage  $\nu$ , find  $(\alpha, c, \theta)$  such that, for all  $t > 0$ ,

$$l\dot{c}(t) + rc(t) + k_e\dot{\alpha}(t) = \nu,$$

$$\ddot{\alpha}(t) [j_m + (m_c + m_p)\Delta^2(\sin \alpha(t))^2] + \dot{\alpha}(t) [b_m + (m_c + m_p)\Delta^2\dot{\alpha}(t) \cos \alpha(t) \sin \alpha(t)] - k_e c(t) - \ddot{\theta}(t) [m_p l_p \cos \theta(t) \Delta \sin \alpha(t)] + \dot{\theta}(t) [m_p l_p \dot{\theta}(t) \sin \theta(t) \Delta \sin \alpha(t)] = 0,$$

$$\ddot{\theta}(t) [m_p l_p^2] - \ddot{\alpha}(t) [m_p l_p \cos \theta(t) \Delta \sin \alpha(t)] - \dot{\alpha}(t) [m_p l_p \cos \theta(t) \Delta \cos \alpha(t) \dot{\alpha}(t)] + m_p g_a l_p \sin \theta(t) + \phi(t) [k_i(l_p \sin \theta(t) + \text{gap}) + c_i(l_p \dot{\theta}(t) \cos \theta(t))] l_p \cos \theta(t) = 0, \quad (4.6)$$

where

$$\phi(t) = \begin{cases} 1, & \text{if } -l_p \sin \theta(t) > \text{gap}, \\ 0, & \text{in all other cases,} \end{cases} \quad (4.7)$$

with the initial conditions,

$$\dot{\alpha}(0) = 0 \quad , \quad \alpha(0) = 0 \quad , \quad \dot{\theta}(0) = 0 \quad , \quad \theta(0) = \pi/2 \quad , \quad c(0) = \frac{\nu}{r}. \quad (4.8)$$

## 4.2 Dimensionless motor-cart-pendulum-barrier system

In this section, the initial value problem to the motor-cart-pendulum-barrier system is presented in a dimensionless form. Taking  $\dot{\alpha}(t) = u(t)$  and  $\dot{\theta}(t) = n(t)$ , the system can be written as a first order system

$$\dot{c}(t) = \frac{-k_e u(t) - rc(t) + \nu}{l},$$

$$\dot{u}(t) = \left\{ -n(t)^2 m_p l_p \sin \theta(t) \Delta \sin(\alpha(t)) - u(t)^2 (m_c + m_p) \Delta^2 \cos(\alpha(t)) \sin(\alpha(t)) - b_m u(t) + k_e c(t) + [\cos(\theta(t)) \Delta \sin(\alpha(t))] [u(t)^2 m_p \cos \theta(t) \Delta \cos \alpha(t) - m_p g_a \sin(\theta(t)) - \phi [k_i(l_p \sin \theta(t) + \text{gap}) + c_i(l_p n(t) \cos \theta(t))] \cos \theta(t)] \right\} \left\{ \frac{1}{j_m + \Delta^2 \sin(\alpha(t))^2 (m_c + m_p \sin(\theta(t))^2)} \right\},$$

$$\dot{n}(t) = \left\{ m_p \cos(\theta(t)) \Delta \sin(\alpha(t)) [k_e c(t) - u(t)^2 (m_c + m_p) \Delta^2 \cos(\alpha(t)) \sin(\alpha(t)) - b_m u(t) - n(t)^2 m_p l_p \sin \theta(t) \Delta \sin(\alpha(t))] + [j_m + (m_p + m_c) \Delta^2 \sin(\alpha(t))^2] [-m_p g_a \sin(\theta(t)) + u(t)^2 m_p \cos \theta(t) \Delta \cos \alpha(t) - \phi [k_i(l_p \sin \theta(t) + \text{gap}) + c_i(l_p n(t) \cos \theta(t))] \cos \theta(t)] \right\} \left\{ \frac{1}{m_p l_p [j_m + \Delta^2 \sin(\alpha(t))^2 (m_c + m_p \sin(\theta(t))^2)]} \right\}.$$

(4.9)

Writing

$$t = \frac{l}{r}s, \quad \alpha \left( \frac{l}{r}s \right) = \gamma(s), \quad u \left( \frac{l}{r}s \right) = \frac{rq(s)}{l}, \quad \theta \left( \frac{l}{r}s \right) = \beta(s), \quad (4.10)$$

$$n \left( \frac{l}{r}s \right) = \frac{ry(s)}{l}, \quad c \left( \frac{l}{r}s \right) = \frac{k_e w(s)}{l},$$

one gets that  $s$  is dimensionless parameter. The functions  $\gamma(s)$ ,  $q(s)$ ,  $\beta(s)$ ,  $y(s)$  and  $w(s)$  are dimensionless functions. By substituting Eq. (4.10) into Eq. (4.9) one obtains

$$w'(s) = -w(s) - q(s) + v_0,$$

$$q'(s) = \left\{ \begin{aligned} & -v_3 q(s) - y(s)^2 v_5 \sin(\gamma(s)) \sin(\beta(s)) - v_6 \sin(\beta(s)) \cos(\beta(s)) \sin(\gamma(s)) \\ & + v_2 w(s) - q(s)^2 \cos(\gamma(s)) \sin(\gamma(s)) [v_9 - v_4 \cos(\beta(s))^2] \\ & - \varphi(s) \cos(\beta(s))^2 \sin(\gamma(s)) [v_{10} \sin(\beta(s)) + v_{11} + v_{12} \cos(\beta(s)) y(s)] \end{aligned} \right\} \\ \left\{ \frac{1}{1 + \sin(\gamma(s))^2 [v_1 + v_4 \sin(\beta(s))^2]} \right\} \quad (4.11)$$

$$y'(s) = \left\{ \begin{aligned} & -v_3 v_7 q(s) \cos(\beta(s)) \sin(\gamma(s)) + q(s)^2 v_7 \cos(\gamma(s)) \cos(\beta(s)) \\ & - v_4 y(s)^2 \sin(\gamma(s))^2 \sin(\beta(s)) \cos(\beta(s)) + v_2 v_7 w(s) \cos(\beta(s)) \sin(\gamma(s)) \\ & [1 - v_9 \sin(\gamma(s))^2] [-v_8 \sin(\beta(s)) - \varphi(s)(v_{13} \sin(\beta(s)) + v_{14}) \\ & + v_{15} y(s) \cos(\beta(s)) \cos(\beta)] \end{aligned} \right\} \left\{ \frac{1}{1 + \sin(\gamma(s))^2 [v_1 + v_4 \sin(\beta(s))^2]} \right\}, \quad (4.12)$$

where

$$\varphi(s) = \begin{cases} 1, & \text{if } -\sin \beta(s) > a_{14}, \\ 0, & \text{if } -\sin \beta(s) \leq a_{14}, \end{cases} \quad (4.13)$$

and where  $'$  denotes the derivative with respect to  $s$  and  $a_i$ ,  $i = 1, \dots, 16$  are dimensionless parameters given by

$$\begin{aligned} v_0 &= \frac{\nu l}{k_e r}, & v_1 &= \frac{\Delta^2 m_c}{j_m}, & v_2 &= \frac{l k_e^2}{j_m r^2}, & v_3 &= \frac{b_m l}{j_m r}, & v_4 &= \frac{\Delta^2 m_p}{j_m}, \\ v_5 &= \frac{m_p l_p \Delta}{j_m}, & v_6 &= \frac{m_p \Delta g_a l^2}{j_m r^2}, & v_7 &= \frac{\Delta}{l_p}, & v_8 &= \frac{g_a l^2}{l_p r^2}, & v_9 &= \frac{(m_c + m_p) \Delta^2}{j_m}, \\ v_{10} &= \frac{k_i l_p \Delta l^2}{j_m r^2}, & v_{11} &= \frac{k_i g_a p \Delta l^2}{j_m r^2}, & v_{12} &= \frac{c_i l_p \Delta l}{j_m r}, & v_{13} &= \frac{k_i l^2}{m_p r^2}, & v_{14} &= \frac{\text{gap}}{l_p}, \\ v_{15} &= \frac{c_i l}{m_p r}. \end{aligned} \quad (4.14)$$

Comparing the dimensionless parameters of the motor-cart-pendulum-barrier system with the dimensionless parameters of the motor-cart-pendulum system given by Eq. 3.9, it can be observed that the internal barrier introduces six new parameters to the equations:  $v_{10}$  to  $v_{15}$ .

### 4.3 Impact energy

As explained in the introduction, the objective of this chapter is to analyze the maximum energy stored in the barrier in each impact in function of some parameters of the electromechanical system. These parameters are  $gap/l_p$  and  $\Delta$ . The maximum impact energy during the  $j$ -th impact,  $\lambda_j$ , occurs when the spring  $k_i$  is compressed to the maximum, that is, when  $l_p \sin(\theta)$  achieves its minimum value during the  $j$ -th impact. Noting as  $\theta^*$  the angle of the pendulum corresponding to this configuration of maximum compression,  $\lambda_j$  is calculated by

$$\lambda_j = \frac{1}{2} k_i (l_p \sin(\theta^*) + gap)^2, \quad \text{with} \quad -l_p \sin \theta^* > gap. \quad (4.15)$$

The average of the maximum impact energy is written as

$$\lambda = \frac{\sum_{j=1}^{N_{\text{imp}}} \lambda_j}{N_{\text{imp}}}, \quad (4.16)$$

where  $N_{\text{imp}}$  is the total number of impacts that occur during time interval  $[0, T]$ .  $T$  is the duration chosen for analysis. The variable  $\lambda$  is chosen to measure the system performance. The bigger  $\lambda$  is, the better will be the system performance.

## 4.4 Numerical simulations of the dynamics of the coupled system

To observe the influence of the coupling between the electrical and mechanical parts in the maximum energy stored in the barrier, two configurations of the vibro-impact system were analyzed separately. In the first one, it is considered no coupling between the motor and the mechanical system, i.e.,  $\Delta = 0$  m. In this case, the motor behaves as if it is turned off and, consequently, the cart does not move. In the second configuration, it is considered coupling, i.e.,  $\Delta > 0$  m.

### 4.4.1 No coupling between the motor and the mechanical system

When  $\Delta = 0$  m, there is no coupling between the motor and the mechanical system. Thus the cart does not move. Considering that there is no energy dissipation in the impact model between the pendulum and the barrier ( $c_i = 0$  Ns/m), the maximum energy stored in the barrier in each impact can be calculated as function of the initial potential and kinetic energies of the pendulum. Calling the initial conditions for the pendulum as  $\theta(0) = \theta_0$  and  $\dot{\theta}(0) = \dot{\theta}_0$ , the initial mechanical energy of the pendulum is

$$\lambda_0 = m_p g \cos(\theta_0) + \frac{1}{2} m_p [(l_p \dot{\theta}_0 \cos \theta_0)^2 + (l_p \dot{\theta}_0 \sin \theta_0)^2]. \quad (4.17)$$

When the spring  $k_i$  is compressed to the maximum during the  $j$ -th impact, a part of  $\lambda_0$  is stored as potential energy in the pendulum and another part as potential energy in spring  $k_i$  ( $\lambda_j$ ). Thus

$$\lambda_0 = m_p g \cos(\theta^*) + \frac{1}{2} k_i (l_p \sin(\theta^*) + gap)^2. \quad (4.18)$$

Observing Eq. (4.17), it is possible to verify that when  $\Delta = 0$  m,  $\lambda_j$  the  $j$ -th impact will be maximum if  $gap/l_p = 0$ . With this configuration, the pendulum begins the impact in the vertical position, exactly when it has its maximum velocity. Thus, this configuration is taken as reference. The impact energy in this configuration represented by  $\lambda^{ref}$  will be used as normalization factor in the analysis of the impact factor. The value of  $\lambda^{ref}$  is computed considering  $k_i = 10^6$  N/m. The graph of  $\lambda/\lambda^{ref}$  as function of  $gap/l_p$  for different values of  $k_i$  is shown in Fig. 4.2. As expected, its maximum occurs when  $gap/l_p = 0$  and its minimum at  $gap/l_p = 1$  (configuration in which there is no impact between the pendulum and the barrier).

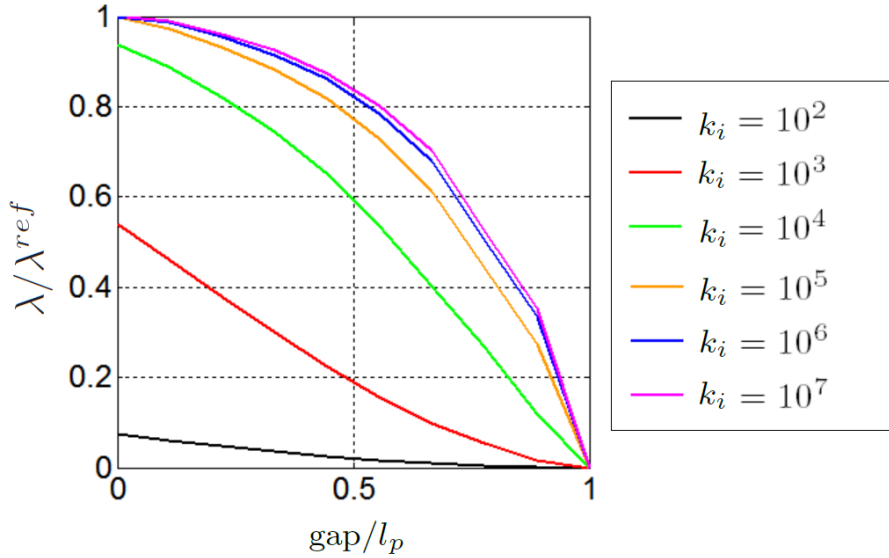


Figure 4.2: No coupling ( $\Delta = 0$  m): normalized average of the maximum impact energy as function of the parameter  $gap/l_p$  for different values of  $k_i$  N/m.

#### 4.4.2 Coupled system

When  $\Delta > 0$  m, i.e., there is coupling between the motor and the mechanical system. The bigger is  $\Delta$ , the more highlighted will be the non-linear behavior of system [42]. Small changes in the values of  $\Delta$  and  $gap/l_p$  can modify a lot the response of the system, as the maximum amplitude

of the pendulum displacement, maximum velocity of the motor shaft and therefore, the impact behavior of the system. The form of the graph of the average of the impact energy changes as shown in Sec. 4.4. Considering just the coupled motor-cart system, i.e., there is no pendulum embarked in the cart, the existence and asymptotic stability of a periodic orbit were already obtained in a mathematically rigorous way in [15, 18]. The influence of the parameters  $\Delta$  and  $\text{gap}/l_p$  in  $\lambda$ , Eq. (4.16), was investigated numerically. For computation, the initial value problem defined by Eqs. (4.6) to (4.8) has been rewritten in the dimensionless form given by Eqs. (4.11) to (4.14). Despite of using the dimensionless initial value problem for numerical simulations, the results are presented in the dimensional form because we believe that in this way they have an easier physical interpretation. Duration is chosen as  $T = 20.0$  s. The 4th-order Runge-Kutta method is used for the time-integration scheme. The specifications of the motor parameters used in all simulations were obtained from the specifications of the DC motor Maxon brushless number 411678 (values could be find at [42](table 1)). The applied voltage was assumed to be constant in time and equal to 2.4 V. The pendulum length was assumed to be 0.075 m. The values of the cart and the pendulum masses were  $m_c = 0.0$  kg and  $m_p = 5.0$  kg, so that the total mass,  $m = m_c + m_p = 5.0$  kg, is equal to the embarked mass, a limit case. The values of the stiffness and damping coefficient used in the simulations were  $k_i = 10^6$  N/m and  $c_i = 0$  Ns/m, so that there is no energy dissipation in the impact model. To investigate the influence of  $\Delta$  and  $\text{gap}/l_p$  in  $\lambda/\lambda^{ref}$ , 700 numerical simulations have been carried out combining the following values of the parameters: 7 values for  $\Delta$  nonuniformly selected in the interval  $[0, 10^{-3}]$  m, and 100 values for  $\text{gap}/l_p$  uniformly selected in  $[0, 1]$ . Figure 4.3 shows the graph of  $\lambda/\lambda^{ref}$  as function of  $\text{gap}/l_p$  for different values of  $\Delta$ . It is noted that for values of  $d$  near zero, as  $10^{-5}$  m and  $10^{-4}$  m, the graph of the impact energy is very similar to the graph with  $\Delta = 0$  m. The average impact energy presents its maximum at  $\text{gap}/l_p = 0$  and its minimum when  $\text{gap}/l_p = 1$ . When  $\Delta$  is bigger, as  $2 \times 10^{-4}$  m,  $5 \times 10^{-4}$  m,  $8 \times 10^{-4}$  m and  $10^{-3}$  m, the form of the graph of the average of the impact energy changes completely. The maximum does not occur anymore at  $\text{gap}/l_p = 0$ . Depending on the value of  $\Delta$ , the maximum occurs at a different value of  $\text{gap}/l_p$ . Among the considered values of  $\Delta$  and  $\text{gap}/l_p$ , the maximum of the average of the impact energy was obtained with  $\Delta = 10^{-3}$  m and  $\text{gap}/l_p = 0.6263$ . Considering  $\Delta = 10^{-3}$  m and varying the value of  $k_i$ , the shape of the curve of the average of the maximum impact energy in function of the parameter  $\text{gap}/l_p$  (shown in Fig. 4.4) changes in an unexpected fashion. Comparing it with Fig. 4.3, it is possible to observe that for small values of

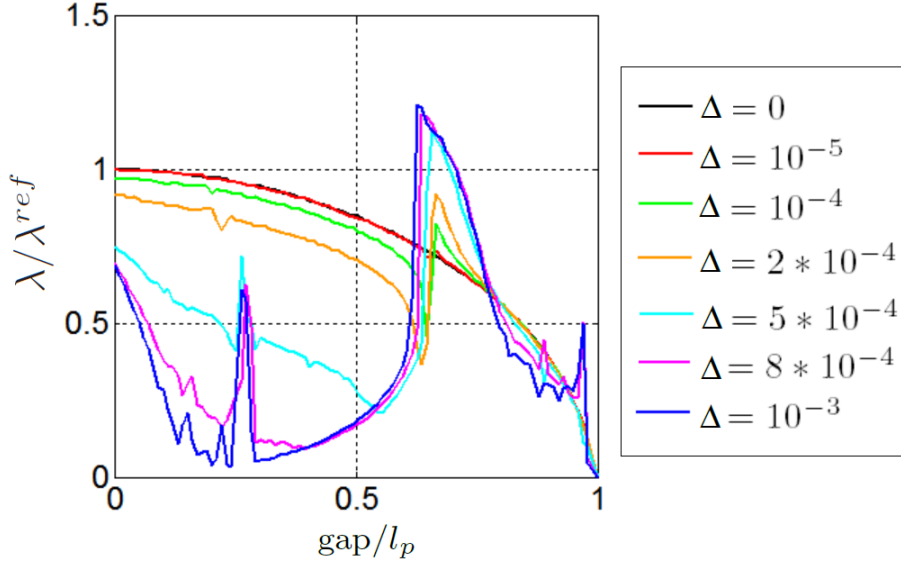


Figure 4.3: Coupled system ( $\Delta > 0$ ): normalized average of the impact energy as function of the parameter  $gap/l_p$  for different values of  $\Delta$  (units in meters).

$k_i$ , as  $10^2$  N/m and  $10^3$  N/m, both graphs are similar. But, when  $k_i$  is bigger, the form of the graph of the average of the impact energy changes completely. Among the considered values of  $k_i$  and  $gap/l_p$ , the maximum of the average of the impact energy was obtained with  $k_i = 10^4$  N/m and  $gap/l_p = 0.293$ . Thus the maximum of the average of the impact energy does not occur anymore with the bigger  $k_i$  as happens in the  $\Delta = 0$  m configuration. To construct the graph of Fig. 4.4, for each value of  $k_i$  selected, 100 values of  $gap/l_p$  equally spaced between 0 and 1 were considered. Thus, in total, 600 numerical simulations have been carried out.

## 4.5 Probabilistic model

The system parameter considered uncertain is  $k_i$ , which is modeled by the random variable  $K_i$ . The probability distribution of this random variable is constructed using the Maximum Entropy Principle [34, 88, 89, 91, 85, 94, 95]. This Principle allows the probability distribution of a random variable to be constructed using only the available information, avoiding the use of any additional information that introduces a bias on the estimation of the probability distribution. The Maximum Entropy Principle states: out of all probability distributions consistent with a given set of available information choose the one that has maximum uncertainty (the Shannon measure of entropy). The available information of the random variable is defined as

1.  $K_i$  is a positive-valued random variable,

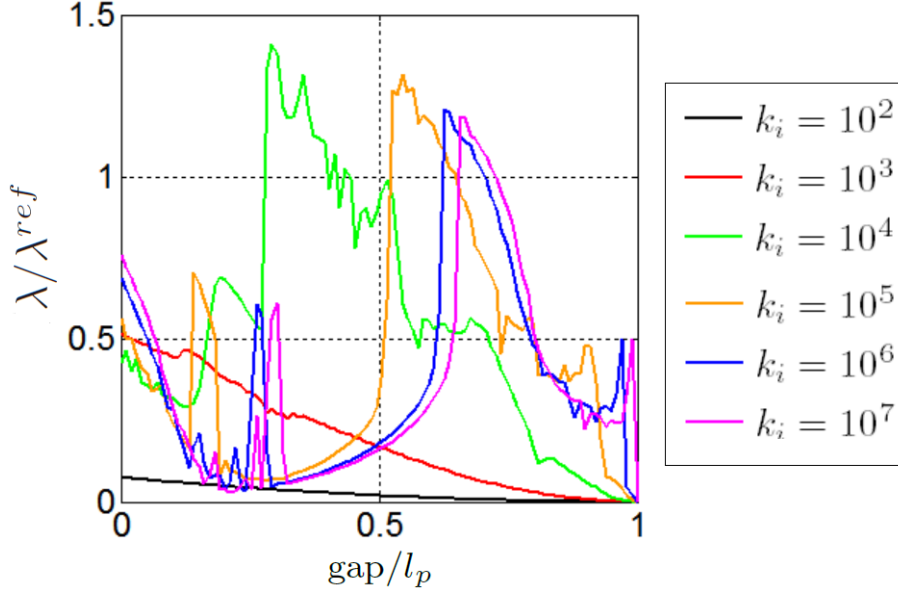


Figure 4.4: Coupled system ( $\Delta > 0$ ): normalized average of the impact energy as function of the parameter  $\text{gap}/l_p$  for different values of  $k_i$  N/m with  $\Delta = 10^{-3}$  m.

2. the mean value is known:  $E\{K_i\} = \mu$ ,
3. in order that the response of the dynamical system be a second-order stochastic process, we impose the following condition:  $\|E\{\log K_i\}\| < \infty$ .

Therefore, the Maximum Entropy Principle using Shannon entropy measure of the probability density function,  $p$ , of  $K_i$  yields the Gamma probability density function, given by

$$p(k_i) = \mathbb{1}_{[0,+\infty)}(k_i) \frac{1}{\mu} \left(\frac{1}{\delta^2}\right)^{\frac{1}{\delta^2}} \frac{1}{\Gamma(1/\delta^2)} \left(\frac{x}{\mu}\right)^{\frac{1}{\delta^2}-1} \exp\left(-\frac{x}{\delta^2\mu}\right), \quad (4.19)$$

where  $\mathbb{1}_{[0,+\infty)}(k_i)$  is an indicator function that is equal to 1 for  $k_i \in [0, +\infty)$  and 0 otherwise, and

- $\Gamma$  is the Gamma function:  $\Gamma(a) = \int_0^\infty t^{a-1} \exp(-t) dt$ ;
- $\delta = \frac{\sigma}{\mu}$  is the coefficient variation ( $\sigma$  is the standard deviation).

## 4.6 Numerical simulations of the stochastic vibro-impact electromechanical system

As it was assumed that the stiffness of the spring,  $k_i$ , in the barrier model is a random variable, the output variables of the stochastic coupled system are random processes [91, 11] and, consequently, the average of the impact energy,

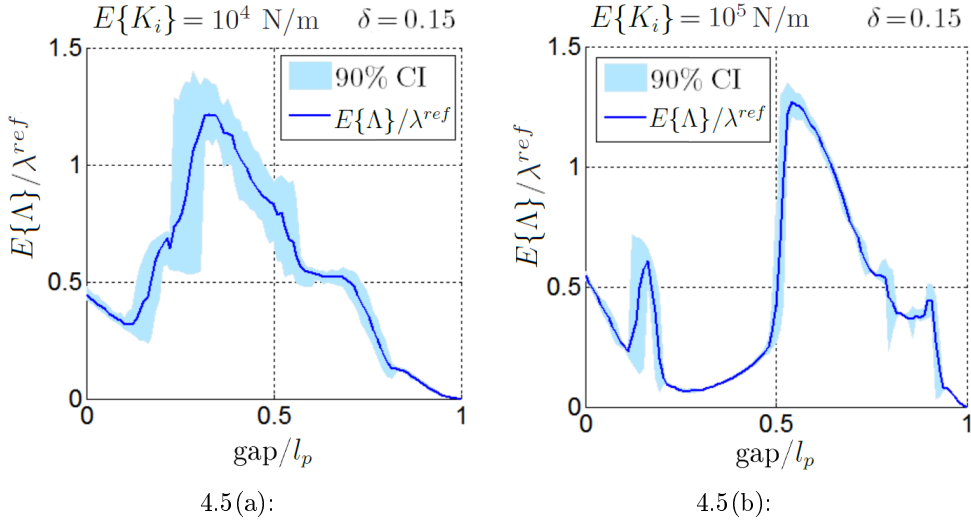


Figure 4.5: Mean and 90% confidence interval of  $\Lambda/\lambda^{ref}$  as function of  $gap/l_p$  with  $\delta = 0.15$  for (a)  $E\{K_i\} = 10^4 \text{ N/m}$  and (b)  $E\{K_i\} = 10^5 \text{ N/m}$ .

$\lambda$ , become a random variable  $\Lambda$ . To make the stochastic analysis, Monte Carlo simulations were employed to compute statistics of  $\Lambda$ , as mean and intervals of confidence, using 100 independent realizations of  $K_i$ . To observe the influence of  $gap/l_p$  in the statistics of the impact energy for different values of  $E\{K_i\}$  and hyperparameter  $\delta$  (which controls the level of uncertainties for  $K_i$ ), the Monte Carlo simulations have been carried out combining the following values of the parameters: 3 values for  $E\{K_i\}$  ( $10^4$ ,  $10^5$ , and  $10^6 \text{ N/m}$ ), 3 values for  $\delta$  (0.15, 0.25, and 0.35) and 100 values for  $gap/l_p$  uniformly selected in the interval  $[0, 1.0]$ . Thus, 90,000 numerical simulations have been carried out in the stochastic analysis. The graphs of  $E\{\Lambda\}/\lambda^{ref}$  and 90% confidence interval as function of  $gap/l_p$  for  $E\{K_i\} = 10^4$ ,  $10^5$  and  $10^6 \text{ N/m}$  with  $\delta = 0.15$  are displayed in Figs. 4.5 and 4.6(a). Comparing these statistics with the results of deterministic simulations shown in Fig. 4.4, it is verified that in relation to the impact energy, deterministic and stochastic systems have similar behavior. However, the 90% confidence interval gets narrower as  $E\{K_i\}$  increases. For  $E\{K_i\} = 10^6 \text{ N/m}$  and  $\delta = 0.15$ , the maximum of  $E\{\Lambda\}/\lambda^{ref}$  occurs at  $gap/l_p = 0.63 \text{ m}$ . The normalized histogram of  $\Lambda/\lambda^{ref}$  with this configuration is shown in Fig. 4.6(b). Figures 4.7 to 4.9 show the graphs of  $E\{\Lambda\}/\lambda^{ref}$  and 90% confidence interval as function of  $gap/l_p$  for  $E\{K_i\} = 10^4$ ,  $10^5$  and  $10^6 \text{ N/m}$  and for  $\delta = 0.25$  and  $0.35$ . These figures show that the bigger  $\delta$  is, the larger is the confidence interval of  $\Lambda/\lambda^{ref}$ .

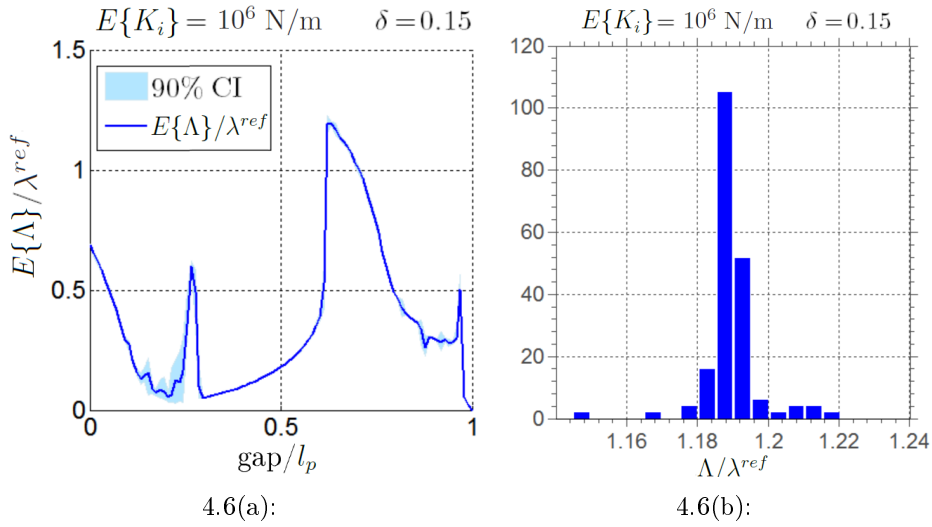


Figure 4.6: (a) Mean and 90% confidence interval of  $\Lambda$  as function of  $gap/l_p$  with  $\delta = 0.15$  and  $E\{K_i\} = 10^6$  N/m and (b) normalized histogram of  $\Lambda/\lambda^{ref}$  for  $gap/l_p = 0.63$  m,  $E\{K_i\} = 10^6$  N/m and  $\delta = 0.15$ .

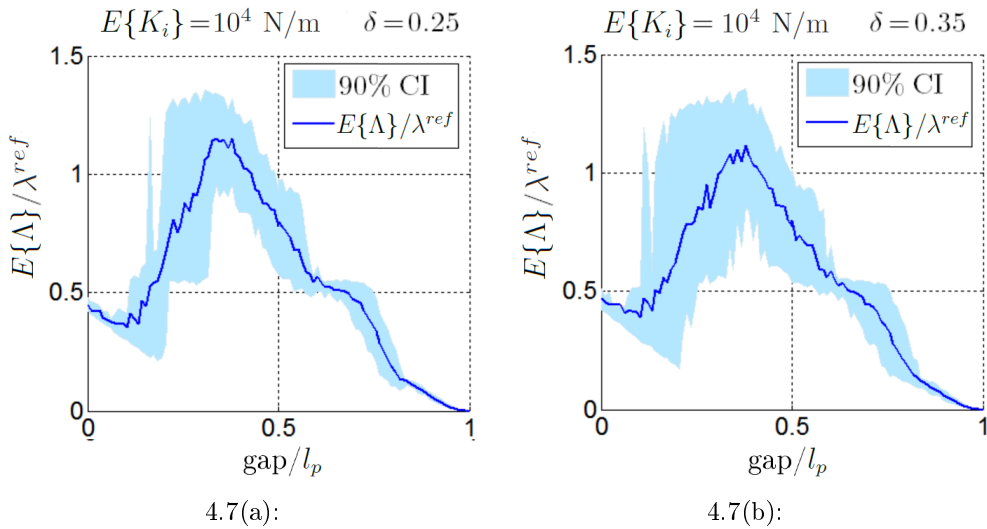


Figure 4.7: Mean and 90% confidence interval of  $\Lambda/\lambda^{ref}$  as function of  $gap/l_p$  with  $E\{K_i\} = 10^4$  N/m for (a)  $\delta = 0.25$  and (b)  $\delta = 0.35$ .

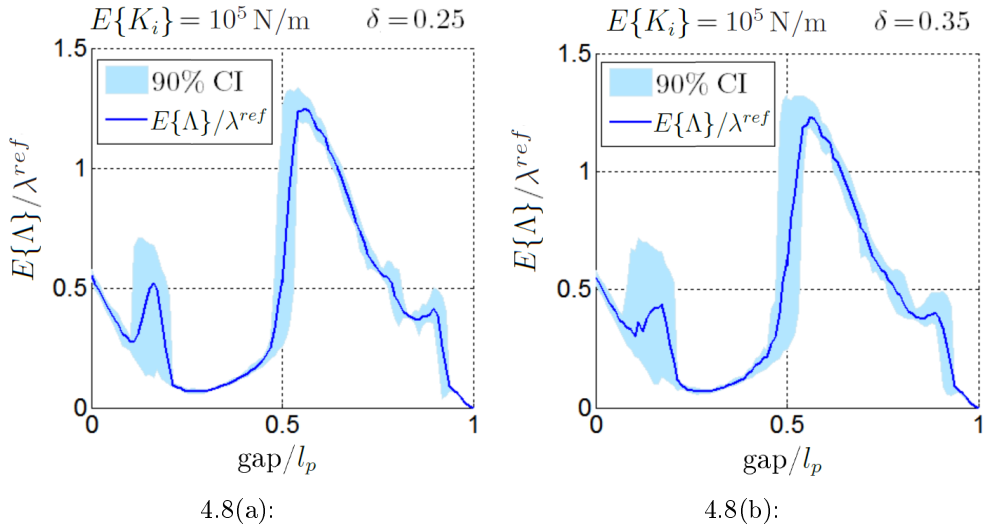


Figure 4.8: Mean and 90% confidence interval of  $\Lambda/\lambda^{ref}$  as function of  $gap/l_p$  with  $E\{K_i\} = 10^5 \text{ N/m}$  for (a)  $\delta = 0.25$  and (b)  $\delta = 0.35$ .

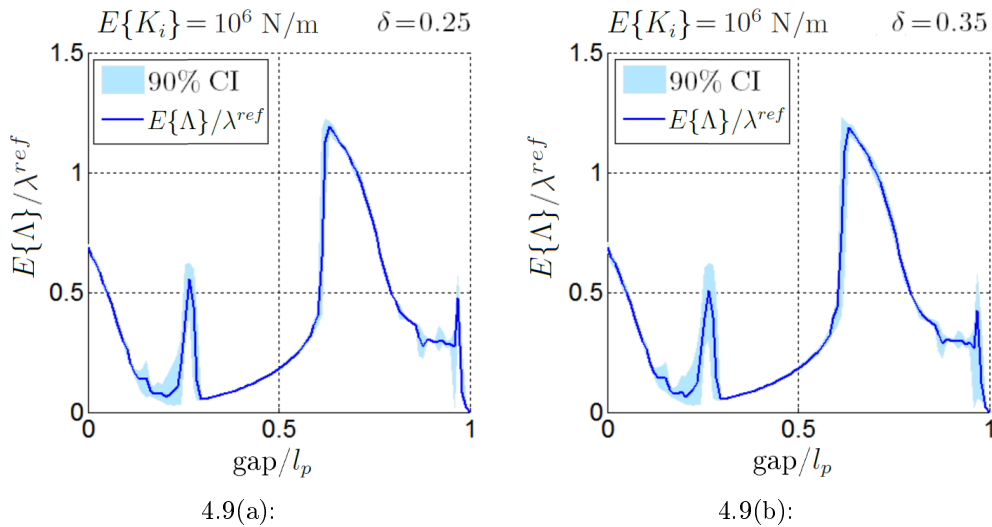


Figure 4.9: Mean and 90% confidence interval of  $\Lambda/\lambda^{ref}$  as function of  $gap/l_p$  with  $E\{K_i\} = 10^6 \text{ N/m}$  for (a)  $\delta = 0.25$  and (b)  $\delta = 0.35$ .

## 4.7 Summary of the Chapter

The purpose of this chapter was to analyze the impact energy of an embarked pendulum in a vibro-impact electromechanical system. A flexible barrier, attached to the cart, constrains the pendulum motion and causes impacts. Since this nonlinear electromechanical system is devoted to the vibro-impact, the time responses exhibit numerous shocks that have to be identified with accuracy and, consequently, a very small time-step is required. To reduce the computation time, the initial-value problem, Eqs. (4.6) to (4.8), was rewritten in the dimensionless form, Eqs. (4.11) to (4.13). While each numerical simulation of Eqs. (4.6) to (4.8) takes approximately 30 seconds to be computed, each numerical simulation of Eqs. (4.11) to (4.13) takes approximately half of this time. In the deterministic analysis, the influence of the parameter  $gap/l_p$  in the impact behavior was numerically investigated for different values of the nominal eccentricity of the pin,  $\Delta$ , the parameter that governs the coupling and the nonlinearity of the system. As  $\Delta$  increases the nonlinearity also increases. It was verified that for values of  $\Delta$  near zero, the graph of the impact energy is very similar to the graph with  $\Delta = 0$  m. This result can be nicely predicted from conservation of energy. However, as  $\Delta$  increases the form of the graph changes completely and in an unexpected fashion. This peculiar behavior is due to the energy taken by the pendulum from the motor. The energy of the mechanical systems varies a lot and the pumping of energy, from the motor to the mechanical system, increases with  $\Delta$ . The systems analyzed show a self-oscillation behavior, in the sense that the generation and maintenance of the motion comes from the motor but the oscillations somehow control the energy taken from the motor. It varies with  $\Delta$ , that is a measure of the nonlinearity of the system. It is worth mentioning that the energy intake is at frequency zero, the constant voltage, but this energy is distributed to all frequencies due to the impacts. The influence of the parameter  $gap/l_p$  in the impact behavior was also investigated for different values of the stiffness,  $k_i$ , with the fixed value  $\Delta = 10^{-3}$  m. Similar to what happens with the parameter  $d$ , it was verified that for small values of  $k_i$ , the graph of the impact energy is very similar to the graph of impact energy with the same  $k_i$  and  $\Delta = 0$  m. However, as  $k_i$  increases the form of the graph changes completely if compared to the graph of impact energy with the same  $k_i$  and  $\Delta = 0$  m. It was also observed that the maximum of the impact energy do not occur anymore with the bigger  $k_i$  as happens in the  $\Delta = 0$  m configuration. In the stochastic analysis, the stiffness of the spring  $k_i$ , in the barrier was modeled as a random variable and the propagation of uncertainties in the

coupled motor-cart-pendulum-barrier system was computed through Monte Carlo simulations. Thus statistics of the impact energy, as mean and 90% confidence interval, were computed for different values of  $\text{gap}/l_p$ ,  $E\{K_i\}$  and  $\delta$ . Comparing these statistics with the results of deterministic simulations, it is verified that in relation to the mean of impact energy, deterministic and stochastic systems have similar behavior. However, the 90% confidence interval decreases as  $E\{K_i\}$  increases and expands as  $\delta$  increases.

## 5

# Robust design optimization with an uncertain model of a nonlinear percussive electromechanical system

The objective of this part of the Thesis is to perform an optimization of a percussive electromechanical system with respect to some chosen design parameters. The optimization consists in maximizing the impact power under the constraint that the electric power consumed by the DC motor is lower than a maximum value. This nonlinear constrained design optimization problem is formulated in the framework of robust design due to the presence of uncertainties in the computational nonlinear dynamics model of the electromechanical system [61, 81, 9].

## 5.1 Dynamics of the vibro-impact electromechanical system

As described in the introduction, the system is composed by a cart whose movement is driven by the DC motor, and by a hammer that is embarked into the cart. The motor is coupled to the cart through a pin that slides into a slot machined in an acrylic plate that is attached to the cart, as shown in Fig. 5.1. The off-center pin is fixed on the disc at distance  $\Delta$  of the motor shaft, so that the motor rotational motion is transformed into a cart horizontal movement. To model the coupling between the motor and the mechanical system, the motor shaft is assumed to be rigid. Thus, the available torque vector to the

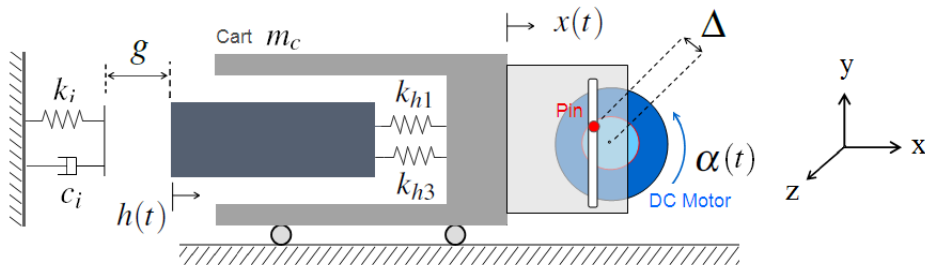


Figure 5.1: Motor-cart-hammer coupled system. The nonlinear component spring is drawn as a linear spring with constant  $k_{h1}$  and a nonlinear cubic spring with constant  $k_{h3}$ .

coupled mechanical system,  $\boldsymbol{\tau}$ , can be written as

$$\boldsymbol{\tau}(t) = \boldsymbol{\Delta}(t) \times \mathbf{f}(t), \quad (5.1)$$

where  $\boldsymbol{\Delta} = (\Delta \cos \alpha(t), \Delta \sin \alpha(t), 0)$  is the vector related to the eccentricity of the pin, and where  $\mathbf{f}$  is the coupling force between the DC motor and the cart. Assuming that there is viscous friction between the pin and the slot, the vector  $\mathbf{f}$  has two components: the horizontal force that the DC motor exerts in the cart,  $f_x$ , and the vertical force,  $f_y$ , induced by the viscous friction. The available torque  $\tau$  and vertical force  $f_y$  are written as

$$\tau(t) = f_y(t) \Delta \cos \alpha(t) - f_x(t) \Delta \sin \alpha(t), \quad (5.2)$$

$$f_y(t) = c_{pin} \Delta \dot{\alpha}(t) \cos \alpha(t), \quad (5.3)$$

where  $c_{pin}$  is the viscous friction. The embarked hammer is modeled as a rigid body of mass  $m_h$  and its relative displacement is  $h$  with respect to the cart. In the adopted model, the constitutive equation of the spring component between the hammer and the cart is written as  $f_s(t) = k_{h1} h(t) + k_{h3} h(t)^3$ . The rate of nonlinearity of the hammer stiffness is defined as  $r_h = k_{h3}/k_{h1}$ . We introduce the natural frequency,  $\omega_h$ , of the hammer suspended to the linear spring with constant stiffness  $k_{h1}$  such that  $\omega_h = \sqrt{k_{h1}/m_h}$ . The horizontal cart displacement is represented by  $x$ . Due to constraints, the cart is not allowed to move in the vertical direction. The spring-damper element modeling the medium on which the impacts occur, is constituted of a linear spring with stiffness coefficient  $k_i$  and a damper with damping coefficient  $c_i$ . The equations of the cart-hammer-barrier system were obtained with the Lagrange principle. They are

$$\ddot{x}(t) (m_c + m_h) + \ddot{h}(t) m_h + c_{ext} \dot{x}(t) = -f_{imp}(t) + f_x(t), \quad (5.4)$$

$$\ddot{x}(t) m_h + \ddot{h}(t) m_h + c_{int} \dot{h} + k_{h1} h(t) + k_{h3} h^3(t) = -f_{imp}(t), \quad (5.5)$$

where,  $c_{ext}$  is the viscous friction coefficient between the cart and the rail and  $c_{int} = 2\zeta_{int}\sqrt{m_h k_{h1}}$  is the viscous friction coefficient between the cart and the hammer ( $\zeta_{int}$  is the damping ratio). The term  $f_x$  is the horizontal coupling force between the DC motor and the cart, and  $f_{imp}$  is the impact force between the hammer and the barrier, which is written as

$$f_{imp}(t) = -\phi(t) \left( k_i (x(t) + h(t) + g) + c_i (\dot{x}(t) + \dot{h}(t)) \right), \quad (5.6)$$

where

$$\phi(t) = \begin{cases} 1, & \text{if } x(t) + h(t) + g < 0 \quad \text{and} \quad \dot{h}(t) + \dot{x}(t) < 0, \\ 0, & \text{in all other cases,} \end{cases} \quad (5.7)$$

in which  $g$  is defined as the horizontal distance from the hammer (when  $\alpha = \pi/2$  rad) to the equilibrium position of the barrier. In the model defined by Eq. (5.7), an impact starts when  $x(t) + h(t)$  is negative and equal to  $-g$  and,  $\dot{h}(t) + \dot{x}(t) < 0$ . During an impact, the action of the barrier on the hammer stops as soon as the total velocity  $\dot{h}(t) + \dot{x}(t)$  becomes positive (the return of the hammer), i.e, the barrier moves irreversibly in one direction, simulating a penetration. Due to the system geometry,  $x(t)$  and  $\alpha(t)$  are related by the following constraint

$$x(t) = \Delta \cos(\alpha(t)). \quad (5.8)$$

Substituting Eqs. (5.2) to (5.8) into Eqs. (2.1) and (2.2), we obtain the initial value problem for the motor-cart-hammer-barrier coupled system that is written as follows. Given a constant source voltage  $\nu$ , find  $(\alpha, c, h)$  such that, for all  $t > 0$ ,

$$l\dot{c}(t) + rc(t) + k_e\dot{\alpha} = \nu, \quad (5.9)$$

$$\begin{aligned} & \ddot{\alpha}(t) (j_m + (m_c + m_h)\Delta^2 \sin^2(\alpha(t))) - \ddot{h}(t) (m_h \Delta \sin(\alpha(t))) - k_e c(t) \\ & + \dot{\alpha}(t) \left( b_m + \dot{\alpha}(t)(m_c + m_h)\Delta^2 \cos(\alpha(t)) \sin(\alpha(t)) \right. \\ & \quad \left. + c_{pin}\Delta^2 \cos^2(\alpha(t)) - c_{ext}\Delta^2 \sin^2(\alpha(t)) \right) \\ & = \phi \left( k_i(\Delta \cos(\alpha(t)) + h + g) + c_i(-d\dot{\alpha}(t) \sin(\alpha(t)) + \dot{h}(t)) \right) \Delta \sin(\alpha(t)), \end{aligned} \quad (5.10)$$

$$\begin{aligned} & \ddot{h}(t)m_h - \ddot{\alpha}(t) (m_h \Delta \sin(\alpha(t))) - \dot{\alpha}(t) (m_h \Delta \dot{\alpha}(t) \cos(\alpha(t))) \\ & \quad + \dot{h}(t)c_{int} + k_{h1}h(t) + k_{h3}h^3(t) \\ & = \phi(t) \left( k_i(\Delta \cos(\alpha(t)) + h + g) + c_i(-\Delta \dot{\alpha}(t) \sin(\alpha(t)) + \dot{h}(t)) \right), \end{aligned} \quad (5.11)$$

where

$$\phi(t) = \begin{cases} 1, & \text{if } \Delta \cos \alpha(t) + h(t) + g < 0 \quad \text{and} \quad \dot{h}(t) - \Delta \dot{\alpha}(t) \cos(\alpha(t)) < 0 \\ 0, & \text{in all other cases,} \end{cases} \quad (5.12)$$

with the initial conditions,

$$\alpha(0) = 0 \quad , \quad \dot{\alpha}(0) = 0 \quad , \quad c(0) = \frac{\nu}{r} \quad , \quad h(0) = 0 \quad , \quad \dot{h}(0) = 0. \quad (5.13)$$

## 5.2 Dimensionless vibro-impact electromechanical system

In this section, the initial value problem to the vibro-impact electromechanical system is presented in a dimensionless form used for simulations. To get the dimensionless form, we take  $\dot{\alpha}(t) = u(t)$  and  $\dot{h}(t) = \eta(t)$ , and rewrite the initial value problem defined by Eqs. (5.9) to (5.13) as a first order system, as follows

$$\begin{aligned}
 \dot{u}(t) &= \left\{ -[b_m + m_c \Delta^2 u(t) \cos(\alpha(t)) \sin(\alpha(t)) + c_{\text{pin}} \Delta^2 \cos(\alpha(t))^2 \right. \\
 &\quad \left. - c_{\text{ext}} \Delta^2 \sin(\alpha(t))^2] u(t) m_h + k_e c(t) m_h - c_{\text{int}} \eta(t) m_h \Delta \sin(\alpha(t)) \right. \\
 &\quad \left. - (k_{h1} h(t) + k_{h3} h^3(t)) m_h \Delta \sin(\alpha(t)) \right\} \\
 &\quad / m_h (j_m + m_c \Delta^2 \sin(\alpha(t))^2) \\
 \dot{\eta}(t) &= \left\{ -[b_m + c_{\text{pin}} \Delta^2 \cos(\alpha(t))^2 - c_{\text{ext}} \Delta^2 \sin(\alpha(t))^2] u(t) m_h \Delta \sin(\alpha(t)) \right. \\
 &\quad \left. + k_e c(t) m_h \Delta \sin(\alpha(t)) - j_m \Delta u^2(t) \cos(\alpha(t)) \right. \\
 &\quad \left. - \phi(t) [k_i (\Delta \cos(\alpha(t)) + h(t) + g) + c_i (-\Delta u(t) \sin(\alpha(t)) + \eta(t))] \right. \\
 &\quad \left. [j_m + m_c \Delta \sin(\alpha(t))^2] \right. \\
 &\quad \left. - [c_{\text{int}} \eta(t) + k_{h1} h(t) + k_{h3} h^3(t)] [j_m + (m_c + m_h) \Delta \sin(\alpha(t))^2] \right\} \\
 &\quad / m_h (j_m + m_c \Delta^2 \sin(\alpha(t))^2) \\
 c(t) &= \frac{1}{l} (\nu - k_e u(t) - r c(t))
 \end{aligned} \tag{5.14}$$

where

$$\phi(t) = \begin{cases} 1, & \text{if } \Delta \cos(\alpha(t)) + h(t) + g < 0 \quad \text{and} \quad \eta(t) - \Delta u(t) \sin(\alpha(t)) < 0, \\ 0, & \text{in all other cases,} \end{cases} \tag{5.15}$$

Writing

$$\begin{aligned}
 t &= \frac{l}{r} s, & \alpha\left(\frac{l s}{r}\right) &= p(s), & u\left(\frac{l s}{r}\right) &= \frac{r q(s)}{l}, \\
 c\left(\frac{l s}{r}\right) &= \frac{k_e w(s)}{l}, & h\left(\frac{l s}{r}\right) &= \Delta a(s), & \eta\left(\frac{l s}{r}\right) &= \frac{r}{l} \Delta y(s)
 \end{aligned} \tag{5.16}$$

one gets that  $s$  is dimensionless parameter. The functions  $p(s)$ ,  $q(s)$ ,  $w(s)$ ,  $a(s)$  and  $y(s)$  are dimensionless functions. By substituting the new functions into the Eq. (5.14) one obtains

$$\begin{aligned}
 q'(s) = & \left\{ -v_3 q(s) - v_1 q^2(s) \cos(p(s)) \sin(p(s)) \right. \\
 & - v_{12} q(s) \cos(p(s))^2 + v_{11} q(s) \sin(p(s))^2 + v_2 w(s) \\
 & \left. - v_9 y(s) \sin(p(s)) - [v_4 a(s) + v_{18} a^2(s) + v_6 a^3(s)] \sin(p(s)) \right\} \\
 & \left\{ \frac{1}{1 + v_1 \sin(p(s))^2} \right\} \quad (5.17)
 \end{aligned}$$

$$\begin{aligned}
 y'(s) = & \left\{ -v_3 q(s) \sin(p(s)) - v_{12} q(s) \cos(p(s))^2 \sin(p(s)) + v_{11} q(s) \sin(p(s))^3 \right. \\
 & + v_2 w(s) \sin(p(s)) + q^2(s) \cos(p(s)) - [v_{10} + v_9 \sin(p(s))^2 (v_8 + 1)] y(s) \\
 & - [v_5 + v_4 \sin(p(s))^2 (v_8 + 1)] a(s) - [v_7 + v_6 \sin(p(s))^2 (v_8 + 1)] a^3(s) \\
 & - \phi(s) [(v_{13} + v_{14} v_8 \sin(p(s))^2) (\cos(p(s)) + a(s) + v_{15}) \\
 & \left. - (v_{16} + v_{17} v_{18} \sin(p(s))^2) (q(s) \sin(p(s)) - y(s))] \right\} \\
 & \left\{ \frac{1}{1 + v_1 \sin(p(s))^2} \right\} \quad (5.18)
 \end{aligned}$$

$$w'(s) = -w(s) - q(s) + v_0 \quad (5.19)$$

$$p'(s) = q(s) \quad (5.20)$$

$$a'(s) = y(s) \quad (5.21)$$

where ' denotes the derivative with respect to  $s$  and  $v_i$ ,  $i = 0, \dots, 19$  are dimensionless parameters given by

$$\begin{aligned}
 v_0 &= \frac{\nu l}{k_e r}, & v_1 &= \frac{\Delta^2 m_c}{j_m}, & v_2 &= \frac{k_e^2 l}{j_m r^2}, & v_3 &= \frac{b_m l}{j_m r}, & v_4 &= \frac{k_{h1} l^2 \Delta^2}{j_m r^2}, \\
 v_5 &= \frac{k_{h1} l^2}{m_h r^2}, & v_6 &= \frac{k_{h3} l^2 \Delta^4}{j_m r^2}, & v_7 &= \frac{k_{h3} l^2 \Delta^2}{m_h r^2}, & v_8 &= \frac{m_c}{m_h}, & v_9 &= \frac{c_{int} \Delta^2 l}{j_m r}, \\
 v_{10} &= \frac{c_{int} l}{m_h r}, & v_{11} &= \frac{c_{ext} l \Delta^2}{j_m r}, & v_{12} &= \frac{c_{pin} l \Delta^2}{r}, & v_{13} &= \frac{k_i l^2}{m_h r^2}, & v_{14} &= \frac{k_i l^2 \Delta^2}{j_m r^2}, \\
 v_{15} &= \frac{g}{\Delta}, & v_{16} &= \frac{c_i l}{m_h r}, & v_{17} &= \frac{c_i l \Delta^2}{j_m r}.
 \end{aligned} \quad (5.22)$$

### 5.3 Measure of the system performance

At time  $t$ , the electric power introduced by the electrical grid in the motor is

$$\pi_{\text{in}}(t) = \nu c(t). \quad (5.23)$$

Let  $t_b^j$  and  $t_e^j$  be the instants of begin and end of the  $j$ -th impact, such that for all  $t$  belonging to  $[t_b^j, t_e^j]$ , we have  $\dot{x}(t) + \dot{h}(t) < 0$ . At time  $t$ , the impact power,  $\pi_{\text{imp}}^j(t)$ , is then written as

$$\pi_{\text{imp}}^j(t) = k_i (x(t) + h(t)) (\dot{x}(t) + \dot{h}(t)), \quad t_b^j \leq t \leq t_e^j. \quad (5.24)$$

The time average of the impact power during the  $j$ -th impact,  $\underline{\pi}_{\text{imp}}^j$ , is written as

$$\underline{\pi}_{\text{imp}}^j = \frac{1}{t_e^j - t_b^j} \int_{t_b^j}^{t_e^j} \pi_{\text{imp}}^j(t) dt. \quad (5.25)$$

The sum,  $\pi_{\text{imp}}$ , of the averages of the impact powers, which is one of the variable of interest in the design optimization problem, is written as

$$\pi_{\text{imp}} = \sum_{j=1}^{N_{\text{imp}}} \underline{\pi}_{\text{imp}}^j, \quad (5.26)$$

where  $N_{\text{imp}}$  is the total number of impacts that occur during time interval  $[0, T]$ . The time average of the electric power consumed in this time interval is

$$\pi_{\text{elec}} = \frac{1}{T} \int_0^T \pi_{\text{in}}(t) dt. \quad (5.27)$$

These two variables,  $\pi_{\text{imp}}$  and  $\pi_{\text{elec}}$ , are chosen to measure the system performance. The biggest  $\pi_{\text{imp}}$  is and the smaller  $\pi_{\text{elec}}$  is, better will be the system performance.

### 5.4 Sensitivity analysis and choice of the design parameters

To understand the role played by each system parameter in  $\pi_{\text{imp}}$  and  $\pi_{\text{elec}}$ , a sensitivity analysis has been done. The objective was to determine what were the system parameters that had the biggest influence in  $\pi_{\text{imp}}$  and  $\pi_{\text{elec}}$ , in order to define those that will be the design parameters for the robust design optimization problem. The initial value problem defined by Eqs. (5.9) to (5.13) has been rewritten in a dimensionless form for computation and some dimensionless parameters were defined. However, in the sensitivity analysis, these dimensionless parameters were not considered as varying parameters since they do not have an easy physical interpretation. The varying parameters used for the numerical simulations are related with the design of the cart and the embarked hammer. They are:

- $m_c/m_h$ , relation between the hammer mass and the cart mass;
- $k_{h1}/m_h$ , relation between the linear stiffness of the spring component and hammer mass (a sort of natural frequency of the hammer);
- $g$ , horizontal distance from the hammer (when  $\alpha = \pi/2$  rad) to the equilibrium position of the barrier;
- $\Delta$ , eccentricity of the pin. This parameter determines the length of the cart path.

The other parameters, related with the motor properties and viscous friction coefficients, are fixed and the values of these fixed parameters are given in Table 5.1. The output responses are  $\pi_{\text{imp}}$  and  $\pi_{\text{elec}}$ . For computation, the

Table 5.1: Values of the system parameters used in simulations.

Parameter	Value	Parameter	Value
$m_c$	0.50 Kg	$\nu$	2.4 V
$r_h$	0.30 1/m <sup>2</sup>	$r$	0.307 $\Omega$
$c_{pin}$	5.00 Ns/m	$l$	$1.88 \times 10^{-4}$ H
$c_{ext}$	5.00 Ns/m	$j_m$	$1.21 \times 10^{-4}$ Kg m <sup>2</sup>
$\varsigma_{int}$	0.05	$b_m$	$1.5452 \times 10^{-4}$ Nm/(rad/s)
$k_i$	$10^6$ N/m	$k_e$	0.0533 V/(rad/s)
$c_i$	$10^3$ Ns/m		

initial value problem defined by Eqs. (5.9) to (5.13) has been rewritten in the dimensionless form given by Eqs. (5.17) to (5.22). The main objective was to reduce the computation time. Duration is chosen as  $T = 10.0$  s. The 4th-order Runge-Kutta method is used for the time-integration scheme for which we have implemented a varying time-step. The time-step is adapted to the state of the dynamical system according to the occurrence or the non occurrence of impacts. When the hammer is not impacting the barrier, the time-step used is  $10^{-4}$  s, but when the hammer is approaching the barrier and when it is impacting it, the time-step is chosen as the value  $10^{-5}$  s. Simulations with different values to the initial conditions, were performed. As it was verified that they do not have a significant influence in  $\pi_{\text{imp}}$  and  $\pi_{\text{elec}}$ , in all simulations the initial conditions were taken as constant, given by Eq. (5.13). Concerning the sensitivity analysis, 20,000 numerical simulations have been carried out combining the following values of the parameters: 10 values for  $m_c/m_h$  selected in the interval  $[0.10, 2.00]$ , 10 values for  $k_{h1}/m_h$  in  $[657, 4410]$  rad<sup>2</sup>/s<sup>2</sup>, 10 values for  $g$  in  $[0, 0.02]$  m, and 20 values for  $\Delta$  in  $[0.003, 0.013]$  m. Due the high numerical cost of these simulations, some strategies were adopted to reduce the computation time:

- the varying time-step integration scheme was used for numerical iterations;
- the initial value problem has been rewritten in a dimensionless form, the computation time of each simulation was reduced from 8 minutes to 5 minutes on average;
- parallelization of the simulations: a cluster in the Laboratoire de Modélisation et Simulation Multi-Echelle of Université Paris-Est with 20 computers was used to make the simulations, as shown in Fig 5.4.

With these strategies, the computational time necessary to perform the 20,000 numerical simulations were approximately 3.5 days. The largest value of  $\pi_{\text{imp}}$ ,

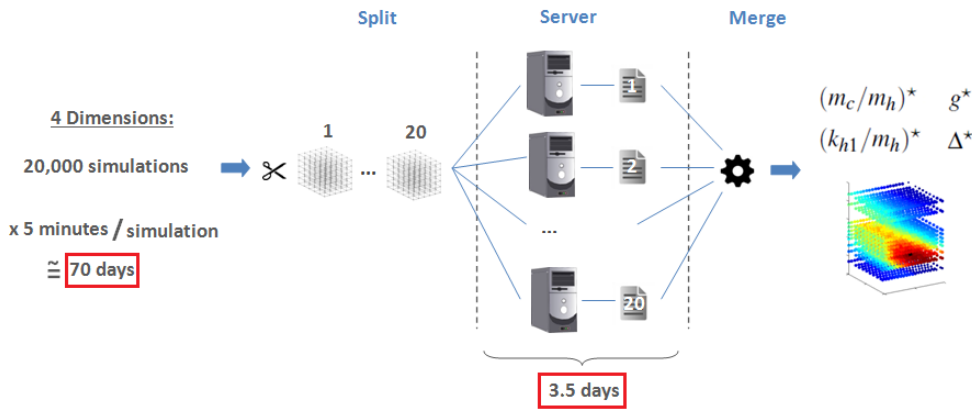


Figure 5.2: Parallelization of the simulations in the sensitivity analysis.

obtained with such numerical simulations, is 5,690 W, and is reached for the following values of the parameters:  $(m_c/m_h)^* = 0.40$ ,  $(k_{h1}/m_h)^* = 1,580 \text{ rad}^2/\text{s}^2$ ,  $g^* = 0.011 \text{ m}$ , and  $\Delta^* = 0.013 \text{ m}$ . With these values, the average of the consumed electric power is  $\pi_{\text{elec}} = 3.93 \text{ W}$ . For  $\Delta = \Delta^*$  and  $m_c/m_h = (m_c/m_h)^*$ , Fig. 5.3 displays  $\pi_{\text{imp}}$  as a function of parameters  $g$  and  $k_{h1}/m_h$ . In Fig. 5.3(a),  $g$  and  $k_{h1}/m_h$  vary in all its range of values, and in Fig. 5.3(b), they vary in  $[0.06, 0.02]$  and  $[1\,250, 1\,953]$  respectively. These figures show that, the optimal value of the design parameter correspond to a global maximum. The influence of each parameter in  $\pi_{\text{imp}}$  and  $\pi_{\text{elec}}$  can be observed through the graphs plotted in Figs. 5.4 to 5.7. Regarding all the graphs of  $\pi_{\text{imp}}$  and  $\pi_{\text{elec}}$  as a function  $m_c/m_h$ ,  $k_{h1}/m_h$ ,  $g$  and  $\Delta$ , it can be seen that small variations on  $g$ ,  $k_{h1}/m_h$ , and  $\Delta$  induce large variations for  $\pi_{\text{imp}}$  and for  $\pi_{\text{elec}}$ , but the same phenomenon does not occur with respect to the parameter  $m_c/m_h$ . Thus, while  $\pi_{\text{imp}}$  and  $\pi_{\text{elec}}$  are not very sensitive to  $m_c/m_h$ , they are sensitive to  $k_{h1}/m_h$ ,  $g$  and  $\Delta$ . It is also seen, that two different kinds of sensitivity can be distinguished among these three parameters. For parameters  $k_{h1}/m_h$  and  $g$ , it can be seen

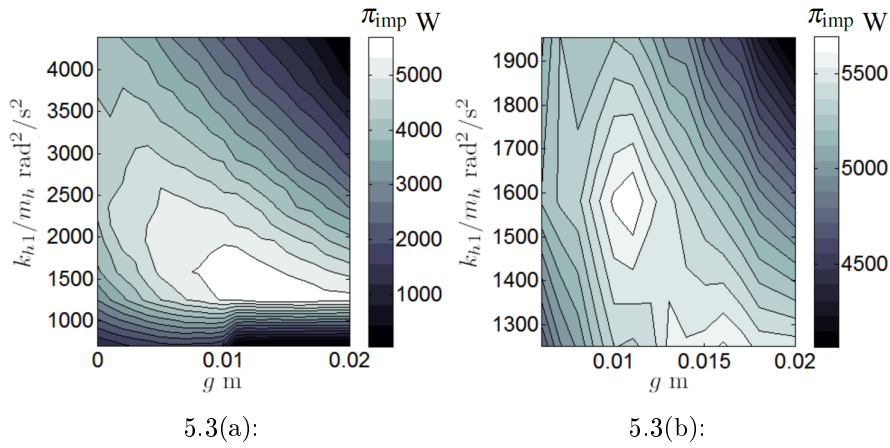


Figure 5.3: For the optimal values  $(m_c/m_h)^*$  and  $\Delta^*$ : (a) graph of  $\pi_{\text{imp}}$  as a function of  $g$  and  $k_{h1}/m_h$  (varying in all its range of values), (b) graph of  $\pi_{\text{imp}}$  as a function of  $g$  and  $k_{h1}/m_h$  (varying in  $[0.06, 0.02]$  and  $[1250, 1953]$  respectively).

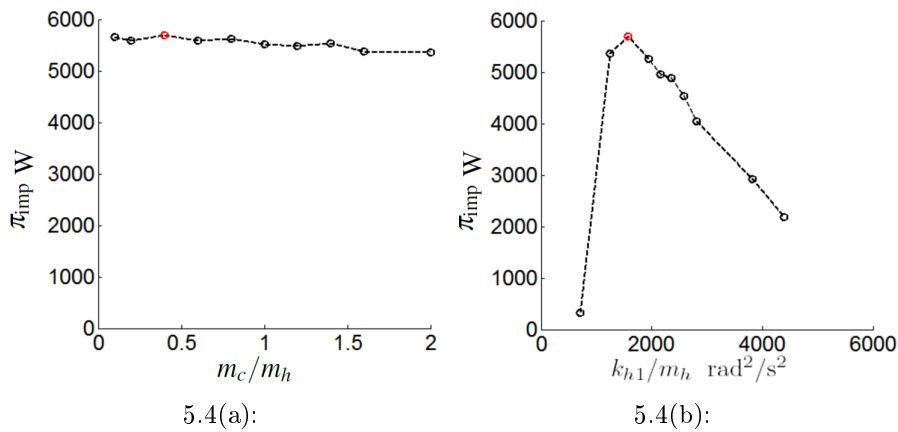


Figure 5.4: (a) Graph of  $\pi_{\text{imp}}$  as a function of  $m_c/m_h$  with  $(k_{h1}/m_h)^*$ ,  $g^*$ , and  $\Delta^*$ . (b) Graph of  $\pi_{\text{imp}}$  as a function of  $k_{h1}/m_h$  with  $(m_c/m_h)^*$ ,  $g^*$ , and  $\Delta^*$ .

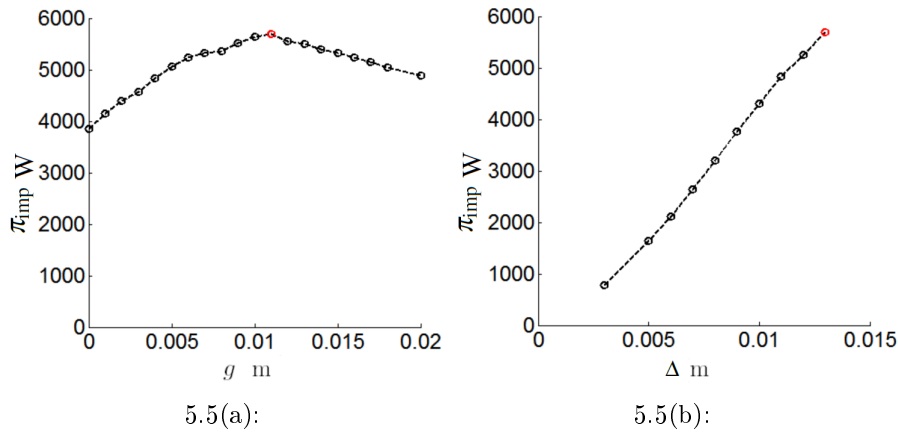


Figure 5.5: (a) Graph of  $\pi_{\text{imp}}$  as a function of  $g$  with  $(m_c/m_h)^*$ ,  $(k_{h1}/m_h)^*$ , and  $\Delta^*$ . (b) Graph of  $\pi_{\text{imp}}$  as a function of  $\Delta$  with  $(m_c/m_h)^*$ ,  $(k_{h1}/m_h)^*$ , and  $g^*$ .

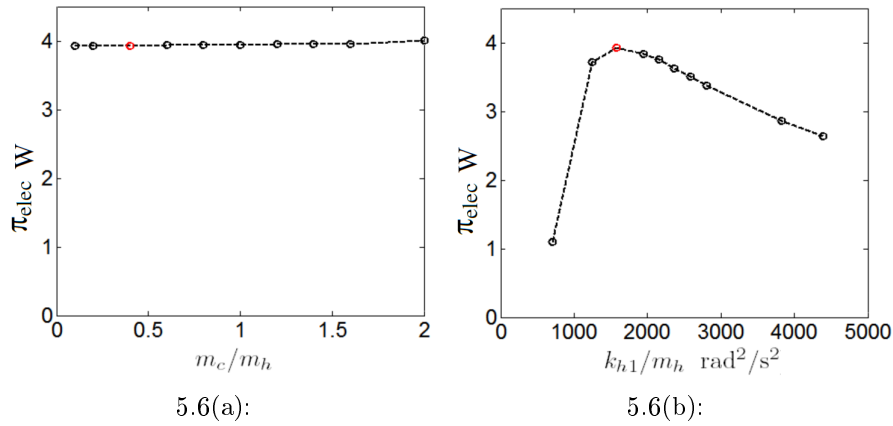


Figure 5.6: (a) Graph of  $\pi_{elec}$  as a function of  $m_c/m_h$  with  $(k_{h1}/m_h)^*$ ,  $g^*$ , and  $\Delta^*$ . (b) Graph of  $\pi_{elec}$  as a function of  $k_{h1}/m_h$  with  $(m_c/m_h)^*$ ,  $g^*$ , and  $\Delta^*$ .

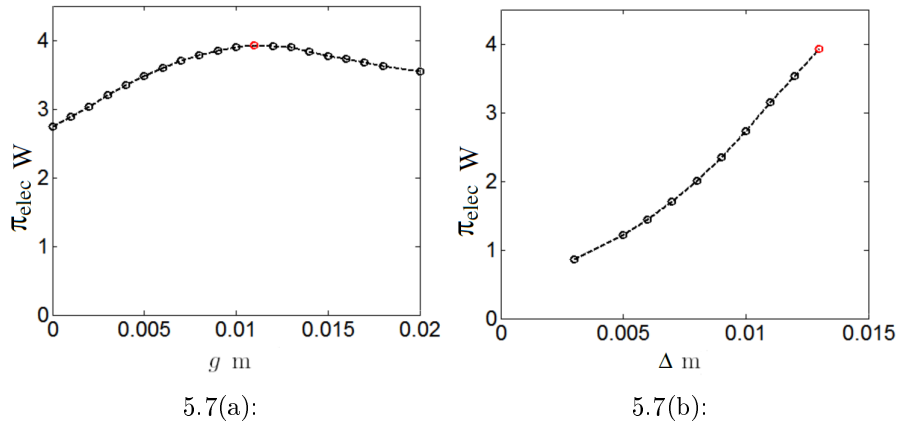


Figure 5.7: (a) Graph of  $\pi_{elec}$  as a function of  $g$  with fix  $(m_c/m_h)^*$ ,  $(k_{h1}/m_h)^*$ , and  $\Delta^*$ . (b) Graph of  $\pi_{elec}$  as a function of  $\Delta$  with fix  $(m_c/m_h)^*$ ,  $(k_{h1}/m_h)^*$ , and  $g^*$ .

that  $\pi_{imp}$  and  $\pi_{elec}$  reach their maxima when  $k_{h1}/m_h$  and  $g$  are equal to 1, 580  $\text{rad}^2/\text{s}^2$  and 0.011 m respectively. For parameter  $\Delta$  varying in its range of values, Figs. 5.5(b) and 5.7(b) show that the highest is  $\Delta$ , the highest are  $\pi_{imp}$  and  $\pi_{elec}$ . It has been considered as not necessarily to verify the behavior of  $\pi_{imp}$  and  $\pi_{elec}$  for a larger range of  $\Delta$  because the value  $\Delta = 0.013$  m is already sufficiently large when compared with the system dimensions and the motor properties. It should be noted that if parameter  $\Delta$  is increased, then, the nonlinearities would increase also, but that is not the objective of the analysis. Considering that  $m_c/m_h$  does not have a significant influence in  $\pi_{imp}$  and  $\pi_{elec}$ , and considering that the sensitivity of the parameter  $\Delta$  is easily predictable, these two parameters will not be considered as design parameters in the robust design optimization problem. Only parameters  $g$  and  $k_{h1}/m_h$  will thus be considered as design parameters.

## 5.5 Construction of the probability model

As explained in the introduction, this chapter deals with the robust design of the electromechanical system in presence of uncertainties in the computational model. The three parameters that are assumed to be uncertain are  $k_{h1}$ ,  $k_i$  and  $c_i$ , which are modeled by the independent random variables  $K_{h1}$ ,  $K_i$  and  $C_i$ . The probability distribution of each one is constructed using the Maximum Entropy Principle [34, 88, 89, 91, 85, 94, 95]. This Principle allows the probability distribution of a random variable to be constructed using only the available information, avoiding the use of any additional information that introduces a bias on the estimation of the probability distribution. If a large amount of experimental data are available, then the nonparametric statistics can be used. If there are no available experimental data, or if there are only a few experimental data, then the Maximum Entropy from Information Theory is the most efficient tool for constructing a prior probability model. The Maximum Entropy Principle states: out of all probability distributions consistent with a given set of available information, choose the one that has maximum uncertainty (the Shannon measure of entropy). The available information of the random variables is defined as

1.  $K_{h1}$ ,  $K_i$  and  $C_i$  are positive-valued independent random variables,
2. the mean values are known:  $E\{K_i\} = \underline{K}_i$ ,  $E\{C_i\} = \underline{C}_i$  and  $E\{K_{h1}\} = \underline{K}_{h1}$ ,
3. in order that the response of the dynamical system be a second-order stochastic process, we impose the following conditions:  $\|E\{\log K_i\}\| < \infty$ ,  $\|E\{\log C_i\}\| < \infty$  and  $\|E\{\log K_{h1}\}\| < \infty$ .

Thus, the Maximum Entropy Principle for each random variable  $K_i$ ,  $C_i$ , and  $K_{h1}$ , yields a Gamma distribution (see [90]),

$$p(a) = \mathbb{1}_{[0,+\infty)}(a) \frac{1}{\mu} \left(\frac{1}{\delta^2}\right)^{\frac{1}{\delta^2}} \frac{1}{\Gamma(1/\delta^2)} \left(\frac{a}{\mu}\right)^{\frac{1}{\delta^2}-1} \exp\left(-\frac{a}{\delta^2\mu}\right), \quad (5.28)$$

where  $\mathbb{1}_{[0,+\infty)}(a)$  is an indicator function that is equal to 1 for  $a \in [0, +\infty)$  and 0 otherwise, and where

- $\Gamma$  is the Gamma function:  $\Gamma(b) = \int_0^\infty t^{b-1} \exp(-t) dt$ ;
- $\delta = \frac{\sigma}{\mu}$  is the coefficient variation of the random variable,  $\mu$  is its mean value representing  $\underline{K}_i$ ,  $\underline{C}_i$ , or  $\underline{K}_{h1}$ , and  $\sigma$  is its standard deviation.

## 5.6 Robust design optimization problem

In order to formulate the robust design problem, the set of all the system parameters is divided into three subsets. The first subset is the family of the fixed parameters that is represented by the vector  $\mathbf{p}_{\text{fix}} = \{ \nu, l, r, j_m, k_e, b_m, c_{\text{pin}}, c_{\text{ext}}, s_{\text{int}}, r_h, m_c, m_h, \Delta \}$ . The second one is the family of the design parameters that is represented by the vector  $\mathbf{p}_{\text{des}} = \{ \underline{K}_{h1}/m_h, g \}$ . The third one is the family of the uncertain parameters that is represented by the random vector  $\mathbf{P}_{\text{unc}} = \{ K_i, C_i, K_{h1} \}$ . Since  $\mathbf{P}_{\text{unc}}$  is a random vector, the outputs of the electromechanical system are stochastic processes and, consequently,  $\pi_{\text{imp}}(\mathbf{p}_{\text{des}}, \mathbf{p}_{\text{unc}})$  and  $\pi_{\text{elec}}(\mathbf{p}_{\text{des}}, \mathbf{p}_{\text{unc}})$ , become random variables  $\Pi_{\text{imp}}(\mathbf{p}_{\text{des}}) = \pi_{\text{imp}}(\mathbf{p}_{\text{des}}, \mathbf{P}_{\text{unc}})$  and  $\Pi_{\text{elec}}(\mathbf{p}_{\text{des}}) = \pi_{\text{elec}}(\mathbf{p}_{\text{des}}, \mathbf{P}_{\text{unc}})$ . The cost function of the robust design optimization problem is defined by

$$J(\mathbf{p}_{\text{des}}) = E\{\Pi_{\text{imp}}(\mathbf{p}_{\text{des}})\}. \quad (5.29)$$

The robust design optimization problem is written as

$$\mathbf{p}_{\text{des}}^{\text{opt}} = \arg \max_{\mathbf{p}_{\text{des}} \in \mathcal{C}_{ad}} J(\mathbf{p}_{\text{des}}), \quad (5.30)$$

in which  $\mathcal{C}_{ad} = \{ \mathbf{p}_{\text{des}} \in \mathcal{P}_{\text{des}}; E\{\Pi_{\text{elec}}(\mathbf{p}_{\text{des}})\} \leq c_{\text{elec}} \}$ , where  $\mathcal{P}_{\text{des}}$  is the admissible set of the values of  $\mathbf{p}_{\text{des}}$ , and where  $c_{\text{elec}}$  is an upper bound.

## 5.7 Results of the robust optimization problem

The hyperparameters  $\delta_{K_i}$  and  $\delta_{C_i}$ , which control the level of uncertainties for  $K_i$  and  $C_i$  are fixed to 0.1. The robust design optimization problem is then solved for three levels of uncertainties for  $K_{h1}$ , defined by the following values of the hyperparameters  $\delta_{K_{h1}} = 0$ ,  $\delta_{K_{h1}} = 0.1$ , and  $\delta_{K_{h1}} = 0.4$ . The optimization problem is also considered without uncertainties in the systems parameters, that is, the deterministic case ( $\delta_{K_{h1}} = \delta_{K_i} = \delta_{C_i} = 0$ ). For  $\mathbf{p}_{\text{des}} \in \mathcal{C}_{ad}$ , the cost function is estimated by the Monte Carlo simulation method using 100 independent realizations of random vector  $\mathbf{P}_{\text{unc}}$  following its probability distribution. The optimization problem (defined by Eq. (5.30)) is solved using the trial method for which the admissible set  $\mathcal{C}_{ad}$  is meshed as follows: for  $\underline{K}_{h1}/m_h$ , 13 values are nonuniformly selected in the interval  $[703, 3830]$ , and for  $g$ , 20 nonuniform values in  $[0, 0.038]$ . Thus, 26,000 numerical simulations have been carried out to solve optimization problem for each level of uncertainties. Due the high numerical cost of these simulations, the same strategies used in the sensitivity analysis were adopted to reduce the computation time. They were:

- a varying time-step integration scheme was used for numerical iterations (described in Section 5.4 with duration  $T = 10.0$  s),
- the initial value problem has been rewritten in a dimensionless form, the computation time of each simulation was reduced from 8 minutes to 5 minutes on average;
- parallelization of the simulations: a cluster in the Laboratoire de Modélisation et Simulation Multi-Echelle of Université Paris-Est with 20 computers was used to make the simulations.

These strategies allowed us to solve the optimization problem (defined by Eq. (5.30)) with the trial method. With the reduction of computation time, different kind of algorithms, as evolutionary algorithms or random search algorithm were not necessary. The computational time necessary to perform the 26,000 numerical simulations were approximately 4.5 days for each level of uncertainties. The values of the fixed parameters are  $m_c = 0.3$  Kg,  $m_h =$

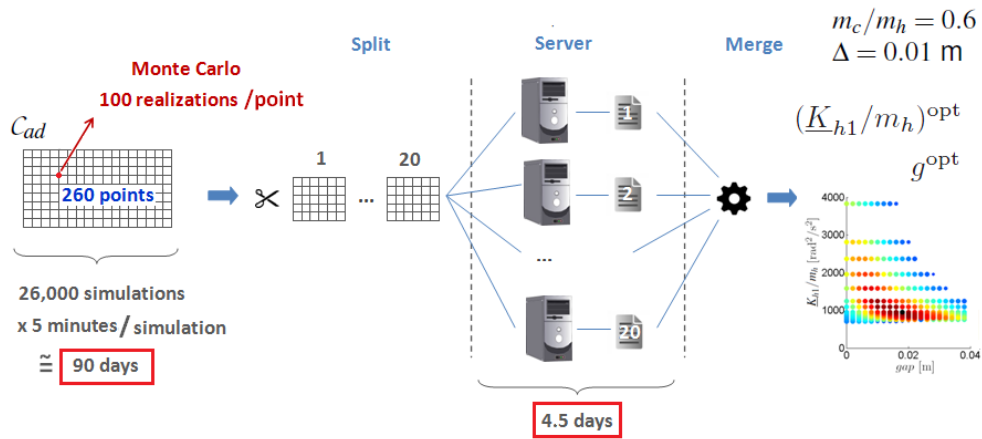


Figure 5.8: Parallelization of the simulations performed to solve the robust optimization problem.

0.5 Kg,  $\Delta = 0.01$  m, and the others are given in Table 5.1. Upper bound  $c_{elec}$  is fixed to the value 6.00 W. For the deterministic case, the components of the optimal solution  $\mathbf{p}_{des}^{opt}$  are  $(\underline{K}_{h1}/m_h)^{opt} = 1,580 \text{ rad}^2/\text{s}^2$  and  $g^{opt} = 0.011$  m. For case with uncertainties, for which  $\delta_{K_i}$  is fixed to 0.1, and  $\delta_{C_i}$  to 0.1, we obtain, for  $\delta_{K_{h1}} = 0$ ,  $(\underline{K}_{h1}/m_h)^{opt} = 957 \text{ rad}^2/\text{s}^2$  and  $g^{opt} = 0.018$  m, for  $\delta_{K_{h1}} = 0.1$ ,  $(\underline{K}_{h1}/m_h)^{opt} = 1,950 \text{ rad}^2/\text{s}^2$  and  $g^{opt} = 0.008$  m, and for  $\delta_{K_{h1}} = 0.4$ ,  $(\underline{K}_{h1}/m_h)^{opt} = 2,360 \text{ rad}^2/\text{s}^2$  and  $g^{opt} = 0.008$  m. Figures 5.9 and 5.10 display the graphs of the cost function defined by Eq. (5.29) as a function of the design parameter for these four cases. These figures show that, for each case, the optimal value of the design parameter correspond to a global maximum in  $\mathcal{C}_{ad}$ . The role played by uncertainties on the optimal values of the design

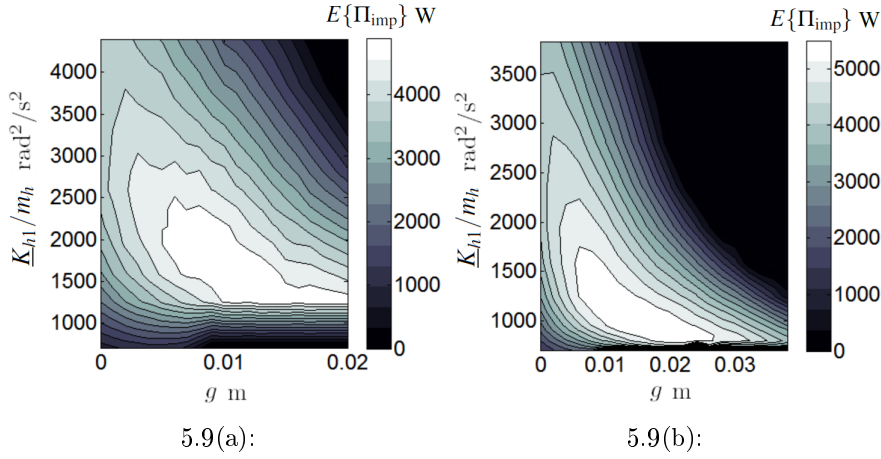


Figure 5.9: (a) Cost function as function of the design parameters for the deterministic case. (b) Cost function as function of the design parameters for the case in which  $\delta_{K_i} = \delta_{C_i} = 0.1$  and  $\delta_{K_{h1}} = 0$ .

parameters can be analyzed through Figs. 5.11 and 5.12, which display the graphs  $g \mapsto E\{\Pi_{\text{imp}}((\underline{K}_{h1}/m_h)^{\text{opt}}, g)\}$ ,  $\underline{K}_{h1}/m_h \mapsto E\{\Pi_{\text{imp}}(\underline{K}_{h1}/m_h, g^{\text{opt}})\}$ ,  $g \mapsto E\{\Pi_{\text{elec}}((\underline{K}_{h1}/m_h)^{\text{opt}}, g)\}$ , and  $\underline{K}_{h1}/m_h \mapsto E\{\Pi_{\text{elec}}(\underline{K}_{h1}/m_h, g^{\text{opt}})\}$ . These figures show that the optimal design point strongly depends on the level of uncertainties. In particular, it can be deduced that the mean value of the electric power increases with the increase of the gap. The robustness of the optimal design point,  $\mathbf{p}_{\text{des}}^{\text{opt}}$ , can be analyzed in studying the evolution of the coefficient variation,  $\delta_{\Pi_{\text{imp}}}(\mathbf{p}_{\text{des}}^{\text{opt}})$ , of random variable  $\Pi_{\text{imp}}(\mathbf{p}_{\text{des}}^{\text{opt}})$  as a function of the uncertainty level. However, in order to better analyze the sensitivity of the responses with respect to the uncertainty level, we have constructed Fig. 5.13 that displays the graphs  $g \mapsto \delta_{\Pi_{\text{imp}}}((\underline{K}_{h1}/m_h)^{\text{opt}}, g)$  and  $\underline{K}_{h1}/m_h \mapsto \delta_{\Pi_{\text{imp}}}(\underline{K}_{h1}/m_h, g^{\text{opt}})$ . For each level of uncertainties, it can be seen that the value  $\delta_{\Pi_{\text{imp}}}(\mathbf{p}_{\text{des}}^{\text{opt}})$  occurs in a region for which the two following functions  $g \mapsto \delta_{\Pi_{\text{imp}}}((\underline{K}_{h1}/m_h)^{\text{opt}}, g)$  and  $\underline{K}_{h1}/m_h \mapsto \delta_{\Pi_{\text{imp}}}(\underline{K}_{h1}/m_h, g^{\text{opt}})$  are minima. This means the optimal design point is robust with respect to uncertainties.

## 5.8 Summary of the Chapter

In this chapter of the Thesis, the formulation and the solution of a robust design optimization problem have been presented for a nonlinear electromechanical vibro-impact system in presence of uncertainties in the computational model. Since this nonlinear electromechanical system is devoted to the vibro-impact optimization, the time responses exhibit numerous shocks that have to be identified with accuracy, and consequently, a very small time-step is re-

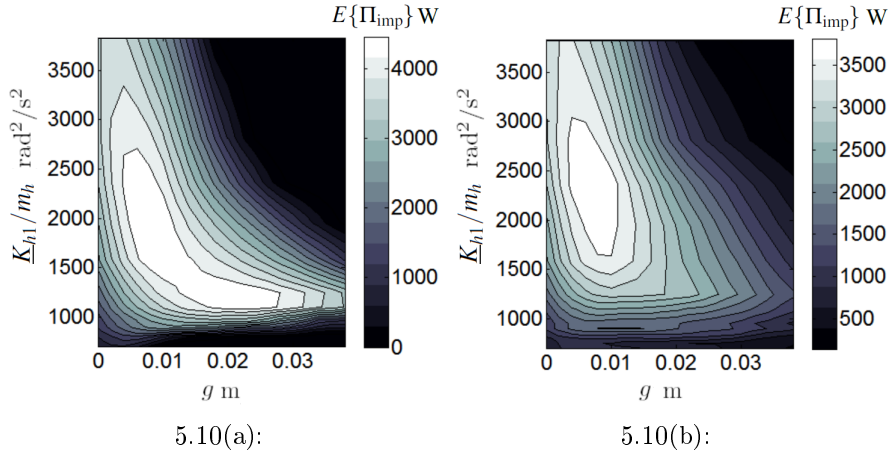


Figure 5.10: (a) Cost function as function of the design parameters for the case in which  $\delta_{K_i} = \delta_{C_i} = \delta_{K_{h1}} = 0.1$ . (b) Cost function as function of the design parameters for the case in which  $\delta_{K_i} = \delta_{C_i} = 0.1$  and  $\delta_{K_{h1}} = 0.4$ .

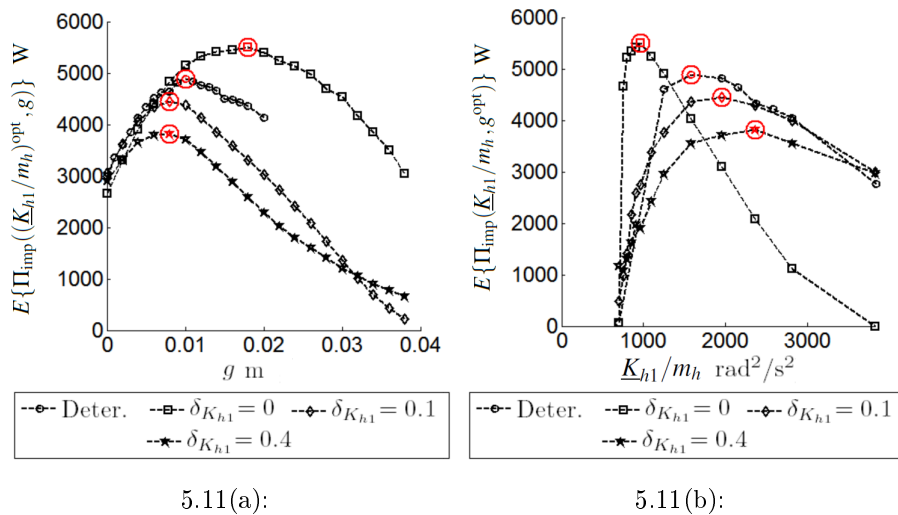


Figure 5.11: (a) Cost function as function of  $g$  with  $(\underline{K}_{h1}/m_h)^{\text{opt}}$ . (b) Cost function as function of  $\underline{K}_{h1}/m_h$  with  $g^{\text{opt}}$ . In both graphs, the  $E\{\Pi_{\text{imp}}(\mathbf{p}_{\text{des}}^{\text{opt}})\}$  is highlighted for each level of uncertainties with markers.

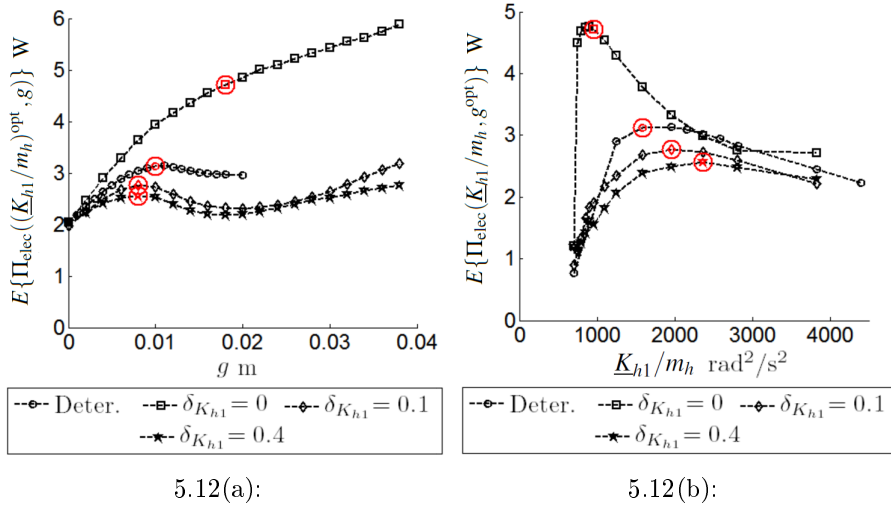


Figure 5.12: (a) Mean value of the time average of electric power as function of  $g$  with  $(\underline{K}_{h1}/m_h)^{\text{opt}}$ . (b) Mean value of the time average of electric power as function of  $\underline{K}_{h1}/m_h$  with  $g^{\text{opt}}$ . In both graphs, the  $E\{\Pi_{\text{elec}}(\mathbf{p}_{\text{des}}^{\text{opt}})\}$  is highlighted for each level of uncertainties with markers.

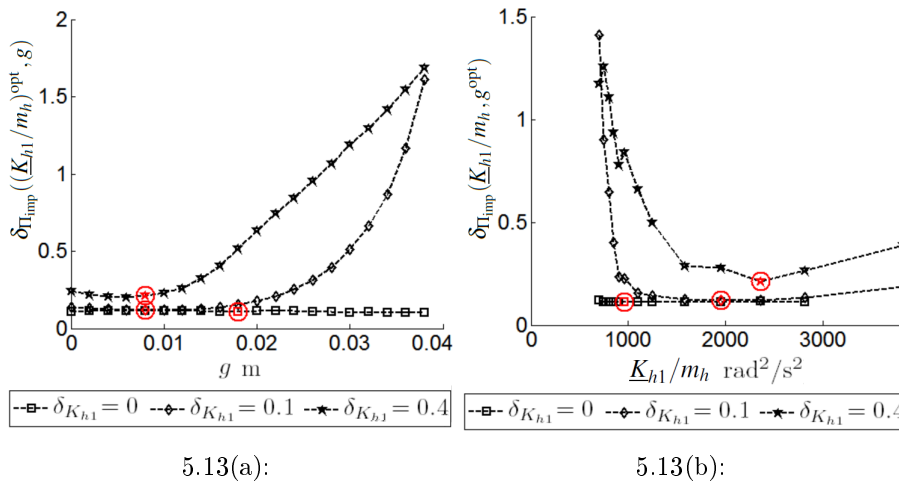


Figure 5.13: (a) Coefficient variation of  $\Pi_{\text{imp}}$  as function of  $g$  with  $(\underline{K}_{h1}/m_h)^{\text{opt}}$ . (b) Coefficient variation of  $\Pi_{\text{imp}}$  as function of  $\underline{K}_{h1}/m_h$  with  $g^{\text{opt}}$ . In both graphs, the  $\delta_{\Pi_{\text{imp}}}(\mathbf{p}_{\text{des}}^{\text{opt}})$  is highlighted for each level of uncertainties with markers.

quired. We have thus chosen an explicit time-integration scheme and not an implicit one. Nevertheless, due to the presence of low-frequency contributions in the time responses, a long time duration is required, which will imply a huge number of integration time-step if the time-step was chosen constant. This is the reason why we have implemented an adaptive integration time-step. It was one of the difficulties encountered for the solver implementation. The use of a varying time-step integration scheme was not the only strategy adopted to reduce the computation time. The initial value problem has been rewritten in a dimensionless form, which reduced the computation time of each simulation from 8 minutes to 5 minutes on average. Furthermore, a cluster with 20 computers has been used to parallelize the simulations carried out in the sensitivity analysis and in the optimization problem. Observing the results of numerical integration, as time histories and phase diagrams, some interesting phenomena were verified, as for example bifurcation. Bifurcation is a typical nonlinear phenomenon, and it is frequently discussed in many works (see for instance [73]). In the analyzed vibro-impact electromechanical system, it appears because depending on the values of the system parameters, the system response will have the occurrence or the non occurrence of impacts. But this topic is an ongoing research that will be object of a future work. The construction of the solution for the design optimization problem, has been prepared by carrying out a sensitivity analysis with respect to all the possible design parameters. This pre-analysis has allowed for reducing the number of design parameters to two parameters. Consequently, a random search algorithm or a genetic algorithm was not necessary, and we have thus used a trail method. It should be noted that in the framework of a robust analysis formulated in the context of the probability theory, and taking into account the types of nonlinearities in the dynamical system, the Monte Carlo numerical simulation method has been used, and this introduces a significant increase of the numerical cost. The design optimization problem of the dynamical system without uncertainties yields an optimal design point that differs from the nominal values, and which can not be determined, *a priori*, without solving the design optimization problem. In addition, the robust analysis that has been presented demonstrates the interest that there is to take into account the uncertainties in the computational model. The optimal design point that has been identified in the robust design framework significantly differs from the design point obtained with the computational model without uncertainties. For this electromechanical system, it has been seen that, the minimum value of the dispersion of the random output occurs in the region of the optimal design parameters, which means that the optimal design point is robust with respect to uncertainties.

## 6

# Summary, future works and publications

This Thesis is a joint work between PUC-Rio and Université Paris-Est in a program of double diploma supported by the Capes-Cofecub project (number 17795/12 – 5).

In relation to the motor-cart system, we analyze the effect of the electromechanical coupling, i.e., the mutual interaction between the mechanical and electric systems. We formulated the time-evolution of the system dynamics as initial value problems, in which the coupling torque appears as a parametric excitation, i.e., a time variation of the system parameters. Numerical simulations were performed for different values of system parameters, and their results, as the graphs the systems variables over time, FFT and *phase portraits* were analyzed. The main results observed were: the existence of a periodic solution with a relation 2:1 between the period of rotation of the disk and the period of the current (a typical phenomenon of parametric excited systems) and, the characterization of the nominal eccentricity of the pin of the motor, as a parameter that controls the nonlinearities of the equations of motion of the system [42]. In [18], the existence and asymptotic stability of a periodic orbit to this motor-cart system were obtained in a mathematically rigorous way.

In relation to the motor-cart-pendulum system, by numerical simulations it was verified that the pendulum introduces a new feature to the system dynamics: it can pump energy from the motor and, in certain cases, revert the relation master-slave [42, 45, 47, 53].

In relation to the electromechanical system with internal impacts, we analyzed from a deterministic and from a stochastic view point the maximal energy stored in the barrier in impacts as function of some parameters of the electromechanical system, as  $\text{gap}/l_p$  and  $\Delta$  [54]. It was verified that for values of  $\Delta$  near zero, the graph of the impact energy as function of  $\text{gap}/l_p$ , is very similar to the graph with  $\Delta = 0$  m (which can be nicely predicted from conservation of energy). However, as  $\Delta$  increases the form of the graph changes completely and in an unexpected fashion.

In relation to the percussive electromechanical system, we performed a robust optimization respect to design parameters in order to maximize the impact power under the constraint that the electric power consumed by the DC motor is lower than a maximum value. The construction of the solution for this robust design optimization problem, has been prepared by carrying out

a sensitivity analysis with respect all the possible design parameters. This pre-analysis has allowed for reducing the number of design parameters to two parameters. The nonlinear constrained design optimization problem was formulated in the framework of robust design. It is solved for different levels of uncertainties, and also for the nominal value of deterministic design. The results are different and this show the importance of the stochastic modeling.

## 6.1 Future works

During the period of the thesis, several research topics arose from the study of electromechanical systems. In relation to the vibro-impact electromechanical system, some of the plans are:

- to analyze the impact power for different models to the barrier, considering for example, plasticity in the displacement, i.e., the barrier moves irreversibly in one direction, simulating a penetration. The objective is to model the propagation of waves in a continuous heterogeneous media, which is unbounded (due to wavelengths that would be generated), and thus there is an additional dissipation by radiation to infinity.
- to develop a controller acting the source voltage in order to synchronize the hammer and the cart movements. Since the total hammer velocity is equal to the cart velocity  $\dot{x}$  added to the relative hammer velocity in relation to the cart  $\dot{h}$ , if we could control the system in a way that  $x$  and  $h$  be in phase, the total hammer velocity could achieve higher values, and consequently, the impact power could grow.
- to consider different variables to measure the system performance, and to include this new variables in the formulation of the robust design optimization problem. Examples of these new variables are the number of impacts and frequency of impacts.

## 6.2 Publications

Concerning publications, during the period of Thesis, we have published three journal papers, see [57, 55, 42]:

[J1] “Robust design optimization with an uncertain model of a nonlinear vibro-impact electro-mechanical system”; R. Lima, C. Soize, and R. Sampaio. *Communications in Nonlinear Science and Numerical Simulation*, 23, pp. 263-273, 2015.

[J2] “Robust design of a vibro-impact electro-mechanical system”; R. Lima, C. Soize, and R. Sampaio. *Mecánica Computacional*, XXXIII(27), pp. 1813-1819, 2014.

[J3] “Stochastic analysis of an electromechanical coupled system with embarked mass”; R. Lima e R. Sampaio, *Mecánica Computacional*, XXXI(14), pp. 2783-2800, 2012.

We have submitted others two journal papers:

[J4] “Two parametric excited nonlinear systems due to electromechanical coupling”; R. Lima e R. Sampaio.

[J5] “Electromechanical system with internal impacts and uncertainties”; R. Lima e R. Sampaio.

During the period of this Thesis other works have been developed besides the work of the Thesis, which have originated four journal papers, see [52, 18, 26, 46]:

[J6] “Stick-mode duration of a dry-friction oscillator with an uncertain model”; R. Lima e R. Sampaio. To be published in *Journal of Sound and Vibration*, 2015.

[J7] “Asymptotically stable periodic orbits of a coupled electromechanical system”; M.J.H. Dantas, R. Sampaio and R. Lima. *Nonlinear Dynamics*, 78, pp. 29-35, 2014.

[J8] “Robust Identification and passive control of vibration of a test rig under uncertain conditions”; C. Fonseca, R. Lima, G. Wagner and R. Sampaio. *Mecánica Computacional*, XXXIII (27), pp. 1767-1781, 2014.

[J9] “Some remarks about stick-slip oscillators”; R. Lima and R. Sampaio. *Mecánica Computacional*, XXXII (8), pp. 647-668, 2013.

In relation to these woks developed besides the work of the Thesis, we have submitted another journal paper:

[J10] “General results of existence and asymptotic stability for a class of

electromechanical systems, M.J.H. Dantas, R. Sampaio e R. Lima.

I published a book [85].

[B1] “Modelagem Estocástica e Geração de Amostras de Variáveis e Vetores Aleatórios”, Sampaio, R. and Lima, R., Notas de Matemática Aplicada, SBMAC, 2012.

We have published fifteen conference papers: [56, 20, 48, 50, 19, 49, 25, 51, 54, 17, 16, 53, 47, 45, 43]. With the financial support of Laboratoire de Modélisation et Simulation Multi-Echelle (MSME) of Université Paris-Est and PUC-Rio, I had the chance to present papers in several international conferences, such as Uncertainties 2012 (Maresias, Brazil), COMPDYN 2013 (Kos, Greece), USNCCM12 2013 (Raleigh, EUA), EUROODYN 2014 (Porto, Portugal), ENOC (Vienna, Austria) and Uncertainties 2014 (Rouen, France). I presented works also in CNMAC 2012(Águas de Lindóia, Brasil), and CMAC-NE 2012 (Natal, Barzil), in which I gave the mini-course “Modelagem Estocástica e Geração de Amostras de Variáveis e Vetores Aleatórios”.

[C1] “Optimal design of a vibro-impact electro-mechanical system with uncertainties”, Lima, R. and Soize, C. and Sampaio, R., 17th International Symposium on Dynamic Problems of Mechanics (DINAME 2015), Natal, RN, Brazil, 2015.

[C2] “General results of existence and asymptotic stability for a class of electromechanical systems”, Dantas, M.J.H. and Sampaio, R. and Lima, R., 35º Congresso Nacional de Matemática Aplicada e Computacional (CNMAC), Natal, RN, Brazil, 2014.

[C3] “Analysis of the stick-slip dynamics with a stochastic approach”, Lima, R. and Sampaio, R., 35º Congresso Nacional de Matemática Aplicada e Computacional (CNMAC), Natal, RN, Brazil, 2014.

[C4] “Stick-mode duration of random dry-friction oscillators”, Lima, R. and Sampaio, R., 8th European Nonlinear Dynamics Conference (ENOC 2014), Vienna, Austria, 2014.

[C5] “Dynamics of an electromechanical system forced near the resonance”, Dantas, M.J.H. and Sampaio, R. and Lima, R., 8th European Nonlinear

Dynamics Conference (ENOC 2014), Vienna, Austria, 2014.

[C6] “The random dynamics of an embarked pendulum in a vibro-impact electromechanical system”, Lima, R. and Sampaio, R., 9th International Conference on Structural Dynamics (EURODYN 2014), Porto, Portugal, 2014.

[C7] “Design of a nonlinear dynamical absorber for an uncertain system”, Fonseca, C and Lima, R. and Wagner, G. and Sampaio, R., 2nd International Symposium on Uncertainty Quantification and Stochastic Modeling (Uncertainties 2014) Rouen, France, 2014.

[C8] “Uncertainties on the stick-slip dynamics”, Lima, R. and Sampaio, R., 2nd International Symposium on Uncertainty Quantification and Stochastic Modeling (Uncertainties 2014) Rouen, France, 2014.

[C9] “A vibro-impact electromechanical system: models of the random dynamics of an embarked pendulum”, Lima, R. and Sampaio, R. and Soize, C., 22nd International Congress of Mechanical Engineering (COBEM 2013), Ribeirão Preto, SP, Brazil, 2013.

[C10] “Stable periodic orbits in an electromechanical system”, Dantas, M.J.H. and Sampaio, R. and Lima, R., Congresso Nacional de Dinâmica e Controle (DINCON 2013), Fortaleza, CE, Brazil, 2013.

[C11] “Existence of periodic orbits in an electromechanical system under parametric and external excitations”, Dantas, M.J.H. and Sampaio, R. and Lima, R., VII Encontro Nacional de Análise Matemática e Aplicações (ENAMA 2013) Rio de Janeiro, Brazil, 2013.

[C12] “Uncertainty quantification of the nonlinear dynamics of electromechanical coupled systems”, Lima, R. and Sampaio, R. and Soize, C., 3rd South-East European Conference on Computational Mechanics (COMPDYN 2013), Kos Island, Greece, 2013.

[C13] “Uncertainty quantification of coupled electro-mechanical systems with an embarked pendulum”, Lima, R. and Sampaio, R., XV International Symposium on Dynamic Problems of Mechanics (DINAME 2013) Búzios, RJ, Brazil, 2013.

[C14] “Stochastic Analysis of mechanical systems with nonideal source of power”, Lima, R. and Sampaio, R., Congresso Matemática Aplicada e Computacional (CMAC-NE 2012), Natal, RN, Brazil, 2012.

[C15] “Analysis of Markov Chain Monte Carlo Method and example of its application in random vibration simulations”, Lima, R. and Sampaio, R., 1st International Symposium on Uncertainty Quantification and Stochastic Modeling (Uncertainties 2012), Maresias, SP Brazil, 2012.

# Bibliography

- [1] R.R. Aguiar. *Experimental investigation and numerical analysis of the vibro-impact phenomenon*. PhD thesis, PUC-Rio, Rio de Janeiro, Brazil, 2010.
- [2] R.R. Aguiar and H.I. Weber. Mathematical modeling and experimental investigation of an embedded vibro-impact system. *Nonlinear Dynamics*, 65:317–334, 2011.
- [3] R.R. Aguiar and H.I. Weber. Impact force magnitude analysis of an impact pendulum suspended in a vibrating structure. *Shock and Vibration*, DOI 10.3233/SAV-2012-0678, pages 1359–1372, 2012.
- [4] J.M. Balthazar, D.T. Mook, H.I. Weber, R.M.L.R.F. Brasil, A. Felini, D. Belato, and J.L.P. Felix. An overview on non-ideal vibrations. *Mechanica*, 38:613–621, 2003.
- [5] A.D. Batako, V.I. Babitsky, and N.A. Halliwell. A self-excited system for percussive-rotary drilling. *Journal of Sound and Vibration*, 259(1):97–118, 2003.
- [6] D. Belato. *Análise Não Linear de Sistemas Dinâmicos Holônomos Não Ideais*. PhD thesis, Department of Mechanical Engineering, Universidade Estadual de Campinas, Campinas, S.P., Brazil, 2002.
- [7] D. Belato, H.I. Weber, and J.M. Balthazar. Escape in a nonideal electro-mechanical system. *Journal of the Brazilian Society of Mechanical Sciences and Engineering*, 24(4):335–340, 2002.
- [8] D. Belato, H.I. Weber, J.M. Balthazar, and D.T. Mook. Chaotic vibrations of a non-ideal electro-mechanical system. *International Journal of Solids and Structures*, 38:1699–1706, 2001.
- [9] E. Capiez-Lernout and C. Soize. Robust design optimization in computational mechanics. *Journal of Applied Mechanics, Transactions ASME*, 75(2):021001-1–021001-11, 2008.
- [10] M. Cartmell. *Introduction to Linear, Parametric and Nonlinear Vibrations*, volume 260. Springer, 1990.

- [11] E. Cataldo. *Introdução aos processos estocásticos*. Notas em Matemática Aplicada, Sociedade Brasileira de Matemática Aplicada e Computacional, São Carlos, Brazil, 2012.
- [12] E. Cataldo, S. Bellizzi, and R. Sampaio. Free vibrations of an uncertain energy pumping system. *Journal of Sound and Vibration*, 332:6815–682, 2013.
- [13] F. L. Chernous'ko. On the motion of a body containing a movable internal mass. *Doklady Physics*, 50(11):593–597, 2005.
- [14] A. P. Christoforou and A. S. Yigit. Fully coupled vibrations of actively controlled drillstrings. *Journal of Sound and Vibration*, 267:1029–1045, 2003.
- [15] M.J.H. Dantas, R. Sampaio, and R. Lima. *Dynamical Systems: Applications (chapter: A nonlinear electromechanical system with stable periodic orbits, pages 353–364)*. Editors: Jan Awrejcewicz, Marek Kazmierczak, Pawel Olejnik, Jerzy Mrozowski, 2013.
- [16] M.J.H. Dantas, R. Sampaio, and R. Lima. Existence of periodic orbits in an electromechanical system under parametric and external excitations. In *VII Encontro Nacional de Análise Matemática e Aplicações (ENAMA 2013)*, Rio de Janeiro, Brazil, 2013.
- [17] M.J.H. Dantas, R. Sampaio, and R. Lima. Stable periodic orbits in an electromechanical system. In *Congresso Nacional de Dinâmica e Controle (DINCON 2013)*, Fortaleza, CE, Brazil, 2013.
- [18] M.J.H. Dantas, R. Sampaio, and R. Lima. Asymptotically stable periodic orbits of a coupled electromechanical system. *Nonlinear Dynamics*, 78:29–35, 2014.
- [19] M.J.H. Dantas, R. Sampaio, and R. Lima. Dynamics of an electromechanical system forced near the resonance. In *8th European Nonlinear Dynamics Conference (ENOC 2014)*, Vienna, Austria, 2014.
- [20] M.J.H. Dantas, R. Sampaio, and R. Lima. General results of existence and asymptotic stability for a class of electromechanical systems. In *35º Congresso Nacional de Matemática Aplicada e Computacional (CNMAC)*, Natal, RN, Brazil, 2014.
- [21] M.J.H. Dantas, R. Sampaio, and R. Lima. Phase bifurcations in an electromechanical system. In *IUTAM - Symposium on Analytical Methods in Nonlinear Dynamics*, Frankfurt, Germany, 2015.

- [22] A. Depouhon, V. Denoël, and E. Detournay. Numerical simulation of percussive drilling. *International Journal for Numerical and Analytical Methods in Geomechanics*, DOI: 10.1002/nag.2344, 2015.
- [23] R. M. Evan-Iwanowski. *Resonance oscillations in mechanical systems*. Elsevier Publ. Co., Amsterdam, 1976.
- [24] A. Fidlin. *Nonlinear Oscillations in Mechanical Engineering*. Springer, Netherlands, 2006.
- [25] C Fonseca, R. Lima, G. Wagner, and R. Sampaio. Design of a nonlinear dynamical absorber for an uncertain system. In *2nd International Symposium on Uncertainty Quantification and Stochastic Modeling (Uncertainties 2014)*, Rouen, France, 2014.
- [26] C. Fonseca, R. Lima, G. Wagner, and R. Sampaio. Robust identification and passive control of vibration of a test rig under uncertain conditions. *Mecánica Computacional*, XXXIII:27:1767–1781, 2014.
- [27] L.F.P. Franca. *Self-excited percussive-rotary drilling in hard rocks*. PhD thesis, PUC-Rio, Rio de Janeiro, Brazil, 2004.
- [28] L.F.P. Franca and H. I. Weber. Experimental and numerical study of a new resonance hammer drilling model with drift. *Chaos, Solitons and Fractals*, 21:789–801, 2004.
- [29] E. Gourdon. *Contrôle passif de vibrations par pompage énergétique*. PhD thesis, Ecole Centrale de Lyon, 2006.
- [30] E. Gourdon, N.A. Alexander, C.A. Taylor, C.H. Lamarque, and S. Pernot. Nonlinear energy pumping under transient forcing with strongly nonlinear coupling: Theoretical and experimental results. *Journal of Sound and Vibration*, 300:522–551, 2007.
- [31] P. Hagedorn. *Non-linear Oscillations*. Clarendon Press, Oxford, second edition, 1988.
- [32] R. Ibrahim. *Vibro-Impact Dynamics: Modeling, Mapping and Applications*. Springer, Berlin, 2009.
- [33] C. Ingar. *Controle de impacto em manipuladores robóticos*. PhD thesis, Department of Mechanical Engineering, PUC-Rio, Rio de Janeiro, Brazil, 2004.

- [34] E. Jaynes. Information theory and statistical mechanics. *The Physical Review*, 106(4):620–630, 1957.
- [35] D.C. Karnopp, D.L. Margolis, and R.C. Rosenberg. *System Dynamics: Modeling and Simulation of Mechatronic Systems*. John Wiley and Sons, 4th edition, New-York, USA, 2006.
- [36] Y. A. Khulief, F. A. Al-sulaiman, and S. Bashmall. Vibration analysis of drillstrings with self excited stick-slip oscillations. *Journal of Sound and Vibration*, 299:540–558, 2007.
- [37] V. O. Kononenko. *Vibrating Systems with a Limited Power Supply*. London Iliffe Books LTD, England, 1969.
- [38] C. Krée, P. Soize. *Mathematics of random phenomena*. D. Reidel Publishing Company, 1986.
- [39] P. Kree and C. Soize. *Mécanique aléatoire*. Dunod, Paris, France, 1983.
- [40] W. Lacarbonara and Stuart Antman. What is parametric excitation in structural dynamics? In *ENOC-2008*, Saint Petersburg, Russia, 2008. ENOC.
- [41] H.S. Lee, I. Incheon, C. Cho, and S.P. Chang. Design and analysis of electro-mechanical characteristics of micromachined stainless steel pressure sensor. In *Proc. of the 5th IEEE Sensors Conference*, IEEE Sensors, pages 659–674, Daegu, South Korea, 2006. IEEE.
- [42] R. Lima and R. Sampaio. Analysis of an Electromechanic Coupled System with Embarked Mass. *Mecânica Computacional*, XXXI:2709–2733, 2012.
- [43] R. Lima and R. Sampaio. Analysis of markov chain monte carlo method and example of its application in random vibration simulations. In *1st International Symposium on Uncertainty Quantification and Stochastic Modeling (Uncertainties 2012)*, Maresias, SP Brazil, 2012.
- [44] R. Lima and R. Sampaio. Stochastic analysis of an electromechanical coupled system with embarked mass. *Mecânica Computacional*, XXXI:2709–2733, 2012.
- [45] R. Lima and R. Sampaio. Stochastic analysis of mechanical systems with nonideal source of power. In *Congresso Matemática Aplicada e Computacional (CMAC-NE 2012)*, Natal, RN, Brazil, 2012.

- [46] R. Lima and R. Sampaio. Some remarks about stick-slip oscillators. *Mecánica Computacional*, XXXII:8:647–668, 2013.
- [47] R. Lima and R. Sampaio. Uncertainty quantification of coupled electro-mechanical systems with an embarked pendulum. In *XV International Symposium on Dynamic Problems of Mechanics (DINAME 2013)*, Búzios, RJ, Brazil, 2013.
- [48] R. Lima and R. Sampaio. Analysis of the stick-slip dynamics with a stochastic approach. In *35º Congresso Nacional de Matemática Aplicada e Computacional (CNMAC)*, Natal, RN, Brazil, 2014.
- [49] R. Lima and R. Sampaio. The random dynamics of an embarked pendulum in a vibro-impact electromechanical system. In *9th International Conference on Structural Dynamics (EURODYN 2014)*, Porto, Portugal, 2014.
- [50] R. Lima and R. Sampaio. Stick-mode duration of random dry-friction oscillators. In *8th European Nonlinear Dynamics Conference (ENOC 2014)*, Vienna, Austria, 2014.
- [51] R. Lima and R. Sampaio. Uncertainties on the stick-slip dynamics. In *2nd International Symposium on Uncertainty Quantification and Stochastic Modeling (Uncertainties 2014)*, Rouen, France, 2014.
- [52] R. Lima and R. Sampaio. Stick-mode duration of a dry-friction oscillator with an uncertain model. *To be published in Journal of Sound and Vibration*, 2015.
- [53] R. Lima, R. Sampaio, and C. Soize. Uncertainty quantification of the nonlinear dynamics of electromechanical coupled systems. In *3rd South-East European Conference on Computational Mechanics (COMPDYN 2013)*, Kos Island, Greece, 2013.
- [54] R. Lima, R. Sampaio, and C. Soize. A vibro-impact electromechanical system: models of the random dynamics of an embarked pendulum. In *22nd International Congress of Mechanical Engineering (COBEM 2013)*, Ribeirão Preto, SP, Brazil, 2013.
- [55] R. Lima, C. Soize, and R. Sampaio. Robust design of a vibro-impact electro-mechanical system. *Mecánica Computacional*, XXXIII:27:1813–1819, 2014.

- [56] R. Lima, C. Soize, and R. Sampaio. Optimal design of a vibro-impact electro-mechanical system with uncertainties. In *17th International Symposium on Dynamic Problems of Mechanics (DINAME 2015)*, Natal, RN, Brazil, 2015.
- [57] R. Lima, C. Soize, and R. Sampaio. Robust design optimization with an uncertain model of a nonlinear vibro-impact electro-mechanical system. *Communications in Nonlinear Science and Numerical Simulation*, 23:263–273, 2015.
- [58] Y. Liu, E. Pavlovskaja, D. Hendry, and M. Wiercigroch. Vibro-impact responses of capsule system with various friction models. *International Journal of Mechanical Sciences*, 72:39–54, 2013.
- [59] Y. Liu, E. Pavlovskaja, M. Wiercigroch, and Z. Pengc. Forward and backward motion control of a vibro-impact capsule system. *International Journal of Non-Linear Mechanics*, 70(0):30–46, 2015.
- [60] Y. Liu, M. Wiercigroch, E. Pavlovskaja, and Yu H. Modelling of a vibro-impact capsule system. *International Journal of Mechanical Sciences*, 66:2–11, 2013.
- [61] R.H. Lopez. *Optimisation en présence d'incertitudes*. PhD thesis, L'Institut National des Sciences Appliquées de Rouen, Rouen, France, 2010.
- [62] A.C.J. Luo and B. Yu. Analytical solutions of period-m motions in a parametric, quadratic nonlinear oscillator. *ENOC-2014, Vienna, Austria*, 2014.
- [63] G. Luo, Y. Zhang, J. Xie, and J. Zhang. Periodic-impact motions and bifurcations of vibro-impact systems near 1:4 strong resonance point. *Communications in Nonlinear Science and Numerical Simulation*, 13:1002–1014, 2008.
- [64] A. H. Nayfeh and D. T. Mook. *Nonlinear Oscillations*. John Wiley and Sons, USA, 1979.
- [65] S. Neumeier, R. Looij, and J. J. Thomsen. Jumps and bi-stability in the phase-gain characteristics of a nonlinear parametric amplifier. *ENOC-2014, Vienna, Austria*, 2014.
- [66] F. Nucera, A.F. Vakakis, D.M. McFarland, L.A. Bergman, and G. Kerschen. Targeted energy transfers in vibro-impact oscillators for seismic mitigation. *Nonlinear Dynamics*, 50:651–677, 2007.

- [67] R. Ohayon and C. Soize. *Advanced Computational Vibroacoustics: Reduced-Order Models and Uncertainty Quantification*. Cambridge University Press, USA, 2014.
- [68] V. Ostasevicius, R. Gaidys, and R. Dauksevicius. Numerical analysis of dynamic effects of a nonlinear vibro-impact process for enhancing the reliability of contact-type mems devices. *Sensors*, 9:10201–10216, 2009.
- [69] M. P. Paidoussis. *System Dynamics: Modeling and Simulation of Mechatronic Systems*. Academic Press, vol.1, London, United Kingdom, 1998.
- [70] E. Pavlovskaja, D. Hendry, and M. Wiercigroch. Modelling of high frequency vibro-impact drilling. *International Journal of Mechanical Sciences*, 91:110–119, 2015.
- [71] N.J. Peruzzi, F.R. Chavarette, J.M. Balthazar, A.L.P. Manfrim, and R.M.F.L. Brasil. On control of a parametrically excited time-periodic "mems". *ENOC-2014, Vienna, Austria*, 2014.
- [72] F. Peterka. Bifurcations and transition phenomena in an impact oscillator. *Chaos Solitons & Fractals*, 7(10):1635–1647, 1996.
- [73] R. Ragulskis and K. Ragulskis. The effect of dynamical self-orientation and its applicability for identification of natural frequencies. *Nonlinear Dynamics*, 50:61–71, 2007.
- [74] T.G. Ritto. *Numerical analysis of the nonlinear dynamics of a drill-string with uncertainty modeling*. PhD thesis, PUC-Rio and Paris-Est, Rio de Janeiro, Brazil, 2010.
- [75] T.G. Ritto, F.S. Buezas, and R. Sampaio. A new measure of efficiency for model reduction: Application to a vibroimpact system. *Journal of Sound and Vibration*, pages 1977–1984, 2010.
- [76] T.G. Ritto, M. Escalante, R. Sampaio, and M. Rosales. Drill-string horizontal dynamics with uncertainty on the frictional force. *Journal of Sound and Vibration*, 332:145–153, 2013.
- [77] T.G. Ritto, M. Gruzman, and R. Sampaio. Fuzzy logic control of a drill-string. In *30th CILAMCE - Iberian Latin-American Congress on Computational Methods In Engineering*, Armação dos Buzios, RJ, Brazil, 2009.

- [78] T.G. Ritto and R. Sampaio. Stochastic drill-string dynamics with uncertainty on the imposed speed and on the bit-rock parameters. *International Journal for Uncertainty Quantification*, 2:111–124, 2012.
- [79] T.G. Ritto and R. Sampaio. Measuring the efficiency of vertical drill-strings: A vibration perspective. *Mechanics Research Communications*, 52(0):32–39, 2013.
- [80] T.G. Ritto, C. Soize, and R. Sampaio. Nonlinear dynamics of a drill-string with uncertain model of the bit-rock interaction. *International Journal of Non-Linear Mechanics*, 44(8):865–876, 2009.
- [81] T.G. Ritto, C. Soize, and R. Sampaio. Robust optimization of the rate of penetration of a drill-string using a stochastic nonlinear dynamical model. *Computational Mechanics*, 45(5):415–427, 2010.
- [82] T.G. Ritto, C. Soize, and R. Sampaio. Stochastic dynamics of a drill-string with uncertain weight-on-hook. *Journal of the Brazilian Society of Mechanical Sciences and Engineering*, 32(3):250–258, 2010.
- [83] Y. Rocard. *Dynamique Générale des Vibrations*. Masson et Cie., Éditeurs, Paris, France, 1943.
- [84] H. Sadeghian and G. Rezazadeh. Comparison of generalized differential quadrature and galerkin methods for the analysis of micro-electro-mechanical coupled systems. *Communications in Nonlinear Science and Numerical Simulation*, 14:2807–2816, 2009.
- [85] R. Sampaio and R. Lima. *Modelagem Estocástica e Geração de Amostras de Variáveis e Vetores Aleatórios*. Notas de Matemática Aplicada. SB-MAC, 2012.
- [86] R. Sampaio, M. T. Piovan, and G. V. Lozano. Coupled axial/torsional vibrations of drill-strings by means of non-linear model. *Mechanics Research Communications*, 34(5-6):497–502, 2007.
- [87] R. Sampaio and C. Soize. On measures of non-linearity effects for uncertain dynamical systems - application to a vibro-impact system. *Journal of Sound and Vibration*, 303(3–5):659–674, 2007.
- [88] C.E. Shannon. A mathematical theory of communication. *Bell System Tech.*, 27:379–423 and 623–659, 1948.

- [89] C. Soize. A nonparametric model of random uncertainties for reduced matrix models in structural dynamics. *Probabilistic Engineering Mechanics*, 15(3):277–294, 2000.
- [90] C. Soize. Maximum entropy approach for modeling random uncertainties in transient elastodynamics. *Journal of the Acoustical Society of America*, 109(5):1979–1996, 2001.
- [91] C. Soize. *Probabilités et modélisation des incertitudes - Eléments de base et concepts fondamentaux*. Université Paris-Est, Marne la Vallée, 2004.
- [92] C. Soize. *Stochastic models of uncertainties in computational mechanics*. ASCE, USA, 2012.
- [93] V. Sorokin. On the response of a nonlinear parametric amplifier driven beyond resonance. *ENOC-2014, Vienna, Austria*, 2014.
- [94] J.E. Souza de Cursi and R. Sampaio. *Modelagem estocástica e quantificação de incertezas*. Notas em Matemática Aplicada, Sociedade Brasileira de Matemática Aplicada e Computacional, São Carlos, Brazil, 2012.
- [95] J.E. Souza de Cursi and R. Sampaio. *Uncertainty quantification and stochastic modeling with Matlab*. ISTE Press, England, 2015.
- [96] M. Trindade, C. Wolter, and R. Sampaio. Karhunen-loève decomposition of coupled axial/bending vibrations of beams subject to impacts. *Journal of Sound and Vibration*, 279(3-5):1015–1036, 2005.
- [97] J. Warminski and J. M. Balthazar. Vibrations of a parametrically and self-excited system with ideal and non-ideal energy sources. *Journal of the Brazilian Society of Mechanical Sciences and Engineering*, 25(4):413–420, 2003.
- [98] X. Yue, W. Xu, and L. Wang. Global analysis of boundary and interior crises in an elastic impact oscillator. *Communications in Nonlinear Science and Numerical Simulation*, 18:3567–3574, 2013.
- [99] S. Zhankui and K. Sun. Nonlinear and chaos control of a micro-electro-mechanical system by using second-order fast terminal sliding mode control. *Communications in Nonlinear Science and Numerical Simulation*, 18:2540–2548, 2013.